THE MESSENGER

EL MENSAJERO

Munich

Paranal

La Silla

Santiago

No. 106 – December 2001

First Fringes with ANTU and MELIPAL

A. GLINDEMANN, P. BALLESTER, B. BAUVIR, E. BUGUEÑO, M. CANTZLER, S. CORREIA, F. DELPLANCKE, F. DERIE, P. DUHOUX, E. DI FOLCO, A. GENNAI, B. GILLI, P. GIORDANO, P. GITTON, S. GUISARD, N. HOUSEN, A. HUXLEY, P. KERVELLA, M. KIEKEBUSCH, B. KOEHLER, S. LÉVÊQUE, A. LONGINOTTI, A. LOPEZ, S. MÉNARDI, S. MOREL, F. PARESCE, T. PHAN DUC, A. RAMIREZ, A. RICHICHI, M. SCHÖLLER, J. SPYROMILIO, M. TARENGHI, A. WALLANDER, R. WILHELM, M. WITTKOWSKI

1. Introduction

On October 30, 2001 at about 1 a.m., the two 8-m Unit Telescopes ANTU and MELIPAL of Paranal Observatory were combined for the first time as a stellar interferometer observing fringes on the star Achernar (see Fig. 1), only seven months and twelve days after the VLTI produced the first fringes with two siderostats. This was the first time that the VLTI was operated as a truly Very Large Telescope Interferometer. The VLT project of designing, building, and operating the VLT observatory and combining the Unit Telescopes as an interferometer, a project that kept most of ESO and many in the ESO community busy for more than a decade, reached one of its most important milestones.

As a preparation for this achievement, the Coudé Optical Trains and the Relay Optics were integrated in the Unit Telescopes, the third Delay Line System (required for using MELIPAL) had its final tests in July, and the beam compressors were assembled in the Beam Combination Laboratory of the VLTI. A new version of the interferometer control software was installed providing the additional functionalities that are required to combine two UTs (see article on page 2). With the support of NEVEC[1], the data pipeline has matured considerably over the last six months, and it now produces results for the visibility, the transfer function and statistical parameters enabling on-line data quality control.

At the beginning of October, the CCD in the VINCI test instrument saw first light with the Unit Telescopes (see Fig. 2) showing an image quality that was well within specifications: the image size was limited only by the seeing of 0.45 arcsec. There was no indication that the 200-m light path and the 28 reflections between the primary 8-m mirror and the CCD affected the image quality.

[1]NEVEC is the NOVA (the Netherlands Research School for Astronomy) – ESO VLTI Expertise Centre at the Leiden Observatory.

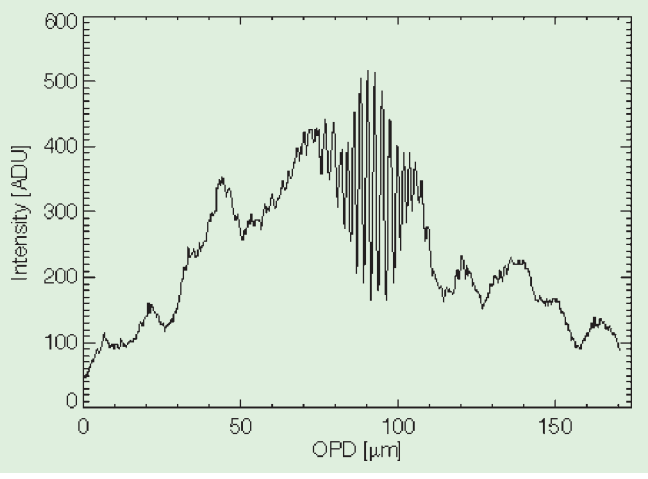

Figure 1: Raw interferometric fringes of Achernar in the K-band, as observed on the computer screen in the VLTI Control Room at the moment of First Fringes.

2. First Fringes

The night of October 29/30 started with tests of the Coudé Optical Trains and the Relay Optics, converting the light from the Coudé focus to a parallel beam in the Delay Line Tunnel. For the history books it should be noted that one of these mirrors (M9) arrived only on the very same night at Paranal, and a small dummy mirror with a diameter of 40 mm – albeit of very good optical quality – on a temporary mount had to be used for First Fringes.

Around midnight, when the UT team finished the tests and the search for fringes could start, not everybody on the mountain would have bet how quickly the search was successful. Before actually seeing fringes with a new baseline, a number of assumptions has to be taken on the internal path lengths in each arm of the interferometer and on the distance between the telescopes. When distances between individual mirrors can be measured with very high precision (some 10 microns), the distance between the telescopes, i.e. the baseline, is only known with a precision of some 10 millimetres. These uncertainties can be corrected after fringes are found on different stars, and the so-called OPD (Optical Path Difference) model of the interferometer is refined. Depending on the discrepancy between the assumed baseline and the real baseline, the first search for fringes can take several hours since the scan for OPD zero position where fringes can be found has to be done at speeds of about 1 mm per minute.

However, barely one hour after we had started, the automatic fringe search routine in VINCI reported 'flecos en el cielo', and the fringes appeared on the screen. We found that the baseline of 102.5 m between ANTU and MELIPAL differed by only 28 mm from their nominal length. After refinement of the OPD model, fringes were subsequently found within 0.4 mm of their calculated position.

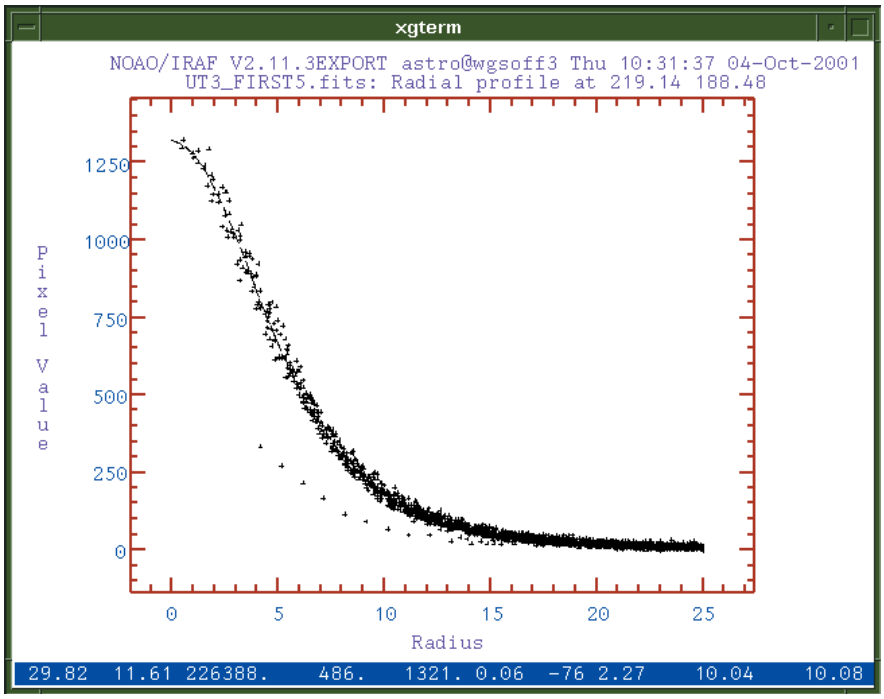

Figure 2: The radial plot of the first stellar image on a CCD at the VLTI focus collected with the 8-m telescopes. After 28 reflections and 200 m of optical path inside the VLTI, the image size of 0.45 arcsec was limited only by the seeing.

With the experience that we had gathered over the last six months of commissioning, 'routine operation' with the 8-m telescopes started almost immediately with a number of scientific observations: the first measurements of the diameter of red dwarfs (Kapteyns star, HD 217987 and HD36395), the precise determination of the diameter of Cepheids (Beta Dor and Zeta Gem), the so-called light houses of the universe, and the first measurement of the core of Eta Carinae (for details see the press release). A total of 17 different stars was observed during this observing run. The technical downtime was less than two hours per night.

The faintest star that could be observed had a magnitude of K = 6.3, and this is all the more remarkable as the 8-m telescopes were used without any adaptive optics correction. The star light in VINCI has to be fed into an optical fibre with a diameter of 6.5 microns which is the diameter of the diffraction limited Airy disk and, thus, a perfect match if the telescopes produced diffraction limited images. Without adaptive optics, this optical fibre is merely fishing for photons in the middle of the speckle cloud with a diameter of about 0.6 arcsec which is 10 times the diffraction limit. The number of photons entering the fibre is then about 100 times or 5 stellar magnitudes smaller than what could be expected with adaptive optics.

We are now looking forward to improving the performance for the following UT observing runs by implementing the tip-tilt correction in the Coudé foci and by tuning the infrared camera readout mode. The general planning for the following years is described in *The Messenger* No. 104, p. 2 (June 2001).

The VLTI Data Flow System: From Observation Preparation to Data Processing

P. BALLESTER[1], P. KERVELLA[1], L.P. RASMUSSEN[2], A. RICHICHI[1], C. SABET[1], M. SCHÖLLER[1], R. WILHELM[1], B. WISEMAN[1], M. WITTKOWSKI[1]

[1]European Southern Observatory, Garching, Germany
[2]ROVSING A/S, Skovlunde, Denmark

In this article we present the Data Flow System (DFS) for the VLT Interferometer (VLTI) that is analogous with that of other telescopes of the VLT. The DFS was first installed for VLTI first fringes utilising the siderostats together with the VINCI instrument and is constantly being upgraded in phase with the VLTI commissioning. A recent VLTI achievement has been the first fringes with the Unit Telescopes (see article on page 1). For this milestone the VLTI

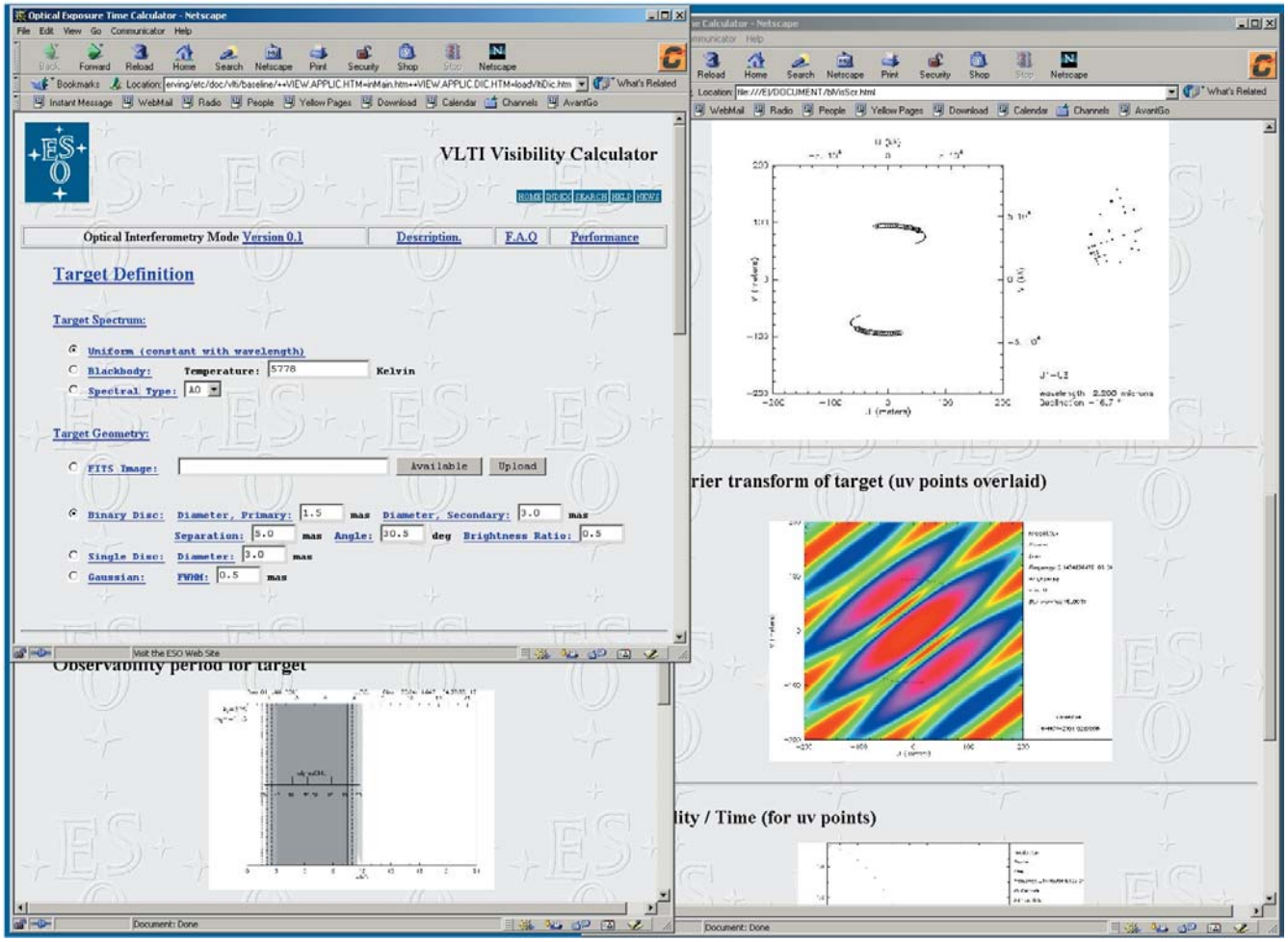

Figure 1: The VLTI Visibility Calculator (preliminary design). The VLTI Visibility Calculator will be an Internet application similar to the ESO Exposure Time Calculators. The prototype is using the ASPRO/JMMC software as a calculation engine.

DFS was also present and operating. Observations of objects with some scientific interest are already being carried out in the framework of the VLTI commissioning, making it possible to test tools under realistic conditions. These tools comprise observation preparation, pipeline processing and further analysis systems. Work is in progress for the commissioning of other VLTI science instruments such as MIDI and AMBER. These are planned for the second half of 2002 and first half of 2003 respectively. The DFS will be especially useful for service observing. This is expected to be an important mode of observation for the VLTI, which is required to cope with numerous observation constraints and the need for observations spread over extended periods of time.

Preparing VLTI Observations

Preparing an interferometric observation involves successive stages, each with specific constraints. In order to assess the technical feasibility of an interferometric observation one needs adequate tools to model the complete interferometer behaviour and to take into account for example shadowing effects, or the range of the delay lines. A typical suite of actions involved in the preparation of an interferometric observation involves the following steps:

• An assumption must be made concerning the intensity distribution of the source. Usually this will be in the form of a model with a uniform or limb-darkened disk, a Gaussian profile, a multiple system or any other shape that can be analytically described or has been obtained by techniques like radiation transfer calculations. The final goal is then to constrain the object parameters by model fitting or image reconstruction.

• The Fourier transform of the source intensity distribution that is the complex visibility function, is calculated. A set of spatial frequencies is identified which is suitable to obtain the required information on the object. A configuration of the interferometer array is selected among the available ones that will make it possible to sample the Fourier space in the adequate domain of spatial frequencies.

• One must make sure that the target is visible from the VLTI platform by all telescopes involved in the observation, taking into account possible shadowing effects. Shadowing effects can be caused for instance by the Unit Telescopes which obscure parts of the sky as seen by the Auxiliary Telescopes.

• The optical path difference must be estimated, in order to evaluate the total time that will be available for the observation.

• Suitable calibrators must be selected for the science object. An interferometric calibrator is a target of (supposedly) known properties that will give a reference value for the measured visibility. Since the transfer function of the interferometer varies with time, calibrators and science objects must be observed alternatively within the finite stroke of the delay lines.

• The visibility amplitude (i.e. the modulus of the Fourier transform) of the target and calibrators can be estimated as well as the required exposure times. Note that in interferometry, it is not just the magnitude of the source that matters, but also the product of the total flux (in the resolution element) and the visibility[1]. For example, between two sources of magnitude 1 and 2, and with visibilities 0.1 and 0.5 respectively, the former will look “fainter” to an interferometer than the latter.

• Once several series of targets and calibrators have been selected, they

[1]Visibility is a measure of the contrast of the interferometric fringes, as a function of the separation between the telescopes. (An unresolved source will have maximum fringe contrast: visibility will be 1. A completely resolved source will have no fringes, and the visibility will be 0.)

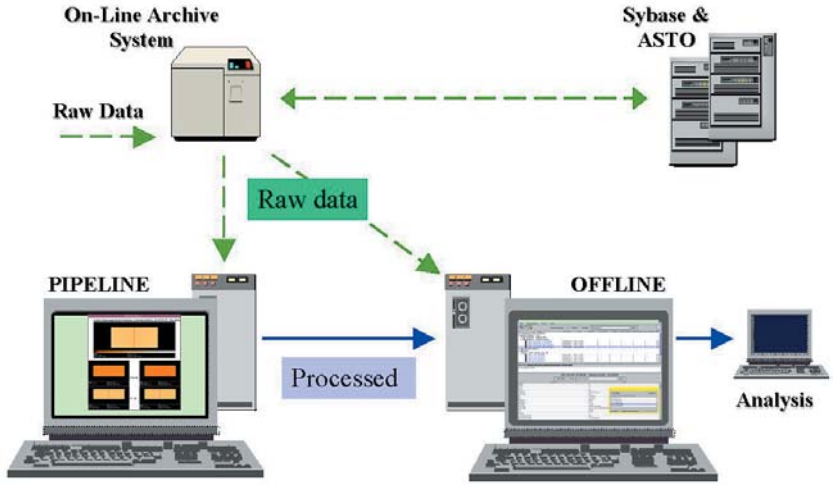

Figure 2: VLTI Data Flow System at Paranal.

must be organised in a schedule of observations, where one will try to optimise the time spent in acquiring data taking into account priorities and observational constraints.

As can be seen from the above list, preparing an interferometric observation requires adequate tools that can handle the geometrical configuration of the array and target/calibrator positions. Most observations in interferometry will involve measurements for different spatial frequencies and are likely to require different configurations and spread over extended periods of time, several weeks or several months. It is therefore expected that service observing will be a dominant mode at the VLTI. The geometrical constraints on the observation of the science and calibrator targets and the limited observability of the objects due to both the range of delay lines and shadowing effects will make it necessary to assess the technical feasibility of observations at both stages of phase 1 and phase 2 preparation. During phase 1, general tools like the WEB-based visibility calculator and exposure time calculators will be provided. In phase 2, the details of the observation can be validated more accurately.

VLTI Visibility Calculator

The VLTI Visibility Calculator is the tool used for such calculations. It computes the fringe visibility as a function of the object model parameters and the array configuration. It takes into account the horizon map of the observatory and shadowing effects induced by telescope domes and structures on the observatory platform. It computes the optical path length, the optical path difference and takes into account the range of the Delay Lines to estimate the period of observation for a given target.

A prototype of the VLTI Visibility Calculator is shown in Figure 1. The current prototype uses as a computation engine the ASPRO software (Duvert & Berio, 2001) provided by the Jean-Marie Mariotti Centre (JMMC) supported by INSU (CNRS and Ministère de la Recherche, France). The prototype is used to identify an efficient and user-friendly procedure for dealing with the numerous interferometric observation constraints. The user-interface of the VLTI Visibility Calculator uses the same technology as the ESO Exposure Time Calculators (ETCs). It will therefore be an Internet tool like the existing VLT ETCs.

An important feature of this Web-based prototype is that the user is provided not only with a visibility map of the source under consideration, but also with the so-called u-v tracks for the chosen VLTI configuration[2]. This enables the user to see immediately which parts of the visibility map can be studied and thereby estimate the usefulness and impact of such measurements.

VLTI Exposure Time Calculators

Observation preparation tools have been provided for the VLT instruments in the form of Exposure Time Calculators accessible over the Internet (http://www.eso.org/observing/etc). The system provides a uniform access to the ETCs provided for the different VLT instruments. Several solutions have been designed to make it possible to efficiently develop and maintain these applications. For instance HTML templates and dictionaries are used to generate the pages on the fly, a macro language is used for prototyping and a database system is utilised to simplify the adjustment of instrument characteristics.

The ETC interface consists of two main pages, the input page and the result page. On the input page, the instrument se-tup and the target of the observations are defined. An HTML form is used to forward this information to a model application, which then performs the calculations and generates the result page. The result page summarises the input parameters and presents the results of the calculations, such as detected number of electrons of the object and sky, as well as various other information. The main result is the signal to noise for the observation, or alternatively, the number of integrations needed to achieve a specified signal to noise. In interferometry the signal-to-noise computations are significantly different from those required for a standard image or spectrum as done so far in the ETCs. The VLTI instruments ETCs will be interfaced to the Visibility Calculator.

[2]u-v plane: also known as Fourier plane or Fourier space, is the counterpart (or inverse) of the image plane in which we measure separations in angles in arcseconds. The coordinates in the u-v plane are in metres and the points that are measured are defined by the baseline vectors (the vectors 'between' the telescopes of the interferometer).

VLTI Data Flow System at Paranal

The hardware system handling the VLTI data is similar to the system installed at the Unit Telescopes (Ballester et al., 2001). Figure 2 shows the logical structure of the VLTI DFS system at Paranal: the instrument data are transferred from the instrument workstation to the On-Line Archive System machine, where they are kept on a Redundant Array of Independent Disks (RAID) system. The Data Handling Server takes care of distributing the data to the pipeline, off-line and archive workstations. Two machines are reserved for archive operations. One is dedicated to the Sybase server, where critical information about the operations is stored in various databases. The other Archive Storage (ASTO) machine is dedicated to media production, in particular CDs and DVDs. The pipeline workstation usually runs in automatic mode, receiving and processing the data, displaying the results and transferring the processed data to the off-line workstation. On the off-line workstation, interactive tools are available for reprocessing and analysing the data for the purpose of commissioning and scientific evaluation.

In the Data Flow system, the instrument parameters are grouped in high-level structures called Templates and Observation Blocks. Templates and Observation Blocks are assembled with P2PP, the Phase 2 Proposal Preparation tool. This Java tool provides a uniform graphical user interface to all VLT and VLTI instruments. In visitor mode the OBs are loaded using P2PP directly at the VLTI. In service mode, the Observation Blocks are ingested in a repository in Garching. The Template activates a standard operation mode of an instrument, for instance for the purpose of internal calibration, observation of calibration objects or scientific observations. Templates are grouped in Observation

Blocks, which in the Data Flow correspond to an unbreakable unit of observation. For the interferometry, a prototype template has been tested which integrates the acquisition and observation of science and calibrator targets. This concept should make it possible to keep track of related observations in the archive and for pipeline processing.

Interferometry data are stored in the form of binary tables. The header of the data follows the ESO Data Interface Control guidelines and provides the FITS keywords necessary for the data handling, processing, archive retrieval and proper documentation of the data.

VINCI Pipeline and Data Quality Control

VINCI (VLT INterferometer Commissioning Instrument) is the beam combiner instrument used to commission the Cerro Paranal VLTI complex (Kervella et al., 2000). The latter is based on the proven concept of FLUOR (Fibre Linked Unit for Optical Recombination) that has been operated since 1995 as a focal instrument of the IOTA interferometer in Arizona. The instrument can receive the beams from the VLTI siderostats or from the Unit Telescopes ANTU and MELIPAL. The Data Flow System to handle VINCI data and the VINCI pipeline were first installed for the VLTI first fringes with the siderostats in March 2001 (Glindemann et al., 2001). The system has been regularly upgraded in particular with the extension of the Data Quality Control facility, which writes a subset of the pipeline results into an operational log-file.

The present VINCI pipeline performs automatically the first stage of processing and prepares FITS files containing the raw visibilities and all the information required for model fitting. The pipeline generates several data products. First the photometry-corrected interferograms are delivered for the purpose of commissioning analysis. This is delivered in ASCII form for further processing. Second, the raw visibilities, together with all the information required for further astrophysical analysis are written in a FITS file.

The pipeline receives the raw data frames from the On-Line Archive system and classifies them in accordance with the specifications given in the pipeline reduction rules. Conditions are evaluated on FITS keywords in order to classify the data. This determines the reduction procedure applied to the data. Before executing the procedure it may be necessary to read additional FITS keywords and to query auxiliary calibration data and tables from the pipeline local calibration database. A reduction block is prepared and sent for execution to a data reduction system. The VINCI measurement set consists of 4 values. These include the Interferometer 1, Interferometer 2, Photometer A and Photometer B measurements at a given time, also corresponding to a given Optical Path Difference (OPD). A scan is a sequence of OPD variation; it typically lasts about 0.1 second with VINCI. Series of scans are taken for different optical configurations: off-source scans, telescope A on-source only, telescope B on-source only, and a longer sequence of interferometric scans with both telescopes on-source. An exposure with VINCI includes the set of 4 batches and all auxiliary information. Each exposure produces a FITS file containing all the information necessary to derive uncalibrated visibilities.

The Quality Control (QC) system includes the tools used inside and outside the pipeline environment in order to control the conditions in which the data have been acquired and processed, in particular the instrumental and observational conditions. Quality control parameters are measured using the data and then written to the log files. The QC parameters have proven to be a very useful method for checking and tracking the health of instruments (Ballester et al., 2000). During the pipeline processing the data quantities characterising the performance of the instrument are measured. These values are written to operational log files. The log files are produced on a daily basis and can be used to produce automatic reports, graphs and summary information. The QC log files are used for diverse applications, for example to establish a catalogue of observed objects, to produce trend graphs of the interferometer transfer function or to verify the quality of the processing by checking the number of scans rejected by the pipeline.

Data Reduction Software

The algorithm for the data processing (Coudé du Foresto et al., 1997) is illustrated in Figure 3. The off-source signal is recorded with both light channels closed. This is processed to estimate the noise power spectral density. The mixed beam signals are recorded while the light passes through telescope A only or telescope B only. They are used to establish the throughput of the interferometer for each beam (transfer matrix) of the interferometer and to calibrate the intensity recorded on each interferometry output with respect to the two photometry signals. Once these preliminary calibrations are performed, it is possible to process the on-source signal. The on-source photometry signal is processed and filtered using information previously collected by the off-source and mixed beam signals. Finally the on-source interferometry signal is processed to yield squared coherence factors together with variance estimates. The processing involves corrections for the dark signal and transfer matrix, and integrating the power spectrum according to the spectral filter.

The calibration of visibilities of interferometry data involves two stages. First the raw visibilities are estimated on both the science and calibrator data. This is the most computing intensive step, during which science and calibrator data are processed in a similar way. Second, the calibrator information is used to estimate the instrument transfer function. This transfer function is then interpolated as a function of time. In interferometry a particular emphasis is placed on the statistical analysis of the data and the accurate estimation of the error bars. This second stage of calibration involves a limited amount of data as it applies to time averaged data. It may also require user interaction for the identification and rejection of calibration points. The calibrated visibilities with error estimates can then be used to determine the science object parameters.

The VINCI data reduction software and pipeline is also an excellent exercise in preparation for the two scientific instruments MIDI and AMBER. MIDI will be the first scientific instrument installed at the VLTI. It will cover the mid-infrared range between 10 and 20 microns. It records spectrally dispersed fringes and at 10 mm can reach a resolution of the order of 20 milli-arc-second. AMBER, which can combine up to three beams will be the first VLTI instrument with some imaging capability. It delivers spectrally dispersed fringes covering the three near-infrared bands J, H and K. Three spectral resolutions of approximately 35, 1000 and 10,000 are supported. By interfering three beams at once it will be possible to obtain images through phase closure

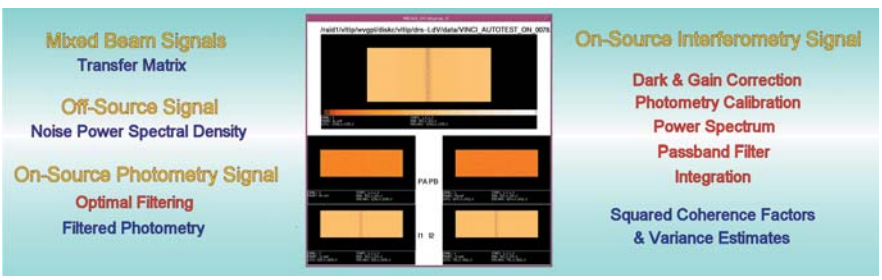

Figure 3: Main processing steps of the VINCI Data Reduction Software.

techniques eliminating the influence of atmospheric turbulence on the fringe position. The system can also be used in differential interferometry mode in order to estimate the phase difference between two spectral channels. Handling dispersed data and three-beam combination will be among the new methods to be installed for the VLTI pipelines.

The data rate for the first VLTI instrument VINCI is less than 1 gigabyte per night. The data rates will be higher for AMBER (0.7 MB/s) and MIDI (2.3 MB/s). For MIDI this translates into more than 40 gigabytes of data per night. The handling of such data volumes brings the current system to its limits, in terms of overall throughput. For example, the DVD production is limited by the media capacity and writing speed. For this reason a new archive technology, based on magnetic disks rather than DVDs, is being evaluated and seems quite promising (Wicenec et al., 2001). The science VLTI instruments like MIDI will set very high requirements in terms of pipeline computation speed. Presently the VINCI pipeline can process data at about the same rate as they are acquired. MIDI will require two orders of magnitude in computation speed to perform this real-time data acquisition and processing. Solutions are being investigated using large VINCI data sets and MIDI simulated data.

Off-Line Processing and Analysis

For the scientific analysis of data, different interactive tools are provided on the off-line workstation, based on commercial data-analysis packages. The data can be browsed and organised by Observation Blocks with the Gasgano tool, which provides means of organising large amounts of data, classify them, view headers and call scripts on selected files. Gasgano can be used as a front-end graphical interface to the data reduction software.

Commands are provided to perform a second stage of calibration on the pipeline results. First the data are glued together and grouped by instrument modes. The calibration information can be tuned and the instrument transfer function is evaluated on the calibrator and interpolated with time. Finally it is possible to apply the calibration to science data and to model the intensity distribution of the source.

Conclusion

In the first phase of system commissioning, most of the calibration and analysis aims at characterising the performance of the interferometer, using two siderostats of 40 cm diameter separated by 16 m. For these tests, the pipeline provides photometry-corrected interferograms, uncalibrated visibilities, and the QC parameters which are instrumental to the assessment of the system performance. After this first stage of processing, data are transferred from the off-line work-station to the dedicated environments used for the performance analysis of each independent subsystem of the VLTI. The prototype tools for observation preparation can be tested for their usability in real conditions of observation.

In particular the interferometer transfer function, environmental parameters such as the atmospheric piston noise or the level of tunnel internal seeing, optomechanical performance and sensitivity of the delay lines are being analysed. A number of stars have been measured and a major criterion for stability could be verified: the equivalent point source contrast, i.e. the interferometer transfer function, was measured to be 0.87 with stability of about 1% over three days. This is far better than the required 5% over five hours. Other commissioning tests aim at verifying that fringes are found on any bright star in the specified field of view (60 degrees of zenith) or that low visibilities (down to 5%) can be measured.

After achieving the first fringes from the interferometer using the Unit Telescopes, the system is now used more intensively for the verification of the science performance of the system. More targets are observed and the pipeline is used to perform a preliminary calibration of the visibilities.

Acknowledgements

Many thanks to Bill Cotton from the National Radio Astronomy Observatory and Walter Jaffe from Leiden Observatory for important contributions to the data-reduction package, to Gilles Duvert from Grenoble Observatory for helping with the VLTI visibility calculator using ASPRO.

References

Ballester, P., Chavan, A.M., Cotton, B., Coudé du Foresto, V., Glindemann, A., Guirao, C., Jaffe, W., Kervella, P., Longinotti, A., Percheron, I., Peron, M., Phan Duc, T., Pirenne, B., Quinn, P.J., Richichi, A., Schöller, M. , Wicenec, A., Wilhelm, R., Wittkowski, M., Zampieri, M., Data Flow System for the VLT Interferometer, *SPIE* Vol. **4477**, Paper No. 31, 2001.

Ballester, P., Modigliani, A., Boitquin, O., Cristiani, S., Hanuschik, R., Kaufer, A., Wolf, S., The UVES Data Reduction Pipeline, *The Messenger* No. **101**, p. 31, Sept. 2000.

Coudé du Foresto, V., Ridgway, S., Mariotti, J.M., Deriving object visibilities from interferograms obtained with a Fibre stellar interferometer, *A&A Suppl*. Vol. **121**, pages 379–392, 1997.

Duvert, G., Berio, P., ASPRO: A Software to PRepare Optical interferometry observations, SF2A-2001: *Semaine de l'Astrophysique Française*, in press.

Glindemann, A., et al., Light at the end of the tunnel – First fringes with the VLTI, *The Messenger* No. **104**, p. 2, June 2001.

Kervella, P., Coudé du Foresto, V., Glindemann, A., Hofmann, R., The VLT INterferometer Commissioning Instrument, in Interferometry in Optical Astronomy, *SPIE* Vol. **4006**, 2000.

Wicenec, A., Knudstrup, J., Johnston, S., 2001, ESO's Next Generation Archive System, *The Messenger* No. **106**, p. 11. Dec. 2001.

Volume Phase Holographic Gratings Made in Europe

S. HABRAKEN[1], P.-A. BLANCHE[1], P. LEMAIRE[1], N. LEGROS[1], H. DEKKER[2] and G. MONNET[2]

[1]Centre Spatial de Liège, Angleur (Belgium). Contact: shabraken@ulg.ac.be
[2]European Southern Observatory (Germany). Contact: hdekker@eso.org

This article is a shortened, combined and updated version of papers given at the August 2001 SPIE conference on Gratings in Astronomy (Monnet et al., 2001 and Habraken et al., 2001).

1. Grisms at ESO

The mission of the ESO Instrumentation Division is to provide our user community with state-of-the-art, operationally and optically efficient, versatile and stable instruments. Grisms have proven to be devices with which our mission can be carried out exceedingly well.

A grism is a surface-relief transmission grating that is applied to the hypotenuse face of a prism. The angle of the prism is chosen in such a way that the central wavelength of the first order spectrum is passed without deviation. Grisms with groove densities of up to 600 g/mm have an optical efficiency in the visible that is comparable to, or slightly better than, that of ruled gratings. Contrary to gratings, their zero deviation wavelength is nearly invariant with respect to slight orientation errors that may be caused by the insertion mechanism

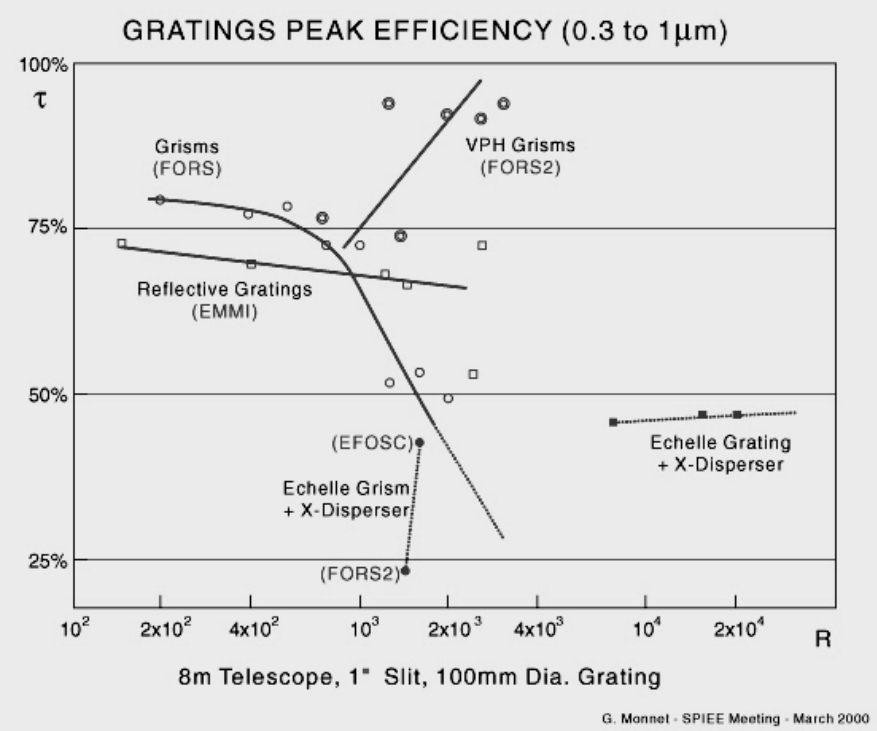

Figure 1: Peak efficiency τ of ESO gratings as a function of spectral resolution R for an 8-m telescope, 1″ slit and a 100 mm grating. The superior efficiency of VPHGs at R ~ 2000–3000 is evident.

or by flexure. Important technical advantages are also that the mechanics are simple, straight-forward and that grisms can be put quite close to the camera entrance which helps to reduce lens dimensions, vignetting and absorption.

ESO has been one of the first observatories to realise the advantages of grisms in combination with Focal Reducer systems and CCD detectors. In the EFOSC (ESO Faint Object Spectrograph and Camera) instrument that was developed for the 3.6-m telescope (Enard and Delabre 1983), focal reducer optics reimage the telescope focal plane to the CCD with the demagnification required to match the pixel size to the seeing disk. By inserting a grism in the parallel beam between the collimator and the camera, (and a corresponding slit in the telescope focal plane) the instrument is converted from an imager-photometer into a spectrograph. This allowed our users to image a field and study the distribution and morphology of faint objects, to do photometry and then to take low-resolution spectra of individual or multi-objects with the same instrument and in some cases even in the same night. In EMMI (ESO Multi-Mode Instrument, Dekker et al. 1986), an instrument for the ESO New Technology Telescope which is in many ways a precursor of the VLT, the same principles were applied. Instruments of the FOSC and MMI family that employ these optical and operational concepts are now in use at many observatories.

Of the 11 instruments, in various states of construction or operation, that were included in the set of first-generation VLT instruments, four Spectro-Imagers, FORS1 and 2, VIMOS and NIRMOS – covering the spectral range 360–1650 nm – are Focal Reducers using grisms. The total projected number of grisms in these instruments is about 50, with sizes matched to beam diameters between 90 and 160 mm.

The initial set of dispersers for these instruments was based on conventional grisms. For the modest spectral resolutions sought at the time (at most R ~ 1,000 for a one-arcsecond slit) they perform well with over 80% peak transmission and have relatively flat efficiency curves with wavelength. In the last years, however, the need for 2–3 times higher spectral resolutions became prominent. One reason is scientific, viz. the strong desire to study very high redshift galaxies, presumably of relatively modest masses since they belong to a prior epoch before small galaxies coalesced to form the giant ellipticals of today. The second one is more technical: roughly in the 630 to 1,650 nm spectral range, strong emission lines dominate the night sky background emission. Higher R ~ 2,000–3,000 permit to detect spectra of very faint objects between these lines, which would have been swamped at smaller resolutions. Attempts to fill that niche with classical grisms have been unsuccessful, with peak transmissions at 50% or lower, a large enough loss to make our instruments non-competitive compared to systems based on reflective gratings which can easily reach such resolutions with good efficiency. This had led ESO to investigate Volume Phase Holographic Gratings (VPHGs).

2. VPHGs – the Present

VPHGs imprint phase differences on the wavefront not by a surface relief, but by locally modulating the refractive index of a thin layer of a medium like Dichromated Gelatin (DCG). This material has for a long time been used for such diverse applications as head-up displays in military aircraft, optical beamsplitters, spectrally selective reflectors for solar concentrators and architectural applications (Stojanoff et al. 1997). Only recently has the

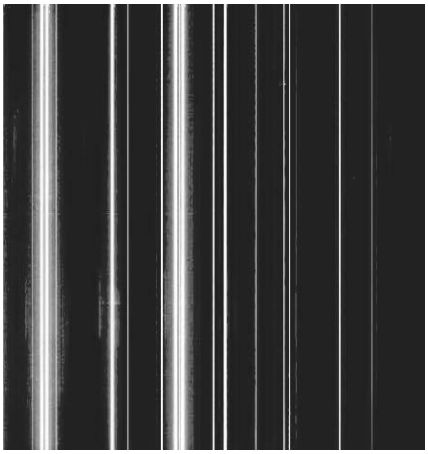

Figure 2: FORS2 He-Ne calibration spectrum with VPHG # 1028z (1028 l/mm blazed at 850 nm).

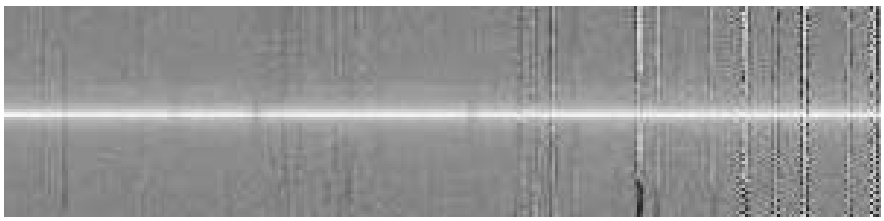

Figure 3: Spectrum of the dwarf galaxy FS27 (courtesy W. Zeilinger, Institut für Astronomie der Universität Wien). Same grism, 0.5 hr integration, resolution 78 km s^{-1}. The Ca II absorption triplet near 850 nm is clearly resolved.

technology been applied to produce dispersing elements for astronomy (Barden et al. 1998 and 2000). VPHGs are recorded holographically by interference of laser beams; subsequent processing in water and alcohol baths and baking results in a layer of the material with the desired index modulation. Because DCG is a hygroscopic organic material, the developed VPHG must be protected by a cemented cover plate.

VPHGs with an index modulation and layer thickness that is well tuned to the desired operating wavelength in first order can have peak efficiencies in excess of 90% at blaze. The blaze peak however is narrower than with surface relief gratings. This effect is less pronounced with larger index modulation and correspondingly thinner DCG. VPHG efficiency does not decrease with increasing line density as is the case with classical grisms; hence they are well suited to be used in existing straight-through focal reducer spectrographs to extend the range of spectral resolutions that can be accessed with good efficiency. (Fig. 1). Fortunately, VPHG/prism combinations also share the rotation invariance property of classical surface relief grisms.

Since 1999, five 92 mm × 92 mm VPHGs from Kaiser Optical Science Incorporated (KOSI) have been mounted and put in operation on the FORS2 at the VLT. Peak efficiencies are ~ 88% as shown in the FORS User Manual (Szeifert and Boenhardt, 2001) and together they cover the 500 to 1,000 nm range, with one arc second slit resolution between 1,000 and 2,700. Image quality is excellent (Fig. 2). Figure 3 shows an early result on a dwarf elliptical galaxy. User acceptance is excellent as shown by the healthy usage statistics since our first offering in October 2000 (Fig. 4).

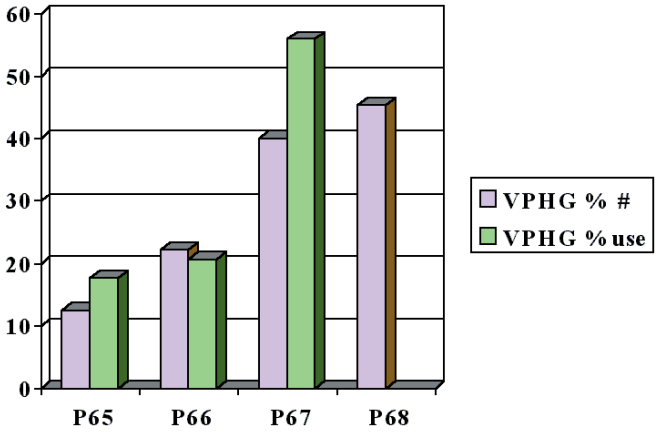

Figure 4: FORS2 VPHG usage statistics during semester allocations from P65 (start April 2000) to P67 (start April 2001 and up to 13 July 2001). Left bars: VPHG - % of all FORS2 grisms. Right bars: VPHG - % of total FORS2 spectrographic observations. From 1 October 1999 to 13 July 2001, total spectroscopic shutter open time at FORS2 was 283 hours.

3. VPHGs – ESO's Future Needs

ESO's current need is to get VPHGs substantially larger than the present 92 mm × 92 mm KOSI limit.

The VIMOS instrument, a 4-channel Visible spectro-imager, essentially to be used for massive redshift surveys of distant galaxies, has five different resolution/central wavelength settings and so it has twenty 150 mm × 150 mm grisms on-board. Twelve of these have bean earmarked for possible replacement by VPHGs.

Looking somewhat further ahead, we see the NIRMOS instrument, a near-infrared clone of VIMOS, which incorporates a –32 ºC cooled optical box to increase efficiency in the H band, above 1550 nm. Higher resolution grisms are mandatory since in the whole wavelength range (1000 to 1650 nm) of the instrument the background is fully dominated by intense night-sky lines (Fig. 5). Cryogenic tests on various VPHGs (KOSI, RALCON, CSL) are being started by Golem-Merate.

On a still longer time scale, in the framework of upgrading the FORS1 instrument in the near-UV (320 to 400 nm), a high-line density, UV-efficient VPHG would be required for the study of tomographic maps of the Inter-Galactic Medium from R ~ 3,000 absorption-line spectroscopy of faint background quasars. The development of such a grating will be studied with CSL.

Finally, for the 2nd-generation VLT instruments, to be developed and deployed in the next 5–10 years, we may well base one or more instruments on the articulated or butterfly spectrograph concept (Bernstein et al. 2001). This approach would be especially useful for a long-slit (possibly fed by an integral field image slicer) spectrograph for the study of the dynamics and abundances of the gaseous and stellar components of external galaxies, with typically R ~ 7,000–10,000.

To satisfy these needs that exist at ESO as well as within the astronomical community at large, the EGUNA Consortium (ESO, Golem-Merate, University of Michigan, NOAO, AAO) has been set up. The short-term aim is to fund best-effort production of a batch of 10 large VPHGs – including 4 for ESO, 2 for Golem-Merate, 2 for the University of Michigan – at a new facility in the vicinity of the Centre Spatial de Liège (CSL) with significant financial help of the local Walloon government. This phase will end by mid-2002. The near-term goal is the creation of a commercially viable spin-off company.

4. The CSL and its Spin-off Activities

The *Centre Spatial de Liège* (CSL) is a group of 100 persons within the University of Liège. Its R&D activities are directed towards space instrumentation, optical metrology and testing (performance evaluation of the optical payloads). To create favourable conditions for the emergence of technological innovations and commercial activities, the Walloon public authorities have set up two resources, as shown in Figure 6.

Some of the CSL projects – mainly space research based – are emerging with high economic potential. A spin-off company incubator, WALLONIA SPACE LOGISTICS (WSL), was created close to the University by the Walloon Economy Ministry. WSL studies each project resulting from space research, and decides whether or

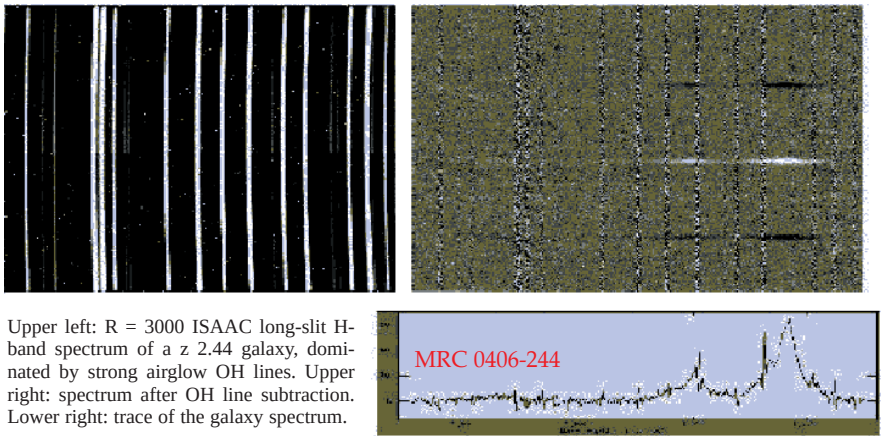

Upper left: R = 3000 ISAAC long-slit H-band spectrum of a z 2.44 galaxy, dominated by strong airglow OH lines. Upper right: spectrum after OH line subtraction. Lower right: trace of the galaxy spectrum.

Figure 5: Demonstrating the need for higher resolution in the NIR

Figure 6: Diagram of resources available at the CSL research centre to spin-off companies

not to support commercialisation, i.e. the creation of a spin-off company. During the incubator phase, the WSL supports and finances the basic needs of the baby spin-off (management, accounting, secretarial support and equipment).

5. CSL Background in Holography

CSL and the University of Liège have been involved in holography R&D programmes for 20 years. Interferometry, recording materials, and optical elements have been extensively studied. Dichromated Gelatin (DCG) is recognised world-wide as the holographic material with the highest diffraction efficiency thanks to its capability to record the highest refractive index modulation. The authors started to investigate that material in 1990 (Habraken et al. 1991) in the field of holographic optical elements. Very efficient reflection and transmission holographic gratings were recorded (Habraken et al. 1995 (1)).

Work was also conducted in the field of surface-relief gratings by recording on a photoresist material (Habraken et al. 1995 (2)). Polariser gratings (Habraken et al. 1995 (1–3)) and master gratings for embossed holography are realised in small size.

The theoretical background of CSL includes the implementation of the Rigorous Coupled-Wave Analysis (RCWA, Gaylord et al. 1983) code since 1994. This powerful tool is very flexible to model the performance of specific gratings.

This background experience of CSL was seen as a realistic starting point for a commercial activity in diffraction gratings. For that reason, the Walloon Research Ministry decided to fund this project. Our major threshold toward the market of Volume Phase Holographic Gratings (VPHG) was certainly the size and the quality criterion that is required.

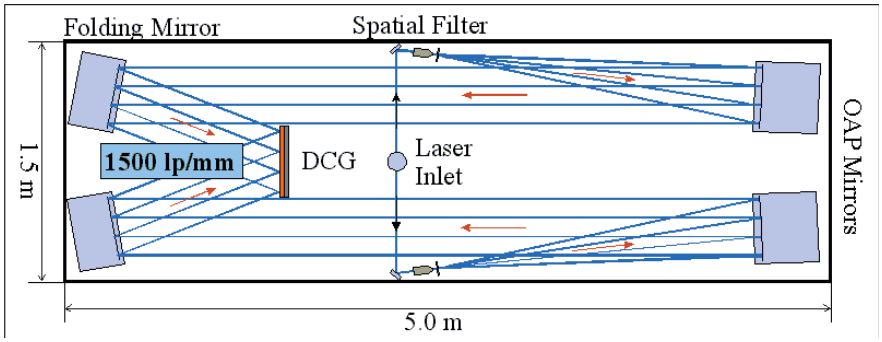

Figure 7: Simplified view of the holographic recording set-up. The laser is mounted below the optical bench.

6. New VPHG Facility: Funding and Construction

Following initial discussions with the five members of the EGUNA consortium, CSL decided to investigate the production of (at least) 30 cm diameter VPH gratings. Total funding amounts to 642 kEuro of which 81% is contributed by the Walloon Government and 19% by the consortium. The definition and procurement activities started in November 2000.

A new DCG coating facility has been subcontracted, built and delivered that can apply DCG layers with thickness values ranging from 5 to 25 μm with high uniformity (local deviation lower than 1 μm PV) over the 40 × 40 cm area.

The holographic recording of plane gratings requires a set-up with two interfering collimated laser beams. Recording is performed on a 1.5 m × 5 m optical bench, using an argon laser delivering 4.8 watts (single line at 488 nm TEM 00). The set-up geometry is shown in Figure 7. Two off-axis parabolic mirrors (38 cm diameter) collimate the beams. To adjust the illumination angle, two flat mirrors fold the beams. Thus, the fringe frequency can be changed continuously from 300 l/mm up to 3000 l/mm. Higher frequency could be recorded with a minor change in the optical set-up.

Laboratory facilities for gelatin development have been set up with large regulated baths and a forced convection oven to dry the final grating before encapsulation.

These three laboratories, i.e. coating, exposure, and development, together cover 100 m^2. They are equipped with air conditioning which regulates temperature, hygrometry and cleanliness up to class 10,000. Laminar flow benches provide local filtering up to class 100 in sensitive areas, utilising the technical know-how of CSL in space optical payload qualification. The hardware deliveries were almost completed by October 2001.

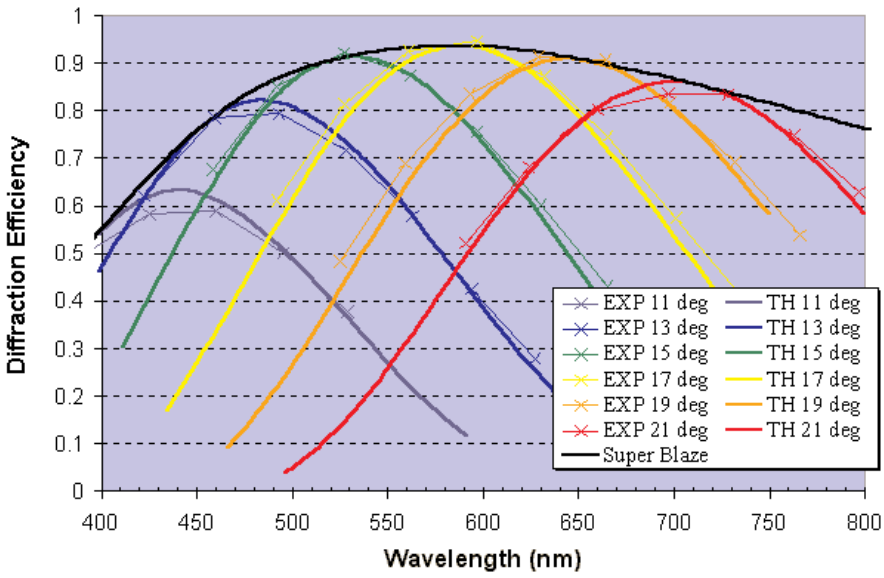

Figure 8: First-order unpolarised intrinsic diffraction efficiency of a 1000 l/mm VPHG sample manufactured at CSL. By tilting a VPHG, the efficiency at a given wavelength can be optimised; the resulting envelope is called the Super Blaze.
Measurements were made at Golem-Brera, assuming 8% surface losses. Actual losses are higher by 3–5%, so peak efficiency will approach 98 %. Theoretical fits based on RCWA assuming grating thickness = 9 µm and Δn = 0.0325.

7. Sample Grating Performance

The initial survey among the members of the Consortium indicated that the CSL should address a wavelength range of 400–1500 nm and a line frequency of 300–3000 l/mm or even more. High efficiency over a wide spectral range is required. With volume phase gratings, this requires a thin layer with the highest possible refractive index modulation.

In parallel to hardware definition and procurement, tests have been performed on small samples to tune the process of recording and development of DCG. Preliminary results are presented below that show potential for further improvement.

DCG offers numerous degrees of freedom. The major parameters are related to the chemical composition, the exposure energy, and the development process. The gelatin thickness must be adapted to the useful wavelength. The easiest theoretical understanding is given by the following relation (Kogelnik 1969):

$$\eta = \mathrm{Sin}^2 \frac{\pi \Delta n d}{\lambda \mathrm{Cos}\theta}$$

where

η is the diffraction efficiency (1st-order TE-polarisation),
λ is the central wavelength in air,
θ is the internal angle of incidence,
Δn is the index modulation,
d is the grating thickness.

From visible to IR wavelengths, the product $\Delta n.d$ must be as high as possible to maximise the diffraction efficiency over a wide wavelength range. When the process optimisation reaches its limits, the only way to increase $\Delta n.d$ is to increase the grating thickness. For that reason, our optimisation phase addressed a variety of thickness. Until now, CSL has reached promising values:

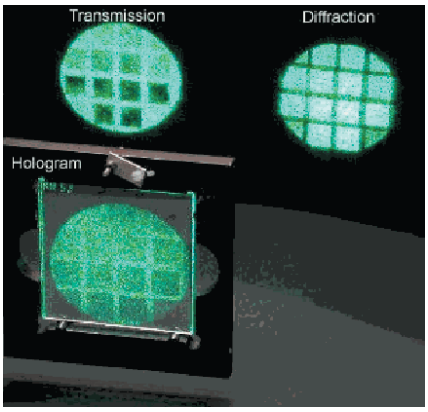

Figure 9: Picture showing the vanishing of the zero-order in VPH grating samples at 514.5 nm.

	Index modulation Δn	
Film Thickness	Measured	Target (2002)
15 μm	0.030	>0.035
10 μm	0.035	>0.040
7 μm	0.040	>0.045

With the above set of parameters, the range of possible blaze wavelengths is 570 nm (and below) to 950 nm. Production of VPHG blazed up to 1500 nm is possible, but would have to be validated on thicker layers.

Accurate spectral measurements have been performed by Golem at Brera Observatory. Figure 8 presents the performance of a 1000 l/mm grating. The physical gelatin thickness is 10.5 μm but the theoretical fitting of the super blaze is consistent with a grating thickness after development of 9 μm and an index modulation of 0.0325[1].

These results demonstrate the progress made by CSL to convince the scientific community, represented by the EGUNA consortium, of our capabilities. Very high diffraction efficiency has been reached even in the near IR.

Figure 9 is a picture of several small gratings diffracting the Ar laser beam (514.5 nm). The high efficiency is evident when the zero-order transmitted beam is vanishing: all the incident energy is transferred to the 1st-order diffracted beam.

8. Next Phases and Schedule

Following these encouraging results, CSL will continue to enhance the DCG process with regard to the index modulation, the diffraction efficiency uniformity and the scatter level on small samples.

The progress should allow us to start the recording of large VPH gratings for the EGUNA Consortium in January 2002. CSL is committed to produce and deliver 10 gratings to the EGUNA consortium by the end of June 2002.

The success of the project and the interest from the astronomical community will be the basis for a decision to set up a spin-off company with the help of WSL in 2002, directly after the delivery of the 10 gratings. The main product of that spin-off will be large-scale VPH gratings but further applications are expected (holographic optical elements, ion-etched surface-relief gratings, etc.) CSL will keep a very close contact with the spin-off company to ensure success; hardware and human resources shall be shared, at least during the first years.

[1]Fitting based on individual spectral measurements indicates a grating thickness of 8.5 μm with $\Delta n = 0.0345$.

Inquiries for future new deliveries should be directed to shabraken@ulg.ac.be

9. Conclusions and Summary

For upgrading of existing ESO instruments, as well as for 2nd-generation VLT instruments, VPH gratings offer significant advantages over conventional grisms and reflection gratings in terms of efficiency and spectral resolution.

The infrastructure necessary to achieve a high quality level in large VPHG manufacturing has been implemented at CSL; process tuning and optimisation shows promising results.

With the demonstration of good performance in VPH grating sizes up to 30 cm diameter, CSL expects to quickly generate a commercial interest.

After the present R&D phase that will end mid-2002, the technological knowledge will be transferred to a new commercial company with core business in the field of holographic optical elements, including gratings.

10. Acknowledgements

The work at CSL is supported by the Walloon Government under the contract RW no. 14559 and by the EGUNA consortium under the ESO contract 63104. The measurements presented in Figure 8 have been performed at Golem-Brera. Special thanks to E. Molinari.

References

Barden S. C., Arns J. A. and Colburn W. S. 1998, Proc. *SPIE* **3355**, 866.
Barden S. C., Arns J. A., Colburn W. S. and Williams J. B. 2000, *PASP* **112**, 809.
Bernstein G. M. et al. 2001, Proc. SPIE 4485, in print. Preprint at: http://www.astro.lsa.umich.edu/users/garyb/PUBLICATIONS/SPIE01/spie.pdf
Dekker H., Delabre B. and D'odorico S. 1986, Proc. *SPIE* **627**, 339.
Enard D. and Delabre B. 1983, Proc. *SPIE* **445**, 552.
Gaylord T.K. and Moharam M.G. 1983, *J. Opt. Soc. Am*., **73**, 1105.
Habraken S. and Roose S. 1991, in HOLO 3 meeting, St Louis France.
Habraken S., Renotte Y., et al. 1995 (1), *Applied Optics* **34**, 3595.
Habraken S., Michaux O., et al. 1995 (2), *Optics Letters* **20**, 2348.
Habraken S., Renotte Y., et al. 1995 (3), Proc. SPIE 2532, 141.
Habraken S. et al. 2001, Proc. *SPIE* **4485**, in print.
Kogelnik H. 1969, *Bell Syst. Techn. J*., **48**, 2909.
Monnet G. , Dekker H. and Rupprecht G. 2001, Proc. *SPIE* **4485**, in print.
Stojanoff C.G., et al. 1997, Proc. *SPIE* **3010**, 156.
Szeifert T. and Boehnhardt H. (eds.) 2001, FORS1+2 Online User Manual, 53. http://www.eso.org/instruments/fors1/userman/index.html

ESO's Next Generation Archive System

A. WICENEC, J. KNUDSTRUP, S. JOHNSTON

Abstract

Early in July 2001 ESO/DMD installed prototype versions of the archiving and buffering units of the Next Generation Archive System (NGAS) at the 2.2-m telescope in La Silla. The two units are the on-site part of an archive system we are currently testing for high data rate/ high data volume instruments like the Wide Field Imager which is mounted at the 2.2-m telescope. The NGAS concept is built around two ideas: the use of cheap magnetic ATA-100 disks as the archiving media and a highly flexible and modular software called NG/AMS, NG Archive Management System. The main goals of the whole system are scalability in terms of data volume, but also the ability to support bulk data processing either by fast data retrieval or by opening the computing power of the archive for data-reduction close to the data themselves. In fact the NGAS scales in such a way that it is possible to process all the data in the archive within an almost *constant* time. In this article we present an overview of the NGAS concept, the NGAS prototype implementation and some of the experience we have made during the first month of operating the system in a real observational environment. We also present the infrastructure of the main archive which supports scalable, decentralised processing, both of which are essential for large-scale scientific programmes submitted to a Virtual Observatory.

Figure 1.

1. Introduction

With the advent of wide-field mosaicing CCD cameras, the data rate of several observatories around the world is literally exploding. While some of these instruments are already in use (e.g. WFI@2p2; CFHT 12k; SLOAN) other, even bigger ones, are under construction or planned (Omegacam, Megacam, VISTA). The current archive system at ESO consists of DVDRs which are written in two copies at the observatory sites. One of the copies is sent to the ESO headquarters in Garching to be inserted into a DVD jukebox. In this way the data are quasi on-line in a juke-box about 10 days (mean) after the observations have been carried out. Given the current set-up of the system, it is possible to archive up to about 15 to 20 GB per night. The data rate coming from the ESO Wide Field Imager (WFI@2p2) easily hits this limit in a typical night and is a lot higher for exceptional programmes (up to 55 GB/night). The expected data rates of Omegacam and VISTA are 4 times and 8 times higher than the one from WFI@2p2, respectively. In order to be able to cope with such data rates, ESO initiated a project (Next Generation Archive System Technologies, NGAST) to come up with alternative archive solutions.

Figure 2: This figure shows three of the NGAS units mounted in a rack. They are fully equipped with eight disks each, giving a total of 1.65 terabyte of on-line storage capacity with three processors running at 1.2 GHz each.

2. Requirements

A new archiving system must resemble the current costs and operational scheme as closely as possible. For the costs it is clear that one has to account for the pure hardware costs, the operational costs and the maintenance costs. The hardware includes the costs for the consumable media, readers, writers (if any) and computers. Apart from scalability in terms of data volume and throughput at the observatory, a Next Generation Archive System has to fulfil a number of basic additional requirements in order to be able to cope with future challenges:

- Homogeneous front-end (archiving at observatory) and back-end (science archive) design
- Access to archive shall be scalable, i.e. the number of entries and volume of data shall not affect the access time to single data sets
- Support bulk data processing mainly for the quality control process, but having Virtual Observatory projects in mind
- Processing capabilities shall scale along with archived data volume, i.e. it should be possible to process all data contained in the archive
- Economic solution using commodity parts to reduce overall costs

The main goal of the first point is to limit maintenance costs, operational overheads and the time-to-archive. Time-to-archive is the total time the complete system needs until data is on-line and retrievable (disregarding access restrictions) from the science archive. The support for bulk data processing is mainly driven by the fact that ESO is already now processing about 50% to 75% of all data, in order to ensure the data quality for service mode programmes, monitor the telescope/instrument parameters and provide master calibrations frames for the calibration data base. With the very high data rate instruments the demands for processing and storage capabilities for quality control will grow tremendously.

3. ESO's Prototype Solution

For the implementation of the prototype units we chose a particular hard-

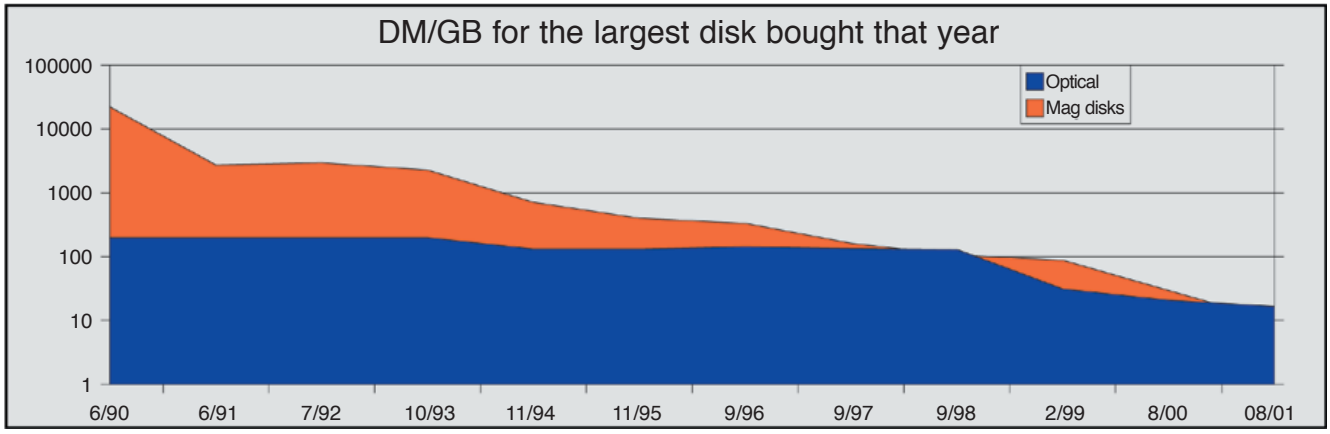

Figure 3: This graph shows the price per gigabyte for the biggest disk bought by ESO during the year indicated on the x-axis. Most of the disks are SCSI disks; only during the last two years also IDE disks have been included in the graph.

ware and software configuration and made some implementation decisions.

3.1 Hardware configuration

The main hardware implementation decisions include the following points:

- Magnetic disks with ATA-100 interface in JBOD configuration
- Standard PC components, like mainboard and network card
- 19 inch rack-mount case with redundant power supply and 8 slots to host the data disks
- Removable hard disk trays (hot-swappable)
- Eight port SCSI to ATA-66 PCI card (3ware Escalade 6800)

3.2 Software configuration

The main software implementation decisions include the following points:

- Linux as the operating system
- Next Generation Archive Management System (NG/AMS) server software written in Python
- Multi-threaded HTTP server implementation
- URL-based command interface to the NG/AMS server
- Plug-in architecture to provide methods for different data types and processing capabilities
- XML-based configuration and message passing

4. NGAS Archive Layout

Magnetic disks are consumables in NGAS and for every eight disks a PC will be added to host those disks and bring them on-line in the archive. Right now we have two operational central units (NCUs, NGAS Central Unit) in Garching with 12 completed disks mounted. Since each NCU is capable of hosting 8 disks, we have to add another NCU end of this year. Each of the NCUs is running a NG/AMS server and every eight NCUs together with a master unit (NMU, NGAS Master Unit) and a network switch will form a Beowulf cluster for processing and data management. In this way CPU power is scaled up together with the data, and processing of all the data in the archive for the first time becomes feasible. The time needed to process *all* the data in an NGAS archive can be kept almost constant as long as the data-to-CPU ration is kept constant. In fact, we are planning to control all the data holding in the NGAS archive permanently by performing CRC checks on a file-by-file level. The NG/AMS is prepared to support large-scale processing in the archive by distributing tasks to the nodes where the data resides. The same software with a slightly different configuration is used to control the archiving process at the telescope as well as the main archive at ESO headquarters in Germany. As soon as a new magnetic disk is formatted and registered in the NGAS data base the location and contents of it is always traceable. Archiving is done in quasi real-time and the data are immediately accessible through the standard archive interface. In principle it is possible to retrieve frames right after they have been observed, but for security and data permission reasons there is a very restricted, fire-wall protected access to the archiving units on the observatory sites. In addition to fire-wall security NG/AMS is configurable to either deny or grant permission to retrieve archived frames.

The ESO Science Archive Facility imposes some additional requirements for the back-end implementation of NGAS. These include seamless integration in the current archive query and request handling system. NGAS has to support fast retrieval of single files, lists of files and files belonging to a specific programme, to name a few retrieval scenarios. Moreover, retrieval of FITS headers only, production of previews and archiving of master calibration frames has to be supported by the main archive part of NGAS. The operational, maintenance, power consumption and physical volume aspects of an ever growing number of PCs have to be addressed as well.

5. Milestones and Performance

The front-end (archiving) system consisting of two NGAS units was installed at the 2.2-m telescope beginning of July 2001. Since then, this prototype installation is archiving data from the ESO Wide Field Imager (WFI). In short, the milestones and performance numbers of this non-optimised prototype look like the following:

- NGAS unit prototype installation on La Silla: July 3 to 13, 2001
- Start of operations on La Silla: July 7, 2001
- First terabyte of data controlled by NGAS: September 18, 2001
- Installation of first two NGAS units for the main archive (NCUs) in ESO HQ: September 25, 2001
- Commissioning and acceptance of front-end NGAS on La Silla: December 2001
- Commissioning and acceptance of back-end NGAS in ESO HQ: February 2002

The prototype front-end NGAS is not yet fully optimised for performance, but the time-to-archive was always shorter than the production time of frames by the instrument. The data flow from WFI between July and September 2001 was 13.7 GB/night (median) with a maximum of 53.8 GB in a single night. The overall throughput of the archiving process during the same period was 3.17 MB/second, including compression and replication of the files. The hardware used in the NGAS units provides very fast write access to all the eight data disks in parallel, summing up to about 100 MB/second (measured), thus there is plenty of room for improvement of the overall system performance.

6. Overall Costs

The overall hardware costs of the NGAS have been carefully calculated.

Media	DM/GB in Juke Box	Number of Media/Terabyte
CD-R	70.3	1625.4
DVD-R (3.95 GB)	16.0	276.8
DVD-R(4.7 GB)	11.6	227.6
DVD-RAM (2 × 4.7 GB)	10.8	113.8
MO	36.8	204.8
SCSI disk farm	8.8	5.7
Sony 12″ Optical Disk	215.7	160.0
RAIDZone NAS	17.7	14.2
NGAS	8.7	14.3

Table 1: Comparison between different media in terms of price/GB of storage and number of media/Terabyte. The SCSI price is remarkably low, because of one of the new 180 GB disks we bought recently under exceptionally good conditions. This kind of comparison is one of the planning tools for the medium term planning of archive media.

Compared to other on-line or quasi on-line random-access data-storage solutions it is the cheapest solution, providing at the same time very low operational costs and very few storage media. Moreover, it is the only solution providing enough computing power to process all archived data with no additional costs. Especially the operational overhead in terms of manual operation drops quite dramatically in the case of the ESO WFI, from about 2 hours/day with the currently used tape procedure to 20 minutes/week. The time-to-archive is also substantially lower (of the order of seconds), because even compared with the DVD system used for the VLT, the data are only on-line when they arrive at ESO HQ about 10 days after the observations; with the tapes the delay is much longer. For very high data volume instruments the number of media/Terabyte becomes a critical parameter, for the production, management and handling.

7. Future of NGAS

NGAS has proven to be a reliable and fast system. Since NGAS is an operational model on top of a hardware/software system, quite different from the one currently used, an implementation for other ESO telescopes/instruments will still take some time. While the prototype system on La Silla will go operational end of this year, other installations on La Silla and Paranal are not required, because the DVD system is able to deal with the data rate of the currently installed instruments. We are planning to use NGAS first for very high data rate instruments like Omegacam which will be operated on the VLT Survey Telescope beginning in 2003. MIDI (VLTI) is another candidate for a NGAS installation. NGAS will certainly be evaluated as one of the building blocks of the Astrophysical Virtual Observatory in the area of scalable archive technologies and it also is already evaluated in the framework of the ALMA archive.

References and Acknowledgements

Most up-to-date information can be found under http://archive.eso.org/NGAST

ESO Wide Field Imager: http://www.ls.eso.org/lasilla/Telescope/2p2T/E2p2M/WFI

AVO: http://www.eso.org/projects/avo

ALMA: http://www.eso.org/projects/alma

We would like to thank especially the 2.2-m telescope team, the La Silla Archive team and Flavio Gutierrez for their on-going support.

News from the 2p2 Team

Personnel Movements

In September we welcomed new team member Linda Schmidtobreick from Germany. Linda is a new ESO Fellow and will be working primarily with the 2.2-m. Before joining ESO, Linda held a two-year postdoctoral position at Padova, Italy. Her research interests include stellar populations, cataclysmic variables and the structure of our Galaxy.

September also saw us farewell Heath Jones from his La Silla duties. Heath will complete the 3rd year of his ESO fellowship at Cerro Calan.

WFI Images

As a Christmas present from the 2p2 team, we have included here colour images of the Dumbbell and Triffid planetary nebulae. These were created from only one of the chips of the Wide Field mosaic by team member Emmanuel Galliano. The separate B, V and R images used to make the pictures were taken under average seeing conditions on June 11/12, 2001.

Figure 1: The Dumbbell nebula from 10 minutes B, V and R images.

Figure 2: The Triffid nebula from 1-minute B, V and R images.

Chilean Astronomy is enjoying a rapid development due to increased funding and access to large telescopes.

Several current projects at different institutes in Chile will be presented in forthcoming issues of The Messenger. The following article is the first in the series.

A panorama of Chilean Astronomy will be presented in the next issue by Professor Leonardo Bronfman, President of the recently founded Sociedad Chilena de Astronomía.

Research in Concepción on Globular Cluster Systems and Galaxy Formation, and the Extragalactic Distance Scale

W. GIEREN, D. GEISLER, T. RICHTLER, G. PIETRZYNSKI, B. DIRSCH,
Universidad de Concepción, Departamento de Física, Grupo de Astronomía, Concepción, Chile

1. Introduction

The Astronomy Group at the Universidad de Concepción is one of the youngest astronomical research groups in Chile. It was formed only six years ago and has grown steadily since. Currently, members of the Astronomy Group include four staff and four postdoctoral fellows. About a year ago, the Physics Department created a PhD programme, with astrophysics being one of the strongest groups in this programme. We are currently educating our first PhD students. Next year our Department will initiate an undergraduate degree programme in astrophysics. We expect that our staff and science activities, as well as the number of undergraduate and PhD students in astrophysics at the Universidad de Concepción, will be boosted in coming years by the recent creation of a FONDAP Institute which is shared by the three major Chilean Astronomy Groups, at the Universidad de Chile, Universidad Católica (both in Santiago), and at Concepción.

Two of our major current research areas deal with the distance scale and with globular clusters. About a year ago, CONICYT (the national science funding agency) approved financing of a 5-year research project for our group which seeks to increase the scientific interaction and scope, and strengthen the links between these areas. It is the purpose of this article to give the reader an impression of what we have been doing so far, and what our scientific goals are for the near future.

2. Research toward Improvements in the Distance Scale

Cepheid variables are generally considered as the best-understood and best-calibrated primary standard candles, and as such they have been widely used to determine distances to galaxies in reach of the Cepheid method (out to about 20 Mpc, at HST resolution). There are, however, still a number of important systematic uncertainties affecting both Cepheid variables and other secondary methods of distance measurement which have so far prevented a truly accurate calibration of the extragalactic distance scale. The astrophysical consequences of such a limitation include a larger uncertainty on the Hubble constant than we would hope for, after almost a century of hard work on this exciting and fundamental problem. The currently weakest link in the whole process of setting up the distance scale is our limited capability to measure truly accurate distances to nearby galaxies which provide the zero point calibration for the extragalactic distance scale. Our difficulties in determining absolute distances to nearby galaxies are best reflected by the current dispersion of the distance values derived for the LMC, the nearest (excluding Sgr) and best-observed galaxy. According to Gibson (2000), current values for the LMC distance modulus obtained with Cepheids, and a variety of other techniques, range between 18.2 and 18.8, corresponding to an embarrassing 30 per cent difference in distance between the extreme values. It is therefore mandatory to investigate, in much more detail, the true capabilities and systematics of the various techniques used to measure the distances to nearby galaxies. Only when these are fully understood, the techniques properly calibrated, with their dependence on environmental properties of the host galaxies (metallicity, age of stellar populations) taken into account, and agreement on the distances of a number of galaxies with a range of environmental properties has been achieved from the various methods, can we trust that the calibration of the local distance scale has finally been achieved with the required accuracy of a few per cent. In this process, we will also learn to distinguish the most accurate standard candles (those with the smallest intrinsic dispersions for distance measurement) from those less useful for distance de-

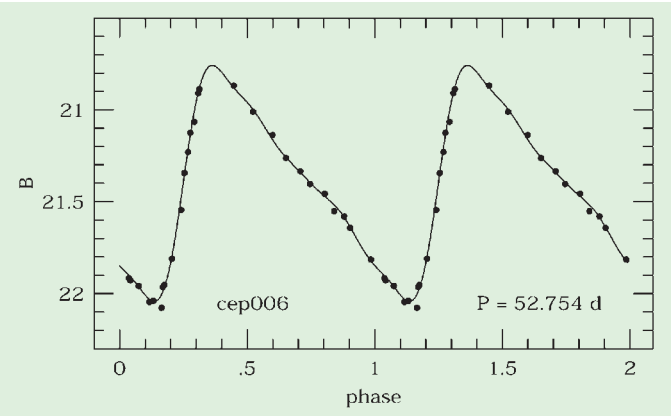

Figure 1: B light-curve of a typical Cepheid in NGC 300. The data were obtained with the ESO-MPA 2.2-m telescope and Wide Field Imager.

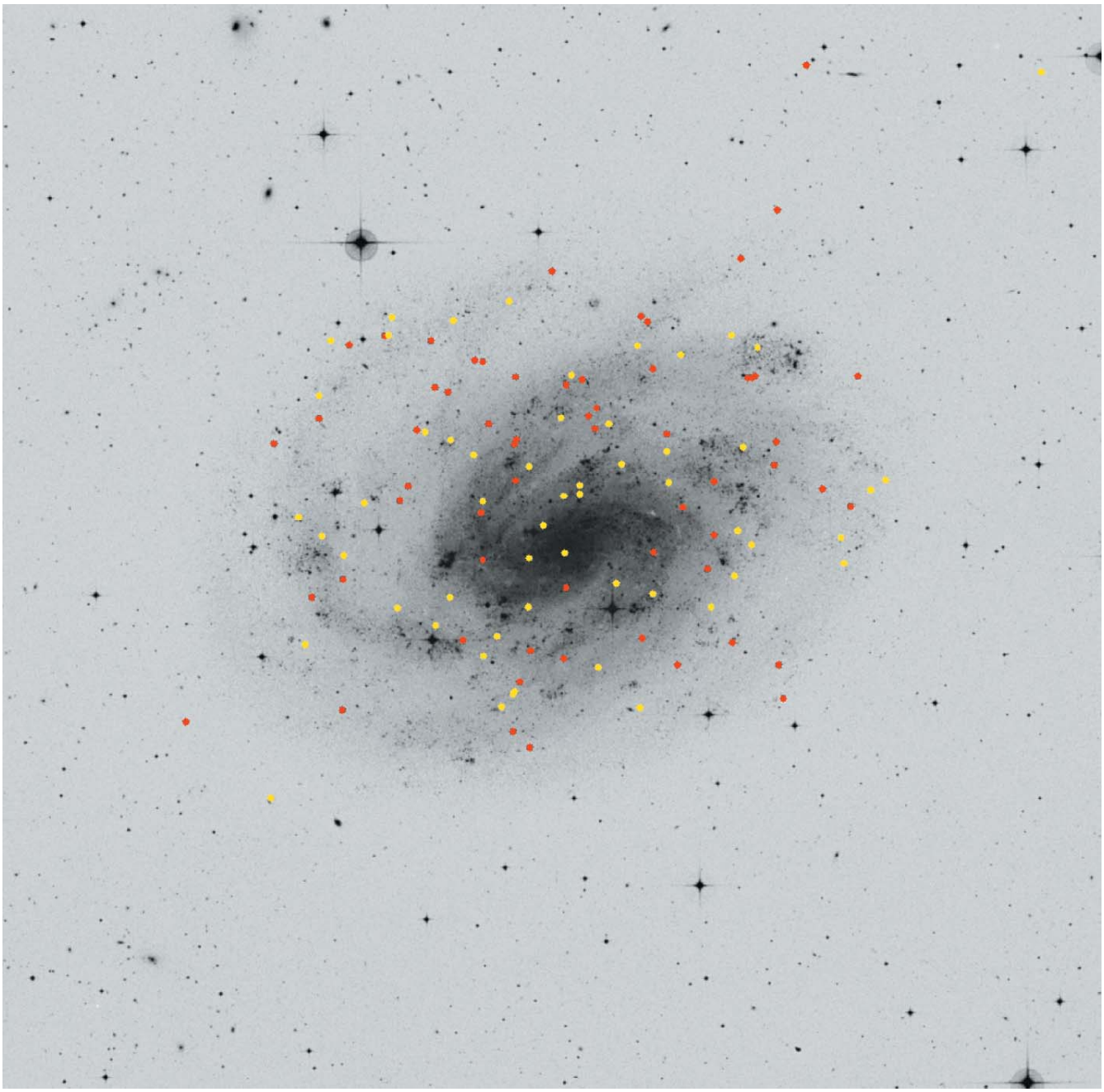

Figure 2: The Sculptor Group galaxy NGC 300, with Cepheids discovered by Pietrzynski et al. (2002) overplotted. Red and yellow points correspond to positions of Cepheids with periods smaller and larger than 15 days, respectively. North is up and east is to the left. The field of view is about 30 × 30 arcmin.

termination. As an added benefit, we will significantly improve our knowledge of many astrophysical properties of the object classes used for distance determination.

2.1. An improved Cepheid distance to the LMC

One of the very promising techniques to derive a truly accurate distance to the LMC (and other nearby spiral and irregular galaxies) is the infrared surface brightness (IRSB) method for Cepheid variables introduced by Fouqué & Gieren (1997). It is a Baade-Wesselink type technique in which a Cepheid's varying surface brightness, as determined from its colour variation during the pulsation cycle, is used to determine its angular diameter variation through the cycle. This information is combined with a knowledge of the variation of its linear diameter which is derived from an integration of its observed radial velocity curve. A linear regression of pairs of angular and linear diameters measured at the same phases yield the distance, and the mean radius of a Cepheid. While the principle of this technique has been known for a long time, its usefulness for distance determination has recently improved dramatically, due to application of the method at infrared wavelengths, first introduced by Welch (1994). Angular diameters calculated from near-infrared colours like V-K are almost an order of magnitude more accurate than those oblained from optical colours, mostly due to two factors: first, the effect of the effective temperature variation of a Cepheid is greatly reduced, at IR wavelengths, compared to its effect on the visual light curve; and secondly, gravity and microturbulence variations in the pulsating atmosphere of a Cepheid, which produce important effects on optical colours, have a negligible influence on infrared colours, which are therefore much better tracers of the Cepheid surface brightness (Laney & Stobie 1995). Gieren, Fouqué & Gómez (1997; GFG97) have shown that the Fouqué & Gieren (1997) calibration of the technique is able to provide distances to individual Cepheids accurate

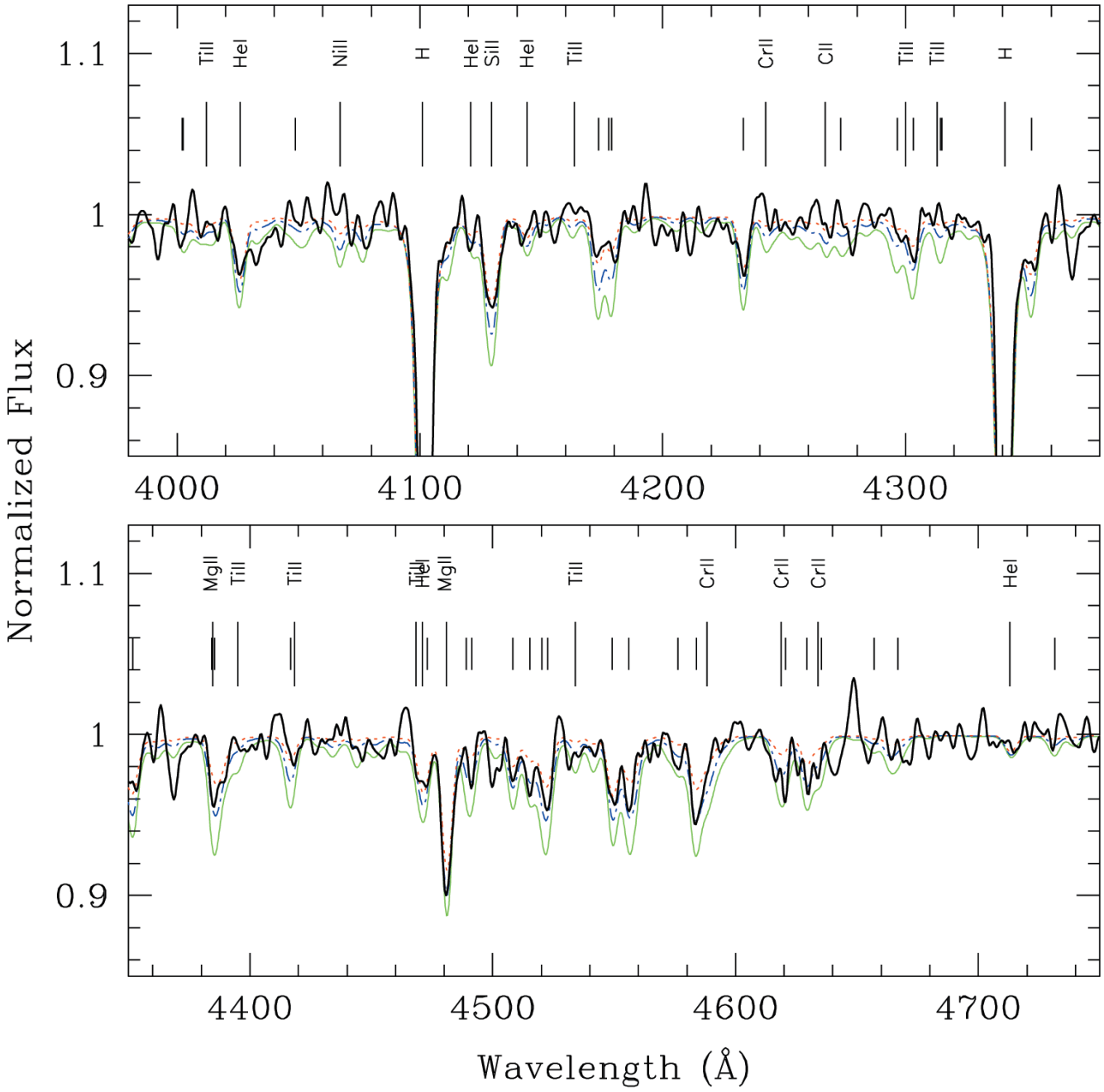

Figure 3: Model fits, corresponding to metal abundances of 0.2, 0.5 and 1.0 solar (red, blue and green curves, respectively), to the spectrum of the B9-A0 supergiant A-8 in NGC 300 (thick black curve). The spectrum was obtained with VLT and FORS1. The metal abundance of this star is about 0.2 solar.

to 4 per cent if the data used in the analysis are of the highest precision. One of the important strengths of the IRSB technique is its very low sensitivity to both reddening and metallicity (GFG97). Also, it is a direct technique which does not require additional, intermediate steps which would introduce additional uncertainties in the distance determination.

In the LMC, the ideal objects on which to apply the IRSB technique are the young, rich clusters, many of which contain substantial numbers of Cepheid variables of similar period and reddening, all at the same distance. We are currently gathering the observational data to carry out IRSB analyses on about a dozen Cepheids in three clusters: NGC 1866, NGC 2031 and NGC 2136/37. First results have been published on the Cepheid variable HV 12198 in NGC 1866, which is the Cepheid "record holder", containing more than 20 Cepheids. For this one object, we have obtained a distance modulus of 18.42, with a total uncertainty of 5 per cent in the distance (Gieren et al. 2000). This value agrees very well with another recent distance determination for NGC 1866 using HST V, I photometry of the cluster main sequence down to V = 25 mag, and ZAMS fitting (Walker et al. 2001), who find 18.35 ± 0.05. Our goal is that at the conclusion of this project (done in collaboration with P. Fouqué (Paris, ESO) and J. Storm (Potsdam)) we will have determined the LMC distance with a remaining uncertainty not exceeding 5 per cent, which would be a giant step towards fixing the zero point of the distance scale. Even further improvement can be expected once we can measure accurate angular diameters of Galactic Cepheid variables directly with VLTI or similar instruments (e.g. Kervella et al. 2001).

2.2. Calibrating the effect of metallicity on Cepheid absolute magnitudes

One of the major uncertainties affecting the distances to galaxies determined from Cepheid period-luminosity (PL) relations is the possibility that

Cepheid absolute magnitudes depend, to a significant amount, on the metallicity. Regarding the size of this effect, empirical tests have led to wildly different claims in the literature over the past few years, from little or no dependence (e.g. Kennicutt et al. 1998; Udalski et al. 2001) to a very strong effect (Allen & Shanks 2001). From theoretical models (Bono et al. 1998; Alibert et al. 1999), even the sign of the metallicity effect is currently under dispute. This shows that there is an urgent need to devise a test capable of giving a precise answer to the problem.

Partly motivated by this open question, about 2 years ago we started a programme with the ESO 2.2-m telescope and Wide Field Imager to carry out a search for Cepheid variables in the Sculptor Group spiral galaxy NGC 300. Given the relative proximity of this galaxy (about 2 Mpc), which allows resolution into stars even in its central regions, its nearly face-on orientation, clear signs of massive star formation, and indications of a substantial metallicity gradient in its disk from previous H II region work, NGC 300 promised to have a large number of Cepheids and to be an excellent target to determine the effect of metallicity on Cepheid luminosities in a similar way as done in M 101 by the HST Key Project team on the the Extragalactic Distance Scale (Kennicutt et al. 1998). Our survey was carried out between July 1999 and January 2000 and has led to the discovery of some 120 new Cepheids, as compared to 16 known from the previous survey of Graham (1984; all his Cepheids were rediscovered by our survey), covering a wide period range from 6 to 115 days (Pietrzynski et al. 2002).

A typical light curve, and the distribution of the Cepheids over the galaxy, are shown in Figures 1 and 2, respectively. In a parallel programme, in collaboration with F. Bresolin and R.P. Kudritzki from the University of Hawaii, we have obtained VLT/FORS multiobject spectra of some 70 blue supergiant candidates in NGC 300 identified from the WFI images, for the purpose of establishing an accurate stellar metallicity gradient in the disk of the galaxy which is needed for the determination of the metallicity effect on Cepheids, and for the independent purpose of improving the use of blue supergiants themselves as standard candles (see next section). More than 60 of our targets were spectroscopically confirmed as blue supergiants, with spectral types ranging from O9 to late A, and first analyses carried out by our team (Bresolin et al. 2002) show that the metallicities determined from the medium-resolution FORS blue spectra (4000–5000 Å) are accurate to about 0.2 dex, and confirm the expected dependence of metallicity on the galactocentric distance (from about solar in the centre to about SMC metallicity in the outskirts of NGC 300). An example of a spectrum is shown in Figure 3.

Once all the spectra have been analysed for their metallicities, using hydrostatic line-blanketed model atmospheres and LTE/NLTE spectrum synthesis, we will proceed with the calibration of the metallicity effect on Cepheid luminosities. Given the amount and quality of the data at our disposal, we are confident that a very accurate result will come from this work.

In yet another, independent approach to this problem we are currently using a sample of metal-poor Galactic outer disk Cepheids, located at galactocentric distances of 12–14 kpc, to determine their distances with the IRSB technique. These metallicity-independent distances will then be compared to those predicted from PL relations calibrated for solar metallicity. Any systematic difference between the two distance determinations should allow us to estimate the effect of metallicity on the absolute magnitudes. A crucial ingredient for this programme to be successful is an accurate knowledge of the metallicities of our target Cepheids. Observing time to obtain these data is scheduled for January 2002 at the ESO NTT. Optical/near-infrared light curves have already been measured from data obtained with the double-channel camera attached to the CTIO YALO telescope, as well as very accurate radial velocity curves (measured with the 1.2-m Swiss telescope on La Silla), which were recently used in a different context to explore the effect of metallicity on the structural properties of Cepheid velocity curves (Pont et al. 2001).

2.3. Blue supergiants as standard candles

The field of extragalactic stellar astronomy is experiencing a time of revival now that the detailed spectroscopic study of single giant and supergiant stars in nearby galaxies has become feasible. Stellar abundance patterns in galaxies can now be studied, and the physical properties of massive stars, in particular those related to their stellar winds, can be used to determine the distances of the parent galaxies. Mass-loss through stellar winds is of fundamental importance in the evolution of stars in the upper H-R diagram. The existence of a relationship between the intensity of the stellar wind momentum and the luminosity of massive stars is a sound prediction of the theory of radiatively driven winds (Kudritzki 1998; Kudritzki & Puls 2000). Briefly, this relationship is summarised as follows:

$$log\ D_{mom} = log\ D_0 + x \cdot log(L/L_\odot)$$

where the modified wind momentum D_{mom} is the product of the mass-loss rate, wind terminal velocity and the square root of the stellar radius. The coefficients D_0 and x must be determined empirically by observations covering blue supergiants (types OBA) of different metallicities. The validity of the Wind Momentum-Luminosity Relationship (WLR) has been demonstrated empirically by Puls et al. (1996) for O-type stars in the Galaxy and the Magellanic Clouds, as well as for supergiants of type B and A in the Milky Way (Kudritzki et al. 1999), M 31 (McCarthy et al. 1997) and M 33 (McCarthy et al. 1995), confirming the expected dependence of the relation on spectral type.

What makes the WLR appealing as an extragalactic distance indicator is the extreme brightness of blue supergiants (up to $M_V = -10$ for A-type supergiants). The basic approach consists in deriving the stellar parameters (temperature, gravity and metallicity) from optical spectroscopy, and modelling the $H\alpha$ line profile to obtain the wind properties (mass-loss rate and terminal velocity). The intrinsic luminosity, and hence the distance, follows from an empirically calibrated WLR, and the knowledge of the stellar apparent magnitude, reddening and extinction. With 8-m-class telescopes, the necessary spectroscopic observations can be carried out to distances of 10–15 Mpc. Previous work of Kudritzki et al. (1999) indicates that the WLR has the potential to yield distances with an accuracy rivalling that of the Cepheid PL relationship. It is also currently the only stellar distance indicator allowing a distance determination on the grounds of spectroscopic analysis alone (but apparent magnitudes and extinction must, of course, be measured from photometry). However, the dependence of the WLR on spectral type and metallicity must first be explored in greater detail before blue supergiants can be used as a new class of accurate, far-reaching stellar distance indicators.

In an effort to obtain such improved calibrations, we have taken VLT/FORS spectra in the blue spectral range of some 60 blue supergiants in NGC 300 to determine their abundances and the systematic stellar abundance variations over the disk of this galaxy. Very recently, we were able to complement these data with red spectra covering the $H\alpha$ line, from which the wind properties of the stars will be determined. From these data, we will be able to populate the WLR diagram, explore in detail its dependence on metallicity and spectral type, and set a zero point to the WLR from the extensive Cepheid sample we have discovered in NGC 300. A first, very encouraging example of a WLR analysis of one of the blue supergiants in NGC 300 is shown in Figure 4 (for more details, see Bresolin et al. 2002).

To improve the Cepheid distance determination beyond what is possible with optical photometric data, we are planning to carry out K-band photometry of the Cepheids, which will allow us to get rid of the problem of reddening and absorption internal to the galaxy. We expect that our current programme on NGC 300 will produce decisive progress for the calibration of the blue supergiant WLR for distance determination, and that subsequently we can use this new tool to derive accurate distances to a number of galaxies out to the Virgo and Fornax clusters.

2.4. The ARAUCARIA project

In addition to performing studies intending to improve Cepheids and blue supergiants as standard candles, we have started a more general programme (called the ARAUCARIA project, after the Chilean national tree, which is common in our southern location) to test the influence of environmental properties of galaxies on a number of other stellar distance indicators. These include RR Lyrae variables, red clump stars (which are currently the only stellar distance indicators which can be geometrically calibrated from HIPPARCOS parallaxes), and planetary nebulae (PN). Our strategy is to obtain and compare distances from all the different stellar candles in a common set of nearby, resolved galaxies which show a wide range of environmental properties. Our work on NGC 300 is a first example of this kind of work. In this particular galaxy we have, in addition to the work mentioned in previous sections, obtained deep narrow-band and *H*α photometry with the ESO 2.2-m telescope Wide Field Imager (in collaboration with R. Méndez, Munich, and R. P. Kudritzki, Hawaii) which will allow us to detect and measure its complete population of PN down to the faintest objects, and to check any possible dependence of the Planetary Nebulae Luminosity Function (PNLF) on the stellar population producing the PN (NGC 300 shows recent star formation, as opposed to the bulge of M 31, which has been the principal calibrator of the PNLF method in the past). To this end, we will use our new accurate Cepheid distance to NGC 300 to set the zero point of the narrow-band fluxes.

Studies of red clump stars in the near-infrared K band, where age and metallicity effects on absolute magnitudes are expected to be less important than for I-band magnitudes (Alves 2000), are underway in the LMC, SMC and several Local Group dwarf galaxies. We also plan to test the red clump star method in NGC 300 in the near future. As an outcome of the ARAUCARIA programme, we not only hope to set the zero point of the extragalactic distance scale with exquisite accuracy,

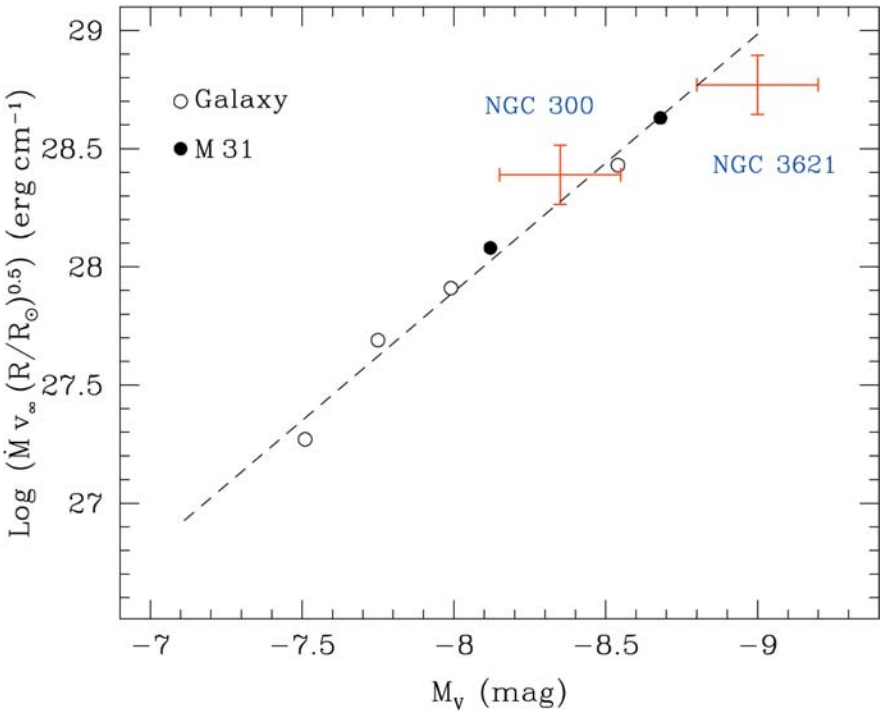

Figure 4: Wind momentum-luminosity relationship for A supergiants, from Galactic (open circles) and M 31 (filled circles) stars (data sources: see text). Also plotted is the A0 supergiant in NGC 3621 analysed by Bresolin et al. (2001), and the A0 supergiant D-12 in NGC 300 analysed by Bresolin et al. (2002).

but we are also confident that a wealth of new astrophysical information about the object classes studied (and individual, particularly interesting objects) will turn up along the way.

3. Globular Clusters and Galaxy Formation

One of the major goals of modern astronomy is an understanding of galaxy formation. What caused the variety of galaxy types we see today? What were the conditions at the time of their formation? When did galaxies form? The crude answer to this last question is, unfortunately, generally very long ago, making it very difficult to investigate this topic by simply observing galaxies which are currently forming. Thus, we must turn to other clues to reveal the distant past.

Globular clusters (GCs) are ideal tools for studying the earliest epochs of galaxy formation, given that they are the oldest easily-dated objects present in all but the least massive galaxies and that they are also among the brightest objects in galaxies, especially giant elliptical galaxies, where they are present in very large numbers over a wide radial range, and thus readily accessible for detailed observations.

3.1. An observational study of galaxy formation using globular clusters

The use of GCs to study galaxy formation beyond the Milky Way has boomed in the last decade. The primary catalyst has been the discovery of multiple (typically 2) distinct subpopulations of GCs in a given galaxy (e.g. Whitmore et al. 1995, Geisler et al. 1996). Such multimodality provides clear evidence for distinct GC, and therefore galaxy formation epochs and/ or processes. Ashman and Zepf predicted bimodality in their 1992 paper on the formation of globular clusters in gaseous mergers. These results have inspired a host of other observational studies (e.g. Gebhardt and Kissler-Patig 1999, Kundu and Whitmore 2001) as well as stimulated a number of theoretical papers suggesting new galaxy formation models and provided the observational constraints used as their input (e.g. Forbes et al. 1997, Côté et al. 1998). This was one of the key topics at the recent IAU Symposium 207 on “Extragalactic Star Clusters” held in Pucon, Chile, in March. This meeting drove home the point that GCs have much to teach us about the formation of galaxies. This was the first ever IAU Symposium in Chile and we note with pride that our Astronomy Group co-organised and hosted this very successful meeting.

Globular clusters provide a wide variety of evidence useful to our quest. Particularly important are metal abundances and kinematic data for a large number of GCs in a galaxy over its entire extent. Such information can help to tightly constrain galaxy formation models. However, the observational requirements for such a study are quite demanding: one needs accurate (~ 0.2 dex) metal abundances and/or radial

Figure 5: The north-east region of NGC 1399, imaged with FORS2 in V and I and an exposure time of 300 s. The rich cluster population is discernable, as well as many galaxies in the field. This image has been obtained during a spectroscopic run with FORS2 and MXU, during which about 500 spectra of clusters were collected.

velocities ($\frac{1}{10}$ 50 km/s) for hundreds of clusters to build up a statistically significant sample to be able to resolve distinct metallicity peaks or discern kinematic differences between any subpopulations. In addition, one needs large spatial coverage within a galaxy to check for any radial trends, which can yield additional constraints on formation models. Such knowledge is only now beginning to become available. We present here some of our recent work along these lines.

3.2. Photometry and Spectroscopy of the Globular Cluster System of NGC 1399

NGC 1399, the central cD-galaxy in the nearby (~ 19 Mpc) Fornax cluster, plays a leading role in the study of extragalactic GCs. Its rich GC system has frequently been the target of investigators (see Kissler-Patig et al. 1999 and references therein), but the most fundamental questions are either still open or under debate. Even the question as to what degree the richness of its cluster system is extraordinary is not conclusively answered because of the huge extension of both the cD-halo and the GC system, which makes the total number of clusters as well as the total luminosity of NGC 1399 difficult to measure. In some previous work, the substructure of its GC system has been recognised (Ostrov et al. 1998), however, without detailing the photometric, spatial and kinematic properties of subpopulations of clusters. The pronounced bimodal colour distribution, and thus very likely also metallicity distribution, suggests a first order distinction between metal-poor and metal-rich clusters, although it is not excluded that the composition may be more complex. We therefore ask: Are metal-rich and metal-poor clusters differently distributed in space? Do their properties correspond to the properties of the underlying field population? Are there kinematical differences and how can they be interpreted in a dynamical context? Finally, what could be a scenario which explains all properties of the GC system?

The two main factors, which make our new photometric data set superior are the use of the Washington system (in fact, we use Washington C and Kron-Cousins R) with its excellent

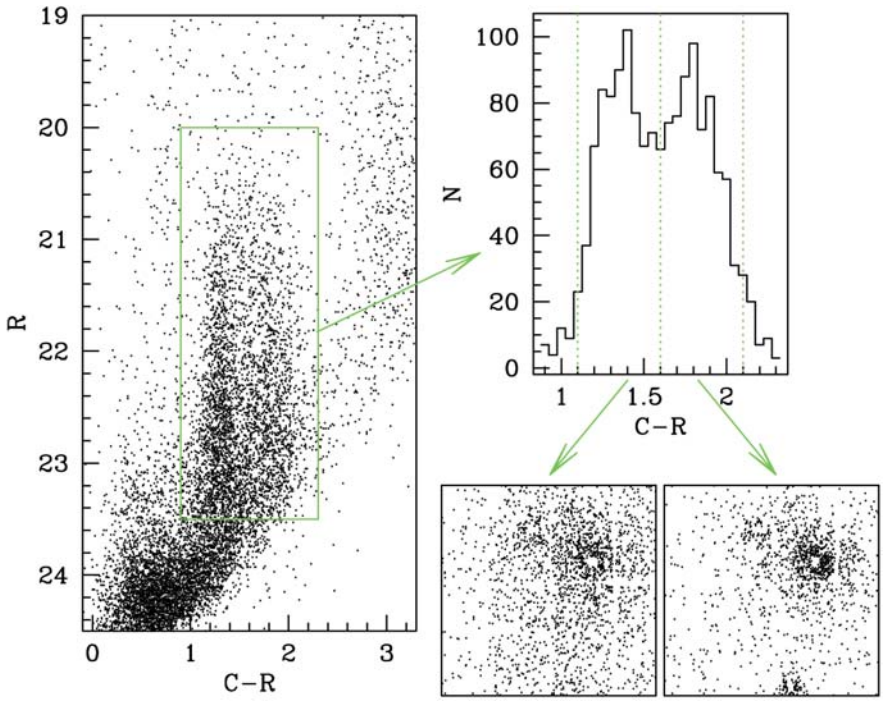

Figure 6: The left panel is the R-(C-R) CMD of all point sources found in the MOSAIC field. The bimodal colour distribution is clearly visible, again demonstrated in the C-R histogram (upper right panel). The lower right panel shows the distribution of blue clusters (left) and red clusters (right) in the 36 × 36 arcmin field. The red clusters are distinctly more concentrated towards NGC 1399. Also NGC 1387 at the lower margin and NGC 1404 left of NGC 1399 are visible, which cannot be seen in the distribution of blue clusters.

metallicity resolution and a large field of 36 × 36 arcmin, which we achieved with the MOSAIC camera of the 4-m telescope at Cerro Tololo. In combination with new and unique spectroscopic data from the VLT we now have the most powerful data set ever oblained for a GC system of an early type galaxy.

Figure 5 shows the north-east region around NGC 1399. The colours have been constructed using V and I exposures from FORS2 at Kueyen, which we took in the course of our spectroscopic run (see next section). The richness of the cluster system is apparent, as is the rich background population of galaxies, which particularly in bad seeing can strongly contaminate a list of GC candidates.

The bimodality of the colour distribution shows up nicely in Figure 6, which is the R vs. (C-R) colour-magnitude diagram of all unresolved objects found on the wide-field images. Since the photometric completeness is controlled by the C images, we have a sharp, inclined completeness limit. The bulk of the faint blue objects are mostly galaxies, which in a V vs. (V-I) diagram merge with the blue GC population and thus contribute significantly to the background contamination. The right panel is a colour histogram of those objects within the rectangle drawn in the CMD, which delimits the expected domain of the brighter half of the GCs. In the plot of the area distributions of blue and red clusters, one notes the much stronger concentration of red clusters toward their host galaxies. Even two neighbouring galaxies, NGC 1404 and NGC 1387, are discernible by the distribution of red clusters, which are not visible if only the blue clusters are plotted.

To be more quantitative, we plot the surface density profile vs. the radial distance for the red and the blue clusters, as well as for the galaxy light in the C and R bands (Fig. 7). The zero-points of the ordinate for all four components have been shifted to make the differences between them best visible. The radial range covered is larger than in any other previous CCD study. We see that in the outermost region the blue and red cluster profiles cannot be distinguished, but the blue cluster profile becomes progressively shallower than that of the red cluster inwards. This difference is also reflected in the galaxy light profile, where the colour gradient becomes best visible between 3 and 10 arcmin. In fact, the galaxy colour gradient resembles nicely the ratio of red to blue clusters at any given radius, so the galaxy "knows" about its bimodal cluster population. We stress that this is very difficult to see in a field smaller than ours. The fact that the galaxy colour profile follows that of the ratio of red to blue clusters is a strong point against any "stripping" scenario, in which the rich cluster system has been built up by stripping globulars from neighbouring galaxies and argues for a scenario in which the field population forms together with the cluster population. We note that we are also investigating the GC luminosity function and its utility as a distance indicator, with particular attention to the metallicity dependence of the turnover.

With the advent of large telescopes like the VLT in combination with a sophisticated and efficient multi-object spectroscopic device like the Mask Exchange Unit (MXU) at FORS2, spectroscopy of objects as faint as V = 23.5 for measuring radial velocities has become feasible. As for the investigation of GC systems of early-type galaxies, two important objectives can now be addressed: firstly, the kinematical be-

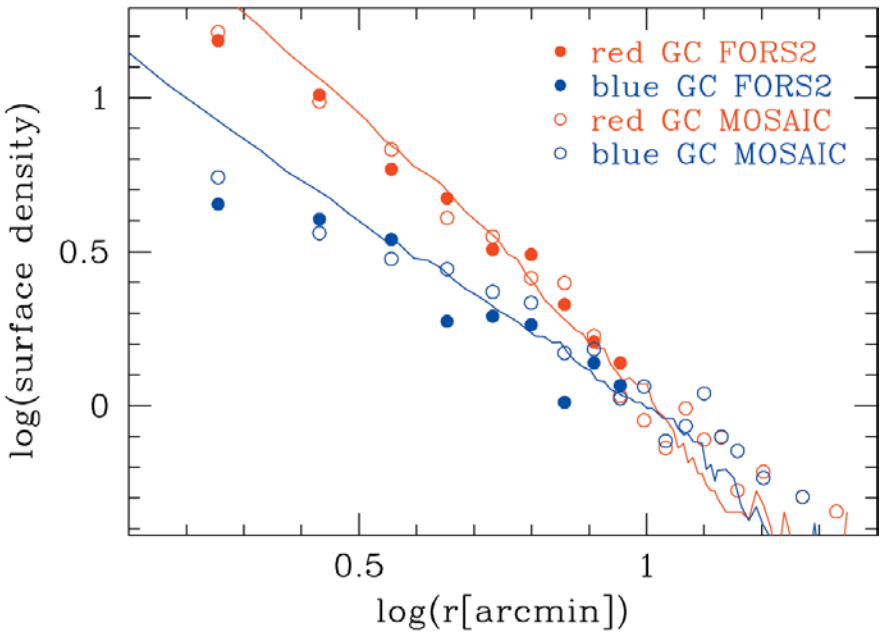

Figure 7: This plot shows the surface density profiles of the radial distribution of red and blue clusters, measured on FORS2 images (filled circles) and MOSAIC images (open circles). The solid lines are the galaxy light profiles in the C filter (blue) and the R filter (red). The zero-points of all four components have been shifted to make the differences most visible. The colour gradient in the galaxy light can be seen best between 0.5 < logr < 1.

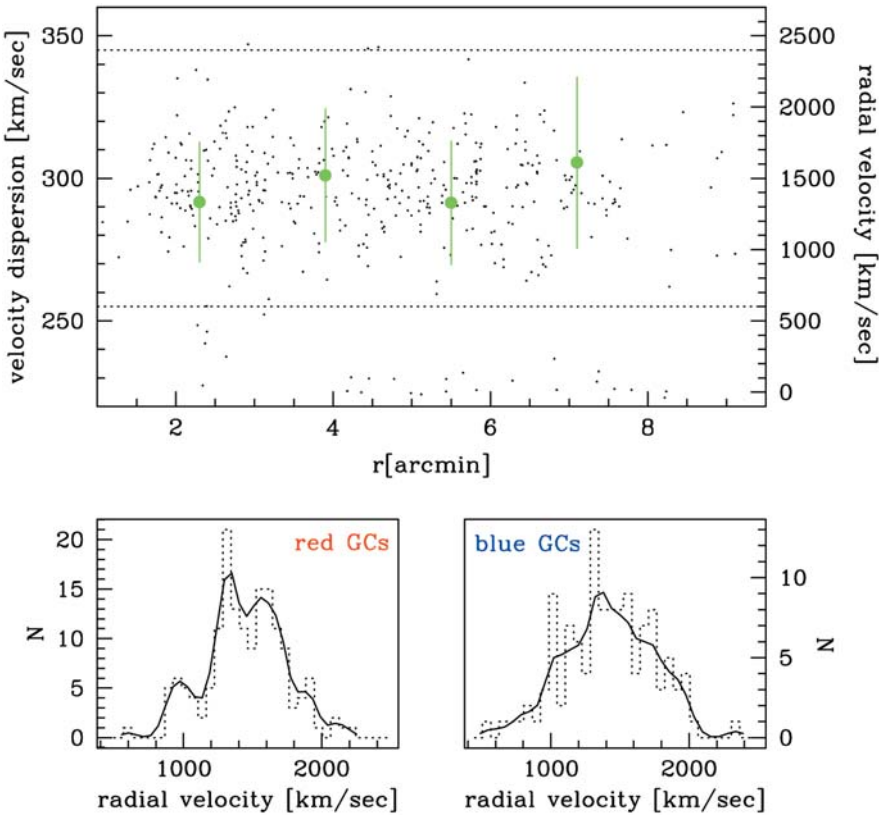

Figure 8: The upper panel is a combination of two figures. The small points are all measured clusters with their velocities (right ordinate) plotted vs. their projected galactocentric distances. The dashed lines indicate the velocity limits which have been applied for calculating the velocity dispersions. The large points are the projected velocity dispersions (left ordinate) in four radial bins with their uncertainties indicated. The lower left panel shows the velocity distribution of the red clusters, the right panel that of the blue clusters. One can see the smaller velocity dispersion of the red clusters, but also that these histograms are not very well approximated by Gaussians. The curves are the result of smoothing the data.

haviour of distinct subpopulations of GCs, and secondly, the use of GCs as probes for the gravitational potential of the host galaxy. Radial velocities of GCs have already been measured for some galaxies (NGC 1399, M87, NGC 4472) using the Keck and 4-m-class telescopes (Kissler-Patig et al. 1999, Cohen et al. 1998, Côté et al. 2001, Zepf et al. 2001), but the VLT vastly improves the situation in terms of accuracy and number statistics. Large sample size is particularly essential for a dynamical analysis, because about 400–500 probes are necessary to disentangle the phase space distribution and the potential (e.g. Merrit 1993).

We therefore started a programme aimed at getting a large sample of GC radial velocities around elliptical galaxies. The first natural target in the southern sky is NGC 1399. In December 2000, we observed with FORS2 and MXU at Unit 2 various fields around NGC 1399. The pre-selection of GC candidates was performed with the aid of our MOSAIC Washington photometry. As the radial velocities showed later on, the distinction of clusters from background galaxies and foreground stars worked excellently, giving a contamination fraction as low as 5%. We used the grism 600B, with which the arc lines have a FWHM of 5 Å. The spectral coverage was from about 3800 Å to 5800 Å, depending on the slit position on the mask. In total we observed 13 masks with varying exposure times between 45 and 90 min. The cluster candidates had R-magnitudes between 20 and 22.5 mag.

The surface density of targets, particularly at small projected galactocentric radii, is very high. Therefore, we decided not to measure the sky through the same slit as the object, but to set independent sky slits, which greatly improved the flexibility of object selection. In that way we could fill one mask with more than 100 slits. The Mask Manufacturing Unit works sufficiently accurately to allow a satisfactory sky subtraction of independent object and sky slits.

The observations resulted in about 500 spectra of cluster candidates together with 300 miscellaneous objects, including galaxies, stars, and clusters which fell outside our photometric selection criteria, which were observed intentionally to take advantage of available slit positions when good GC candidates were not available. We have measured radial velocities for about 450 clusters by both cross-correlation techniques and direct measurements of line positions. The uncertainty for most objects is in the range 20–50 km/s. The final sample will probably contain about 450 GC velocities, which is the largest sample of dynamical probes ever obtained for an early-type galaxy.

Figure 8 (top) shows both the individual velocities and the velocity dispersion (right and left ordinates) and their radial dependence. Because the work is still in progress, we can only give preliminary results. We do not see any significant rotation for most of the cluster population except perhaps for the outer metal-poor clusters, for which a marginal rotation signature might be present. Considering the entire sample, the projected velocity dispersion seems to be constant with radial distance and has a value of 310 ± 20 km/s.

We use a colour of C – R = 1.4 to separate the metal-poor from the metal-rich clusters. The metal-poor and the metal-rich subsamples show slightly different velocity dispersions of 330 ± 18 km/s and 291 ± 16 km/s, respectively, and again do not indicate a change with radial distance (Fig. 8, bottom).

Although the proper dynamical analysis still has to come, a few interesting remarks can already be made. If we assume spherical symmetry, we may apply the spherical Jeans equation (e.g. Binney & Tremaine 1987):

$$\frac{G \cdot M(r)}{r} = -\sigma_r^2 \cdot \left(\frac{d\ln\rho}{d\ln r} + \frac{d\ln\sigma_r}{d\ln r} + 2\beta\right)$$

where G is the constant of gravitation, r the galactocentric distance, M(r) the mass contained within r, σ_r is the radial component of the velocity dispersion, ρ(r) the density profile of clusters, $\beta = 1 - \frac{\sigma_\Theta^2}{\sigma_r^2}$ with σ_Θ being the tangential velocity dispersion. Unless β is non-zero, a radially constant *projected* velocity dispersion implies a constant σ_r and $\frac{d\ln\sigma_r}{d\ln r} = 0$. Within our radial range, the red and the blue clusters show different density profiles (Dirsch et al. 2001), $\frac{d\ln\rho}{d\ln r} \sim -2.5 \pm 0.1$ and -1.8 ± 0.1, respectively. The difference of the density profiles could account completely for the difference in the velocity dispersions, if β would be zero.

A handy formula for the mass inside a radius r is ($\beta = 0$)

$$M[M_\odot] = 2 \cdot 10^{10} \cdot r[kpc] \cdot \left(\frac{\sigma_r^2}{300km/s}\right)^2 \cdot \alpha$$

where α is the logarithmic slope of ρ(r) and where a distance of 19 Mpc has been assumed. The mass inside 10 kpc is $4.2 \cdot 10^{11}$ $M_\odot$ and inside 40 kpc $1.7 \cdot 10^{12}$ $M_\odot$, which is in good agreement with the values given by Jones et al. (1997) based on X-ray analyses and indicates that isotropy is not grossly violated. We note that we are performing a detailed investigation of the mass and M/L distribution in NGC 1399 based on

these data, in collaboration with K. Gebhardt (University of Texas), D. Minniti, L. Infante, M. Rejkuba (Universidad Católica), J.C. Forte (Universidad La Plata), M. Hilker (Universität Bonn), S. Larsen (Lick Observatory), V. Alonso (Cordoba Observatory), E. Grebel (MPIA Heidelberg). A progress report has been given in Richtler et al. (2001).

3.3. What can this study teach us about Galaxy Formation?

NGC 1399 possesses roughly three times as many GCs per unit galaxy luminosity as is "normal" for an early-type galaxy, a property that is shared with other central galaxies in clusters. There have been numerous attempts to interpret this finding, ranging from the concept of a universal GC formation efficiency (McLaughlin 1999) to cluster formation in mergers (Ashman & Zepf 1992) and infall of dwarf galaxies (Hilker et al. 1999; Côté et al. 1998). Here we want to give a few remarks regarding our present view of NGC 1399 and its cluster system.

There is evidence that (for whatever reason) the efficiency of GC formation increases with the star formation rate (Larsen & Richtler 2000), which is also supported by the rich young cluster systems in present-day mergers (Whitmore & Schweizer 1995). The centre of a galaxy cluster obviously is a favourite place for rapid and perhaps multiple merger events. A multiple merger at early times in which gas-rich and chemically unevolved disk galaxies participated is an attractive framework for explaining the properties of NGC 1399. In this scenario, most of the clusters, both metal-rich and metal-poor, could have formed already in the pre-merger phase, either as halo/bulge/disk clusters of the involved spiral galaxies well before the actual merger took place or during the starburst, which probably accompanied the early merger phases, when the galaxies are still detached. This is suggested by the declining amount of molecular gas in evolving present-day mergers (Gao & Solomon 1999). After the merger the remaining gas rapidly falls towards the centre (Barnes & Hernquist 1996) and forms stars and preferentially metal-rich clusters, which mix with the already existing cluster population and cause a steeper concentration of metal-rich clusters. If "normal" elliptical galaxies in low-density regions are formed by the merging of typically two disk galaxies with already moderate gas fractions, one may not expect a very high specific frequency. NGC 1316 (Fornax A) may be considered as an example (Gómez & Richtler 2001, Goud frooif et al. 2000) for such a merger. In the case of the central cD, NGC 1399, the much higher specific frequency may be due to a much higher gas fraction and deeper potential well, which makes it harder for the gas to escape, and thus forced a higher gas fraction to be involved in violent star formation processes.

Within such a scenario, one would expect to find the same radial colour gradient in the galaxy light as is seen in the clusters, just as we observe. The difference in the velocity dispersions of red and blue clusters simply reflects the difference in the density profiles. Also almost isotropic orbits are expected, if the majority of blue and red clusters already existed before the merger remnant achieved its present dynamical state. Our programme for the future is to look at other early galaxies with rich cluster systems where we can obtain data similar to that in hand for NGC 1399. The most attractive candidates are NGC 5128 (Centaurus A) where it will be possible to observe the majority of its GCs, and NGC 4636, a relatively isolated galaxy located at the southern extension of the Virgo cluster, which nevertheless has an unusually rich cluster system. The VLT and forthcoming VIMOS will provide an unrivalled combination for this endeavour.

Finally, we would like to extend a warm invitation to those astronomers ready to take a few extra hours on their next trip to Chile to see our place, talk to our people and, if possible, give a seminar about their research.

4. Acknowledgements

We gratefully acknowledge support from FONDECYT Lineas Complementarias Grant 8000002. We are also very grateful to ESO for providing the necessary observing time which has made possible most of the work described in this article, and to the ESO Comité Mixto for their great generosity, which has helped us to build up our Group and its programme to its current level.

References

Alibert, Y., Baraffe, I., Hauschildt, P. & Allard, F. 1999, *A&A*, **344**, 551.
Allen, P.D. & Shanks, T. 2001, astro-ph/0102447.
Alves, D. 2000, *ApJ*, **539**, 732.
Ashman, K.M., & Zepf, S.E., 1992, *ApJ*, **384**, 50.
Barnes, J.E., Hernquist, L. 1996, *ApJ*, **471**, 115.
Binney, J., & Tremaine, S. 1987, in "Galactic Dynamics", Princeton University Press, p. 204.
Bono, G., Caputo, F. & Marconi, M. 1998, *ApJ*, **497**, L43.
Bresolin, F., Gieren, W., Kudritzki, R.P., Pietrzynski, G. & Przybilla, N. 2002, *ApJ*, in press (astro-ph/0111070).
Cohen, J.G., Blakeslee, J.P., & Ryzhov, A. 1998, *ApJ*, **486**, 808.
Côté P., Marzke R.O. & West M.J., 1998, *ApJ*, **501**, 554.
Côté P., McLaughlin, D.E., Hanes, D. et al. 2001, *ApJ* **559**, 828.
Dirsch, B., Richtler, T., Geisler, D. et al. 2001, Proceedings of IAU Symposium No. 207, Extragalactic Star Clusters, ASP Conf. Series, ed. E. Grebel, D. Geisler, D. Minniti, in press.
Forbes D.A., Brodie J.P. & Grillmair C.J., 1997, *AJ*, **113**, 1652.
Fouqué, P. & Gieren, W. 1997, *A&A*, **320**, 799.
Gao, Y., Solomon, P.H. 1999, *ApJ*, 512, L99.
Gebhardt, K., & Kissler-Patig, M. 1999, *AJ*, **118**, 1526.
Geisler, D., Lee, M.G., & Kim, E. 1996, *AJ*, **111**, 1529.
Gieren, W., Fouqué, P. & Gomez, M. 1997, *ApJ*, **488**, 74.
Gieren, W., Storm, J., Fouqué, P., Mennickent, R.E. & Gomez, M. 2000, *ApJ*, **533**, L107.
Gómez, M., Richtler, T., Infante, L., Drenkhahn, G., 2001, *A&A* **371**, 875.
Goudfrooij, P. Mack, J., Kissler-Patig, M., Meylan, G., Minniti, D. 2001, *MNRAS* **322**, 643.
Graham, J.A. 1984, *AJ*, **89**, 1332.
Hilker, M., Infante, L., Richtler, T. 1999, *A&AS*, **138**, 55.
Jones, C., Stern, C., Forman, W. et al. 1997, *ApJ*, **482**, 1431.
Kennicutt, R.C., et al. 1998, *ApJ*, **498**, 181.
Kervella, P., Coudé du Foresto, V., Perrin, G., Schoeller, M., Traub, W.A. & Lacasse, M.G. 2001, *A&A*, **367**, 876.
Kissler-Patig, M., Grillmair, C.J., Meylan, G. et al. 1999, *AJ* **117**, 1206.
Kudritzki, R.P. 1998, in Stellar Astrophysics for the Local Group (eds Apariclo, A., Herrero, A. & Sanchez, F.), p. 149–262 (Cambridge University Press, Cambridge).
Kudritzki, R.P., Puls, J., Lennon, D.J., Venn, K.A., Reetz, J., Najarro, F., McCarthy, J.K. & Herrero, A. 1999, *A&A*, **350**, 970.
Kudritzki, R.P. & Puls, J. 2000, *ARA&A*, **38**, 613.
Kundu, A. & Whitmore, B.C. 2001, *AJ*, **121**, 2950.
Laney, C.D. & Stobie, R.S. 1995, *MNRAS*, **274**, 337.
Larsen, S., Richtler, T. 2000, *A&A* 354, 836.
McCarthy, J.K., Lennon, D.J., Venn, K.A., Kudritzki, R.P., Puls, J. & Najarro, F. 1995, *ApJ*, **455**, 135.
McCarthy, J.K., Kudritzki, R.P., Lennon, D.J., Venn, K.A & Puls, J. 1997, *ApJ*, 482, 757.
McLaughlin 1999, *AJ*, **117**, 2398.
Merrit D. 1993, *ApJ*, **413**, 79.
Ostrov, P.G., Forte, J.C., Geisler, D. 1998, *AJ*, **116**, 2854.
Pietrzynski, G., Gieren, W., Fouqué, P. & Pont, F. 2002, *AJ*, in press.
Pont, F., Kienzle, F., Gieren, W. & Fouqué, P. 2001, *A&A*, **376**, 892.
Puls, J., et al. 1996, *A&A*, **305**, 171.
Richtler, T., Dirsch, B., Geisler, D., et al. 2001, Proceedings of IAU Symposium No. 207, Extragalactic Star Clusters, ASP Conf. Series, ed. E. Grebel, D. Geisler, D. Minniti, in press.
Walker, A.R., Raimondo, G., Di Carlo, E., Brocato, E., Castellani, V. & Hill, V. 2001, *ApJ*, **560**, L139.
Welch, D.L. 1994, *AJ*, **108**, 1421.
Whitmore, B.C, Schweizer, F. 1995, *AJ* **109**, 960.
Whitmore et al. 1995, *ApJL*, **454**, 73.
Udalski, A., et al. 2001, astro-ph/0109446.
Zepf, S.E., Beasley, M.A., Bridges, T.J. 2000, *AJ*, **120**, 2928.

Harvesting the Results from the REFLEX Cluster Survey: Following-up on an ESO Key Programme

H. BÖHRINGER[1], P. SCHUECKER[1], P. LYNAM[1], TH. REIPRICH[1, 4], C.A. COLLINS[3], L. GUZZO[2], Y. IKEBE[1], E. MOLINARI[2], L. BARONE[2], C. AMBROS[1]

[1]*Max-Planck-Institut für Extraterrestrische Physik, Garching, Germany*
[2]*Osservatorio Astronomico di Brera, Milano/Merate, Italy*
[3]*Astrophysics Group, Liverpool John-Moores University, Liverpool, UK*
[4]*Department of Astronomy, University of Virginia, Charlottesville,USA*

1. Introduction

The prime achievement of 20th century cosmology is clearly the establishment of the expanding universe model and the approximate measurement of the parameters, H_0, Ω_m, and Λ_0 governing the dynamics of the expansion and of space-time geometry. This development will practically reach its goal in the next decade with precise measurements of all parameters involved and we will have a good measure of the statistics of the large-scale structure of the dark matter distribution as well. So what is left for cosmological research to do for the 21st century? These results are actually only describing the Universe of the dark matter. But how this invisible Universe is related to the Cosmos we observe with our telescopes is still to a large part an open question. Aiming towards this general goal we are using galaxy clusters as cosmological laboratories to address some of these fundamental questions.

The formation time of galaxy clusters is comparable to the Hubble time. Therefore clusters are still evolving today and their evolution is closely connected to the evolution of the large-scale structure. Clusters are also well characterised laboratories in which the matter composition can be measured and taken to be approximately representative of the Universe, and the galaxy population can be studied in a controlled environment. The most important cluster characteristics is the measurement of the total gravitational mass – which can be determined quite reliably e.g. from X-ray imaging and spectroscopy of the million degree hot intergalactic gas. One of the interesting findings of X-ray astronomy is that there is about a factor five times more mass in this hot gas (~ 17% of the total mass) than in the cluster galaxies (~ 3–4%) in massive clusters. Thus, the majority of the gas seems to be left over and was not used to form galaxies.

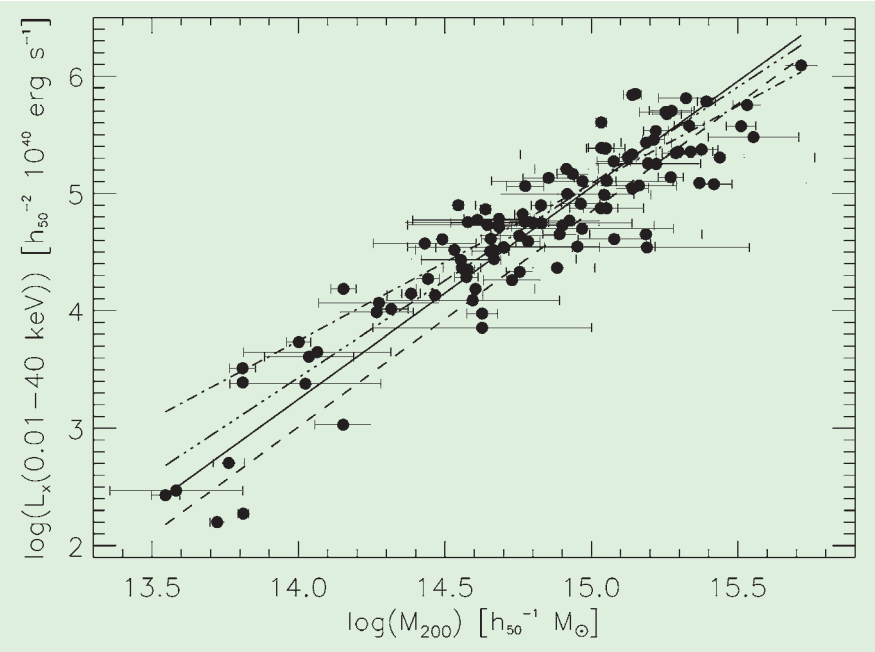

Figure 1: Relation of X-ray luminosity and gravitational mass of the brightest galaxy clusters in the ROSAT All-Sky survey (Reiprich & Böhringer 2001). The mass, M_{200}, was determined inside the virial radius taken to be the radius at which the mean density averaged over the cluster is 200 times the critical density of the Universe.

Therefore some of the major questions that we address with our studies are: How can cluster masses be estimated from easily observable cluster properties? What are the most massive dynamically relaxed objects that we can find in our Universe? How important are clusters and how much mass are they contributing to the matter in the Universe? What are precisely the mass fractions of the galaxies, the hot gas, and the dark matter in clusters, and are there significant system-to-system variations? Are these possible variations linked to variations in the galaxy formation efficiency? How fast do clusters grow at the present epoch by cluster mergers? Does the cluster growth rate depend significantly on the local matter density in the Universe? Are there properties of the galaxy population that are related to the cluster dynamical state, in particular for clusters in a state of merging?

For the study of cluster and galaxy evolution not only observations as a function of time are important, but also the study of the dependence on environment. There are two interesting aspects of the environmental dependence of evolutionary effects. On the one hand, we know from basic cosmological considerations that structure formation is more advanced and continues more vigorously in a denser environment. On the other hand, in a dense environment such as a cluster or protocluster of galaxies we expect a higher frequency of galaxy collisions and galaxy mergers which are believed to be the processes by which at least some of the elliptical galaxies are formed. A particularly important parameter characterising galaxy evolution is the star-formation rate, which can be monitored by optical line spectroscopy. A historic record of star formation is also contained in the abundances of heavy elements that can be derived from the occurrence of element lines in the X-ray spectra of the intracluster gas. These elements are solely produced by stellar processes (notably supernova explosions). Therefore it is important to ask if there are correlations of cluster properties, properties of the

galaxy population in the clusters, and element abundances as a function of location in the cluster and from system to system, that could guide our understanding of the evolution of these components.

To answer these questions, we are conducting a series of systematic studies on galaxy clusters. A progress report with preliminary results is given in the subsequent sections. Such studies should not be conducted on any cluster that is found to have an appealing appearance, but we have to know for each study object what part of the cluster population and which characteristics of the large-scale structure it represents. Therefore the basis of our work is a detailed census of the galaxy cluster population in the Universe out to intermediate redshifts (z ~ 0.4) that we achieved with the REFLEX (ROSAT-ESO Flux-Limited X-ray) Cluster Survey. The survey was conducted as an ESO key programme based on X-ray selected galaxy clusters providing a highly complete X-ray flux limited cluster sample. With the X-ray flux limit we are essentially sampling the most massive clusters in each redshift shell (as will be explained below). The prime goal of the REFLEX survey is the assessment of the large-scale structure. This was previously described in *The Messenger* (Böhringer et al. 1998, Guzzo et al. 1999). The most important information retrieved from the large scale structure measurement is given in a statistical form by the X-ray luminosity function of the REFLEX clusters (Böhringer et al. 2002), the two-point correlation function (Collins et al. 2000), and the density fluctuation power spectrum (Schuecker et al. 2001a). This analysis provides the most important scientific result that the observations are only consistent with a mean matter density of the Universe clearly below the critical limit above which the Universe would recollapse in the future. The allowed range of the density parameter is roughly, Ω_m = $0.12h^{-1}$ – $0.26h^{-1}$ (where h is the Hubble expansion parameter in units of 100 km s^{-1} Mpc^{-1}). Thus the REFLEX programme has made an important contribution to the above-described achievement in cosmology in the last century.

For the follow-up work described below, REFLEX is now providing a highly complete cluster catalogue from which the most appropriate clusters for study can be selected.

2. Weighing the Galaxy Cluster Population

The theoretical description of structure formation as well as N-body simulations of the evolution of the dark matter Universe both describe galaxy clusters by their basic parameter, their mass. Therefore, to interpret our observations in terms of cosmological models, we need to know the link between cluster mass and X-ray luminosity. The cluster mass is not an easily observable parameter, however, but it can be deduced for example from detailed X-ray observations on the density and temperature distribution of the hot, X-ray emitting intracluster gas and the estimation of the gravitational potential needed to hold this hot gas in place. We have used such detailed X-ray observations for the 63 brightest galaxy clusters in the REFLEX catalogue and its northern complement, the NORAS Cluster Sample (Böhringer et al. 2000) to determine the masses of the clusters and to establish the correlation properties of mass and X-ray luminosity (Reiprich & Böhringer 2001). The resulting diagram is shown in Figure 1. Indeed we find a very good correlation of the two cluster properties, and the systematic study also allows us to characterise the scatter. This correlation and its scatter is an essential ingredient for the modelling of cosmological tests with the REFLEX cluster sample (see e.g. Schuecker et al. 2001a).

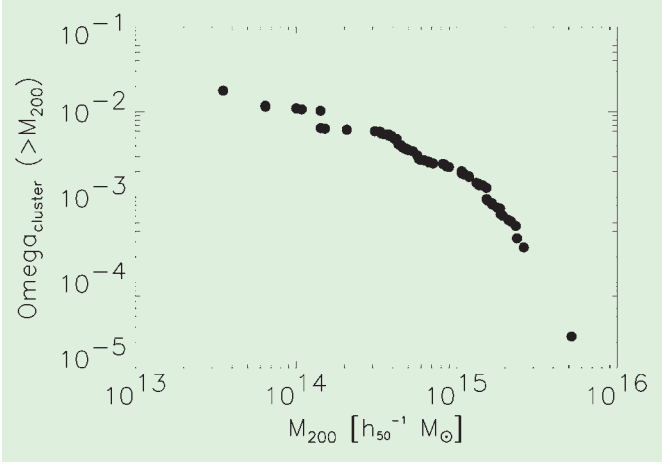

Figure 2: Cumulative mass density function of galaxy clusters normalised to the density of a critical universe ($\Omega_{cluster} = \rho_{cluster}/\rho_{critical}$; Reiprich & Böhringer 2001).

Since the clusters used in this study form a complete flux-limited sample, we can also construct the mass function of clusters. A very interesting result comes from the integral of the mass function, normalised to the mean density of a critical universe as shown in Figure 2. We observe that the matter density bound in clusters with a mass above ~ $6.4 \cdot 10^{13}$ $M_\odot$ is about 2% of the mean density in a critical density universe. For the currently most favoured cosmological model with a density parameter Ω_m ~ 0.3 we find that clusters contain presently about 6% of the total matter in the Universe (Reiprich & Böhringer 2001).

3. Going to Extremes

One of the interesting aspects of large surveys is the discovery of rare but important objects. During the REFLEX survey the so far X-ray brightest galaxy cluster RXCJ1347-1145 and the so far hottest galaxy cluster, RXCJ0658-5557 were discovered (the latter was independently found in the *EINSTEIN* Slew Survey by Tucker et al. 1995). The high temperature of the cluster RXCJ0658-5557 was first found in ASCA follow-up observations, with results of ~ 17 keV (Tucker et al. 1998) and around 14–15 keV in an analysis conducted by us (see also Andreani et al. 1999) making this cluster the record holder for the highest temperature, superseding the previous incumbent, A2163. The high temperature also suggests that this may be the most massive gravitationally relaxed object discovered to date.

Therefore we applied for a deep X-ray study of this object with XMM-Newton, an observation that was conducted recently. Figure 3 shows an image of the observation with the EPN detector on board of XMM. The cluster is obviously featuring a merger of two subcomponents, since we know already from the deep ROSAT HRI observation that both maxima visible in Figure 3 are associated with extended X-ray emission. The high throughput of XMM-Newton allows us to collect enough photons (in a useful exposure time of ~ 14 ksec in the present case) to perform a spectral analysis for several concentric rings in the cluster and to get a good temperature estimate. Figure 4 shows a very preliminary temperature profile from an analysis centred on the maximum of the Eastern main cluster while the Western cluster component was excised. The temperature profile shows that the cluster is indeed very hot around 13–15 keV over a large radial range to at least $0.6h^{-1}$ Mpc. Note that the results are preliminary and the cause of the temperature drop seen in the outermost bin still has to be explored in detail, since it could be an artefact of the very delicate background subtraction in the faint surface brightness region at large radii. From the temperature profile and the gas density distribution obtained from the X-ray image under the assumption of spherical symmetry we can estimate the cluster mass. Inside a radius of $1.5h^{-1}$ Mpc we find a mass of about

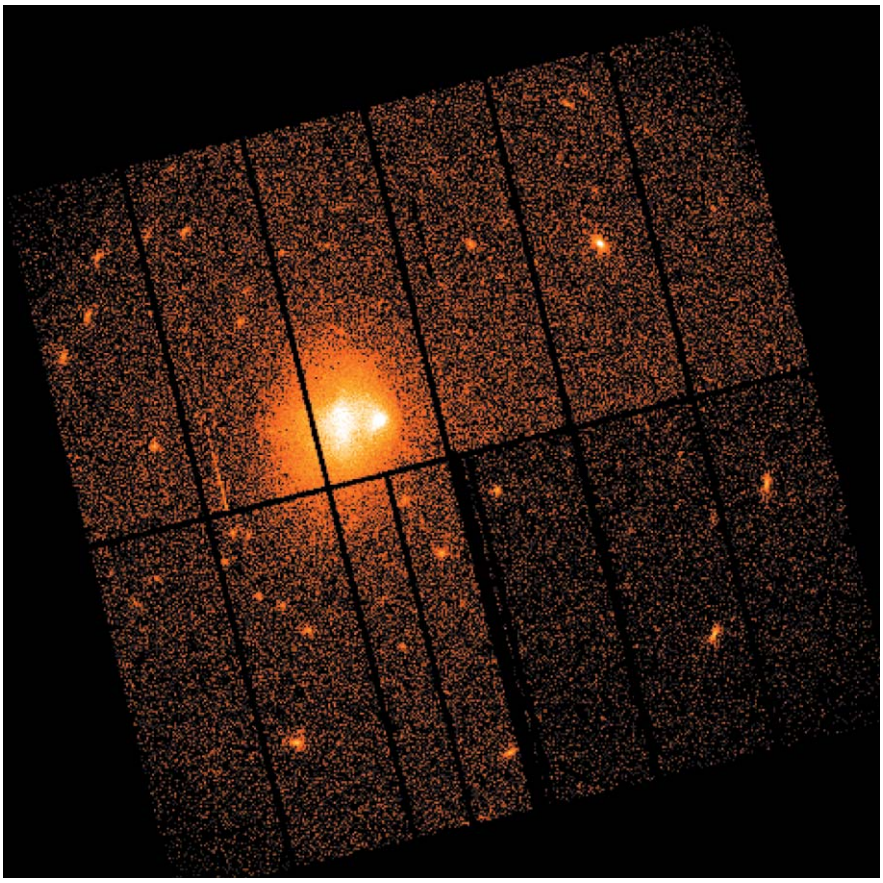

Figure 3: XMM Newton image of RXCJ0658-5557 taken with the EPN X-ray CCD detector in the energy range 0.5 to 5 keV.

$3 \cdot 10^{15}$ M_0 . The virial radius of the cluster is estimated to lay at around $2.5h^{-1}$ Mpc out to which the integral mass may by higher by another factor of two, but we have no observational data that extend so far out. With these numbers this cluster is the most massive dynamically relaxed object known in our Universe. We can use our census of the cluster population to ask how large the search volume has to be to find such a rare, massive cluster. We conclude that one such object should be found in a volume of a few Gpc^3 h^{-3}. Considering that these very massive objects have formed only recently and that the chance to observe them at larger distances becomes increasingly smaller, there should only be a few of these massive objects in the whole visible Universe.

4. The Statistics of Cannibalism

We know from observations as well as from N-body simulations that galaxy clusters evolve and grow by the subsequent merging of subunits. Within the theoretical framework of gravitational growth of structure we expect that the present rate at which clusters merge is a function of the mean matter density of the Universe. Thus in a critical density universe there will at any time be overdense regions which are bound to collapse, while in a universe with low density the growth of structure will essentially be stopped when the density parameter, Ω_m, starts to diverge from unity. What is true for the Universe on average should also be true for large, local regions of higher or lower density. Therefore, we can use density variations in the very large-scale structure to test this structure formation paradigm.

The REFLEX survey is the first survey large enough and sufficiently well defined to perform such a study. The first, quite difficult step of the study is to develop an index for the likelihood that a cluster is in a state of merging. This index was derived from the X-ray morphology of the clusters as seen in the ROSAT All-Sky Survey for the brighter part of the REFLEX sample and for northern clusters (Schuecker et al. 2001b). Figure 5 shows two examples, a merging cluster and a well-relaxed system. These examples are among the best in the sample, being bright and characterised by a large number of X-ray photons. Unfortunately the exposure time for each cluster in the ROSAT Survey is only a few hundred seconds and therefore we have only typically a hundred to few hundred X-ray photons. Therefore regular clusters and mergers cannot be identified with certainty and the derived index has to be considered primarily as a statistical measure.

Figure 6 shows the statistical results of the study based on the two indices found to be most efficient, the β-method which tests for mirror symmetry and the Lee-Statistics which is sensitive to asymmetric substructure (Schuecker et al. 2001b). The parameter shown in this plot is the significance that the cluster is regular (and unlikely to be a merger) as found in two different tests. This parameter is plotted as a function of the cluster density, where the cluster density was derived from the mean distance to the five nearest neighbours. Each data point in the plot is the mean significance value of a number of clusters falling into the density interval. We clearly note that the mean significance for the clusters to be regular is decreasing with the local cluster density. Thus the likelihood to find cluster mergers is highest in the densest regions, as expected from theory.

A closer look shows that this signal is not only providing statistical information. An inspection of the location of those clusters which have a high significance to be mergers shows that these objects lay predominantly in prominent superclusters as can clearly be seen in Figure 7. The most striking structure of the dense clustering regions is the well-known Shapley Supercluster at a redshift of about 0.05 (a velocity of about 15,000 km s^{-1}).

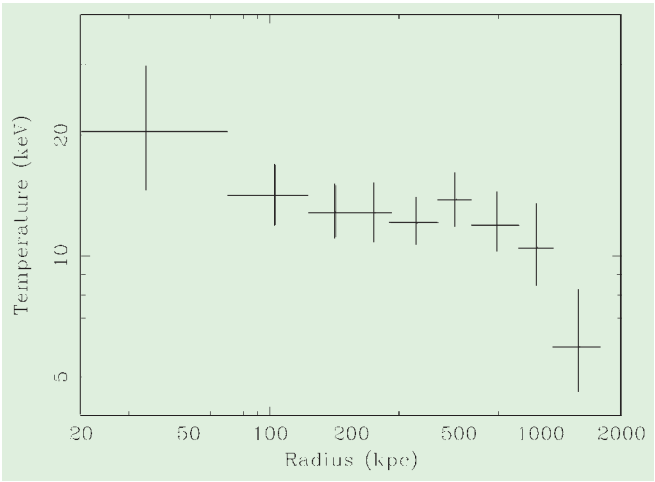

Figure 4: Temperature profile of the hot intracluster gas of RXCJ0658-5557 as obtained from the recent XMM Newton observation. The radial scale is given for a Hubble parameter of, H_0 = 50 km s^{-1} Mpc^{-1}

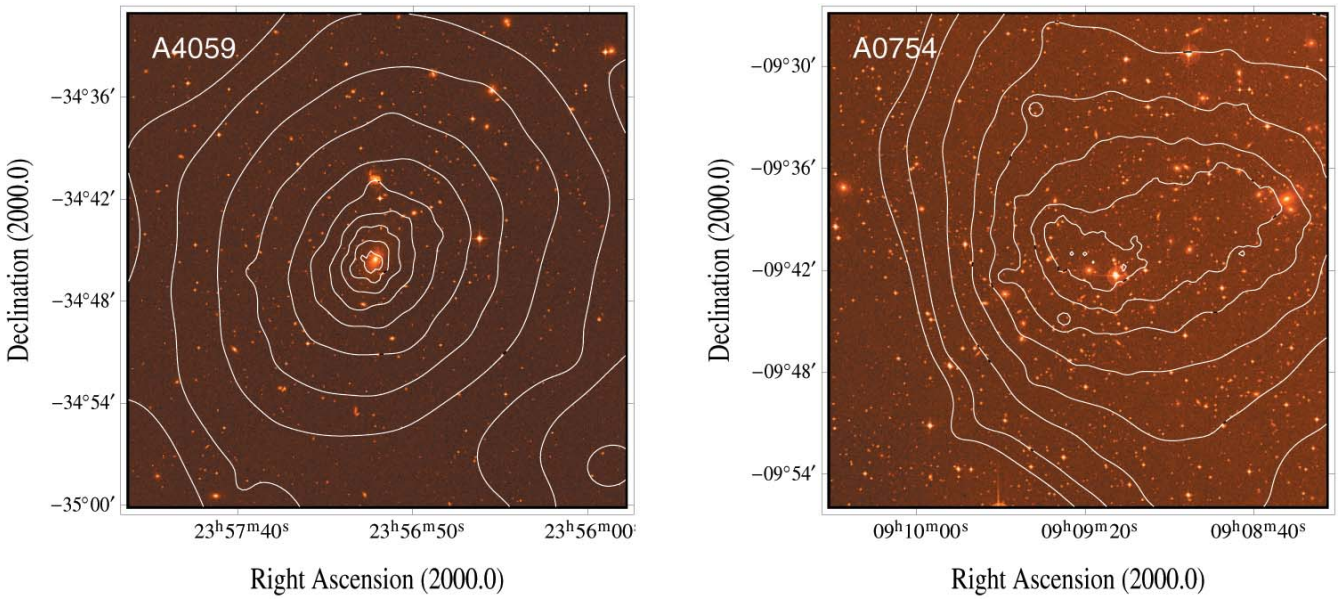

Figure 5: Example of a clearly regular cluster (left) and merging cluster (right). These clusters are among the brightest examples in the REFLEX sample.

5. Probing Large-Scale Motions

The observation of large-scale peculiar flows in the Universe is a very important addition to the study of the large-scale matter distribution. The knowledge of both allows us to investigate the origin of peculiar velocity and to test the paradigm that the flows are caused by the gravitational effects of the density inhomogeneities. The prerequisite for the study of peculiar motion patterns is the establishment of an absolute distance indicator that together with measured redshifts allows us to reconstruct the cosmic flows. Traditionally the brightest cluster galaxy (BCG) has been used as such a distance indicator since the pioneering time of Hubble. The method is based on the recognition that BCGs span a relatively small range of absolute magnitudes.

A few years ago a refined use of BCGs as distance indicators was applied to the study of streaming flows. The refinement is based on the finding that the absolute magnitude of BCGs is correlated to the structure of the galaxies, best characterised by the slope of the surface brightness profile with the slope parameter, α. This correlation can be used to reduce the uncertainty in the BCG distance estimate (Lauer & Potsman 1994). From the study of the "Abell Cluster Inertial Frame" involving 119 Abell clusters Lauer & Postman found very surprisingly a large-scale streaming velocity of 689 ± 178 km s^{-1} on scales of ~ 120h^{-1} Mpc pointing in a direction more than 90 degrees away from the streaming direction indicated by the cosmic microwave background dipole. Thus, both the direction and the magnitude of this effect on these large scales is unexpected in standard cosmological modelling. Several follow-up studies tested the method of Lauer & Postman and did not find an error in the method.

We have therefore embarked on a similar survey now including the X-ray information on the clusters involved (Lynam et al. 2002). The survey sample is constructed from the brightest REFLEX and NORAS Abell and Abell, Corwin & Olowin clusters. In contrast to the earlier studies the BCG candidate was selected to be the brightest elliptical galaxy closest to the centroid of the X-ray emission – which is marking the centre of the gravitational potential of the clusters. In most cases the X-ray luminous clusters have a bright, dominant central galaxy and the identification of the BCG is unambiguous. Only in a handful of cases the coincidence of the X-ray maximum and the BCG position is less obvious. The first interesting finding of this study comes from a comparison of the BCGs identified for the objects in common with the Lauer & Postman survey. In 14 out of 57 common objects the optically selected BCG taken by Lauer & Postman was located far from the X-ray maximum, and in three cases the redshift of the BCG and the cluster differs. Figure 8 shows with Abell 147 one of the examples of different BCG identification. In 80% of these cases Lauer & Postman find a low α-parameter while in the present work always a significantly higher α-value was found (Lynam et al. 2002).

This leads to the second crucial finding. Figure 9 shows the distribution of α-parameters as found in the Lauer & Postman (1994) survey in comparison to the present work. There is a clear difference in the distribution of α in the samples. The major difference is that the present sample lacks the systems with low α and has a much more compact distribution function. This is very suggestive of the observation of two different galaxy populations, X-ray coinci-

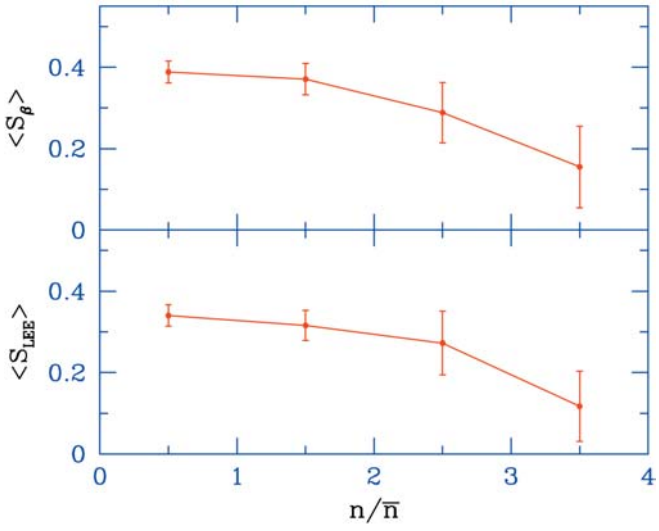

Figure 6: Mean significance of clusters to be regular as a function of local cluster density. Each data point is the mean result for a subsample of clusters. The statistics shows a clear trend that cluster merging occurs more frequently in dense large-scale structure regions.

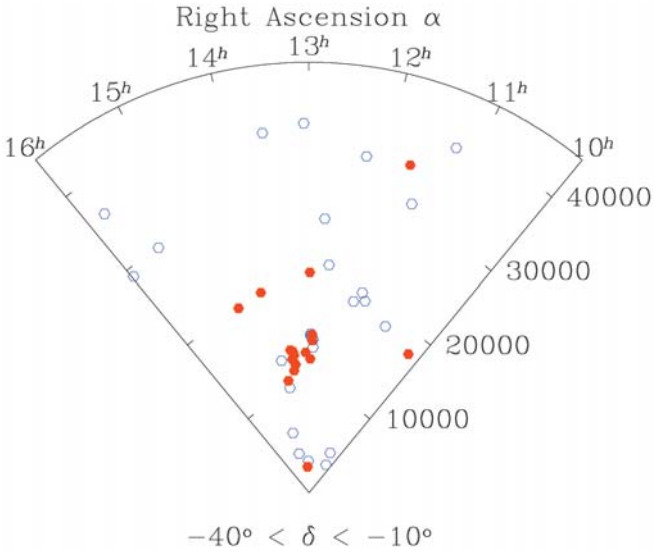

Figure 7: Spatial distribution of the clusters which show a high significance of being regular (open blue dots) and low significance (red dots). There is a clear concentration of the likely merging clusters in dense superstructures. The densest concentration in the plot is the Shapley Supercluster.

dent BCGs and other bright cluster galaxies, which are characterised by different distributions of the α-parameter. While the present sample contains only the X-ray BCG population with a seemingly Gaussian α-distribution, the Lauer & Postman sample is presumably composed of a bimodal population. This is also revealed by some other contemporary studies. A major aim of our further work in this project is therefore to establish more clearly this population difference. The Wide-Field Camera cluster survey described in the next section is particularly useful for this work.

Taking now this population difference into account and re-inspecting the α-luminosity correlation shows that for the X-ray BCGs there is no correlation effect, and therefore no improvement on the distance estimate for these galaxies is possible. The preliminary results of our survey, based on this revision of the method and on the sample of 173 clusters, do not show a significant signal of a large-scale streaming flow (Lynam et al. 2002). This is supported by almost all other independent tests not confirming the Lauer & Postman streaming signal and consistent with the expectations within the standard model..

6. Galaxy Demography

Working with galaxy clusters, it is of course most interesting to know what the clusters are made of and in particular what is the mass ratio of the two forms of visible matter, the hot gas and the galaxies, and the mass-to-light ratio. Are these ratios variable indicating that galaxy formation can be different in different clusters? To answer these questions we are conducting a detailed combined X-ray/optical study of a well selected subsample of massive REFLEX clusters at intermediate redshifts (z = 0.14–0.45) using XMM-Newton observations and the Wide-Field Imager (WFI) at the MPIA/ESO 2.2-m telescope. Having with a large effort finally tackled the reduction of dithered mosaic images and having the first XMM observational data sets at hand we can start our comparison. A first example of these combined observations is shown in Figure 10, the massive REFLEX cluster RXCJ1131.9-1955 at a redshift of z = 0.306. The image is a colour composite produced from exposures with B, V, and R filters. The image is showing a fraction of about 6% of the total mosaic frame. The zooming was chosen to still allow the recognition of galaxy images.

In the further analysis the galaxies are identified and separated from stars by their shape with the object recognition software S-EXTRACTOR (Bertin & Arnouts 1996). In Figure 11 we show the distribution of the objects identified as galaxies with symbols indicating their magnitudes and elongations. The cluster concentration is well visible in this image. The image scale is 26.4 × 30.5 arcmin^2 (4.4 × 5h^{-2} Mpc^2) compared to a virial radius of the cluster which is estimated to be about 1.8–2h^{-1} Mpc. The image is thus covering the whole cluster as virialised object as well as some surrounding background. The image suggests that there is filamentary structure stretching out from the cluster beyond the virial radius. The significance of these structures will be addressed with photometric redshift estimates as well as with further redshift work (see below). Also overlayed on this image are the surface brightness contours of the X-ray image obtained for this cluster with XMM-Newton. The original XMM EPN image is also shown in Figure 12. The morphology of the cluster is traced in a similar way by the hot gas as well as the galaxy component of the cluster. This implies that presumably both components are well tracing the gravitational potential and thus the dark matter distribution. We see a massive compact cluster core in the centre of the image

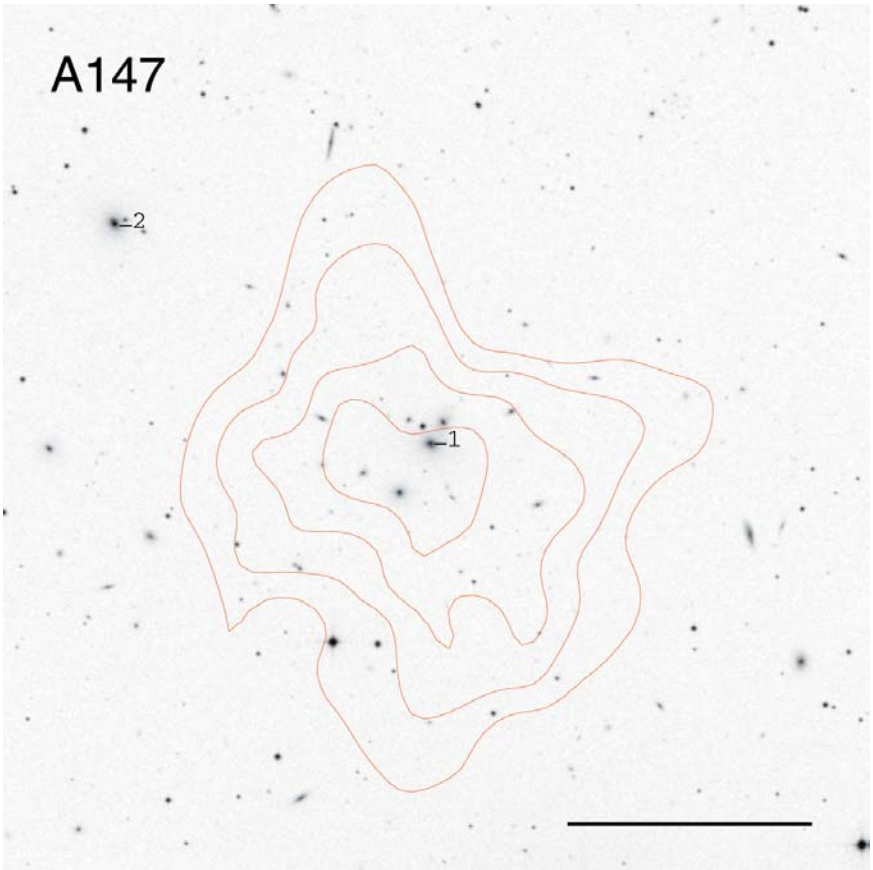

Figure 8: Example of an optically misidentified BCG in the Lauer and Postman (1994) sample. Position 1 marks the X-ray coincident BCG, while the optically selected BCG of Lauer & Postman is at location 2.

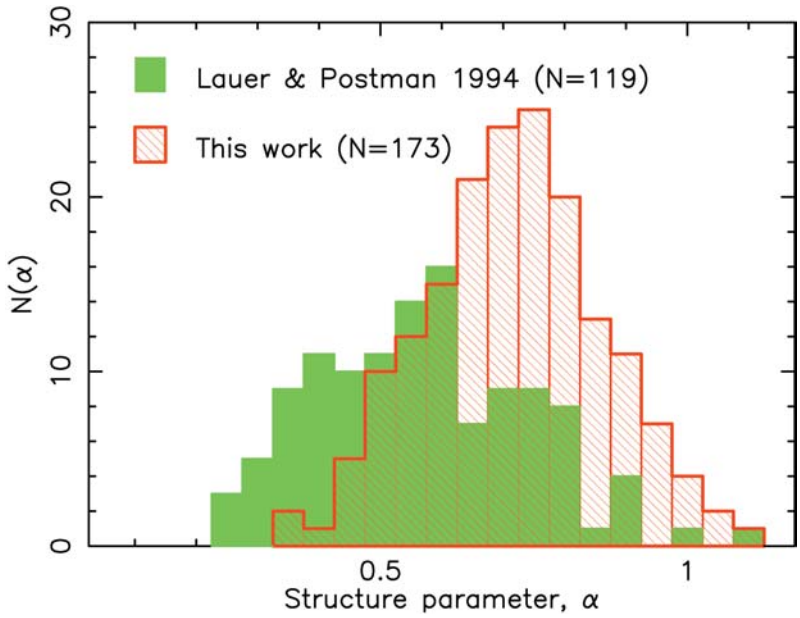

F *Figure 9: Distribution of the shape parameter, α, for the Lauer & Postman (1994) sample and the work by Lynam et al. (2002). There is a clear difference in the two distributions. Most remarkable is the extension towards low values of the α-parameter in the Lauer & Postman sample which gives this distribution a bimodal appearance and which does not appear in our survey.*

Figure 10: Central region of a MPIA/ESO 2.2-m WFI image of the distant REFLEX cluster RXCJ1131.9-1955. The size of the image is ~ 8.12 × 8.12 arcmin². For the production of the colour image we used a programme kindly provided by J. Engelhauser.

H

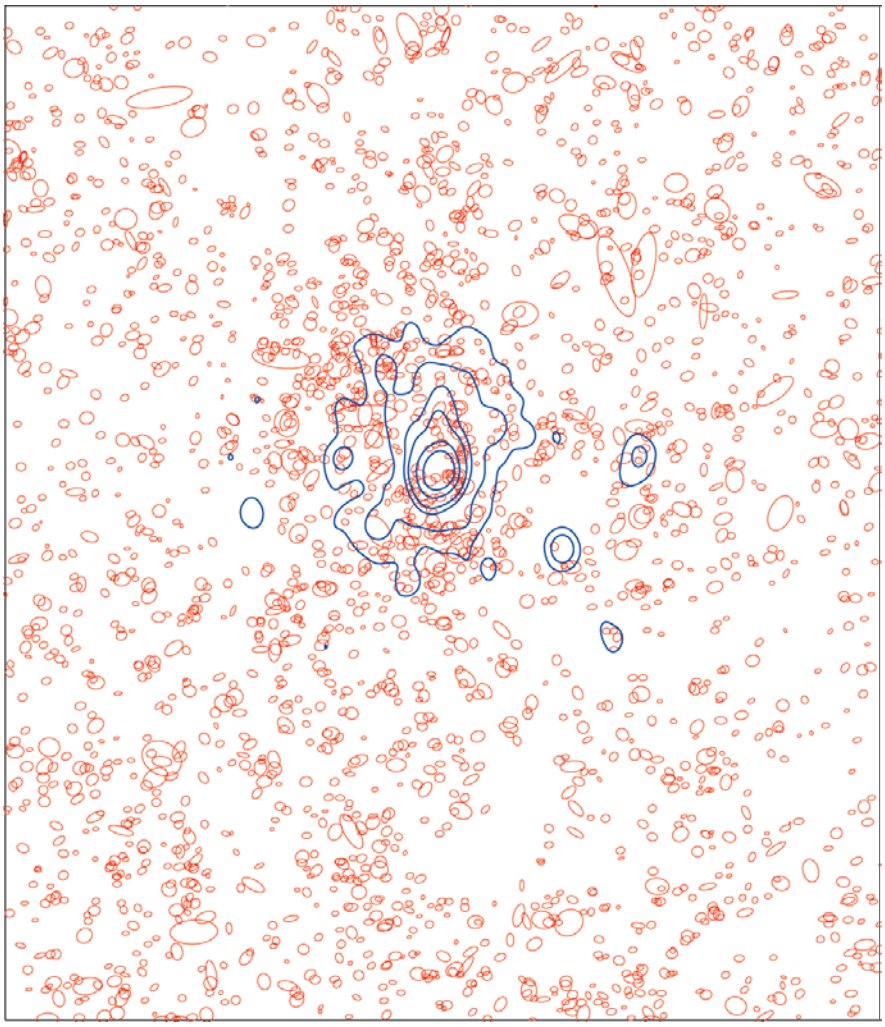

Figure 11: Galaxy distribution in the field of the cluster RXCJ1131.9-1955 as identified in the image shown in Figure 10 displayed by symbols indicating the brightness and orientation of the galaxies. The blue contours show the surface brightness distribution of the XMM EPN X-ray image. This figure illustrates that the hot X-ray emitting gas and the galaxies are displaying a very similar morphology due to the fact that both cluster components are tracing the same gravitational potential.

and a second slightly more diffuse cluster component stretching out to the North-East.

To assess the gravitational mass of this cluster we use the hot gas density profile obtained from the X-ray image and the temperature distribution in the hot gas derived from the X-ray spectra (the temperature profile is similar to that shown in Figure 4 but indicating a bulk temperature around 7 keV). From this very preliminary analysis we estimate a mass of about $2 \cdot 10^{15}$ $M_{\odot}$ within a radius of $1.5h^{-1}$ Mpc.

This is only one of a well-selected sample of 16 REFLEX clusters which have already been scheduled for XMM-Newton observations and which we are also studying and plan to study in the optical. The results of these studies will provide very important details on the cluster composition, dynamical state, and galaxy population of these systems and on the system-to-system variations. They will also help to solve another important problem. Selecting galaxy clusters in X-rays and in the optical yields quite different clusters samples e.g. only about two thirds of the REFLEX catalogue are clusters found by Abell and co-workers (1958, 1989), while these optical catalogues find about five times as many clusters in the REFLEX area as contained in REFLEX. While the X-ray emission clearly flags a three-dimensional mass concentration, the optical identifications are expected to be partly due to projection effects. Therefore, it is very important to understand the relation between the appearance of clusters in the two-wavelength regimes and why there is such a difference. For this we need to include morphological parameters in the optical and X-rays and to look for their correlation properties. We already know that cluster compactness plays a crucial role in these relations. The final goal here is to provide the means to predict from the well-characterised ap-

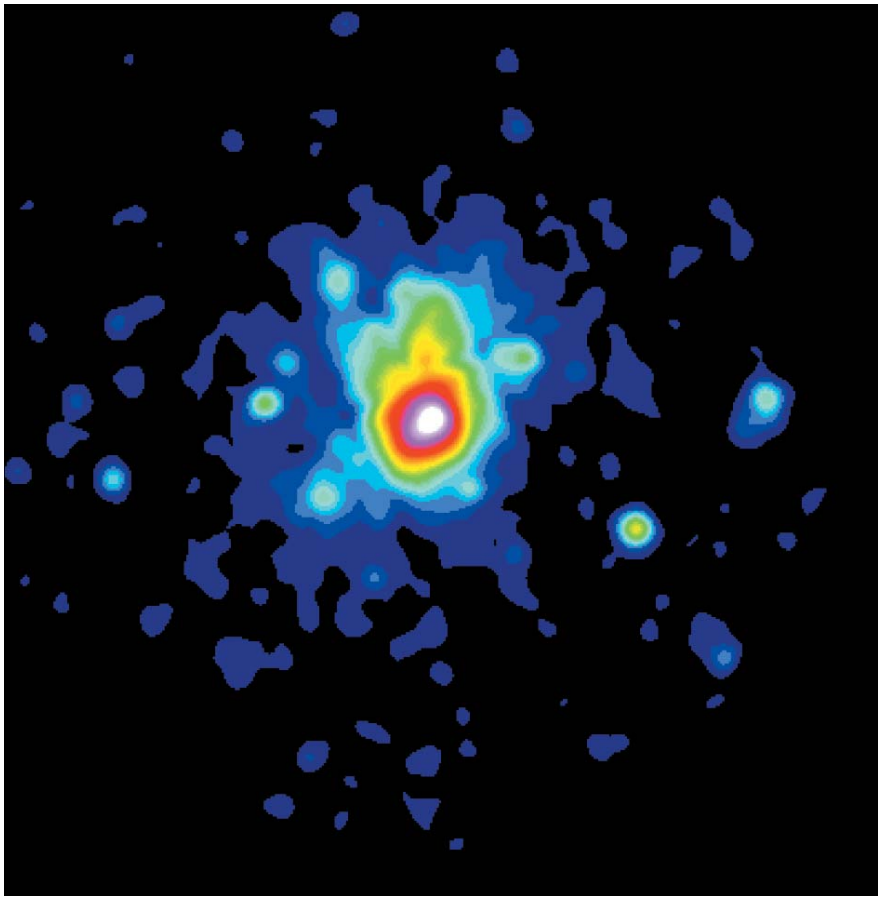

Figure 12: XMM-Newton EPN image of RXCJ1131.9-1955. The image was smoothed by a Gaussian filter with σ = 16 arcsec.

pearance of the cluster in one wavelength band its properties in the other. This would be very valuable for the many planned future surveys either in X-rays or the optical.

To extend this work to the study of star-formation rates as a function of galaxy and matter density in the cluster environment, a closer inspection of the dynamical state of clusters by comparison of optical velocity data and X-ray results, and a better understanding of the connection between the cluster structure and the large-scale structure filamentary network, we have proposed detailed spectroscopic studies with the forthcoming VIMOS instrument. Of the order of 2000 galaxy spectra could be obtained in less than one night, providing an unprecedented spectroscopic census of the galaxy population of the clusters and their surroundings almost into the dwarf regime. This in-depth study is bound to provide new insights into cluster as well as galaxy evolution.

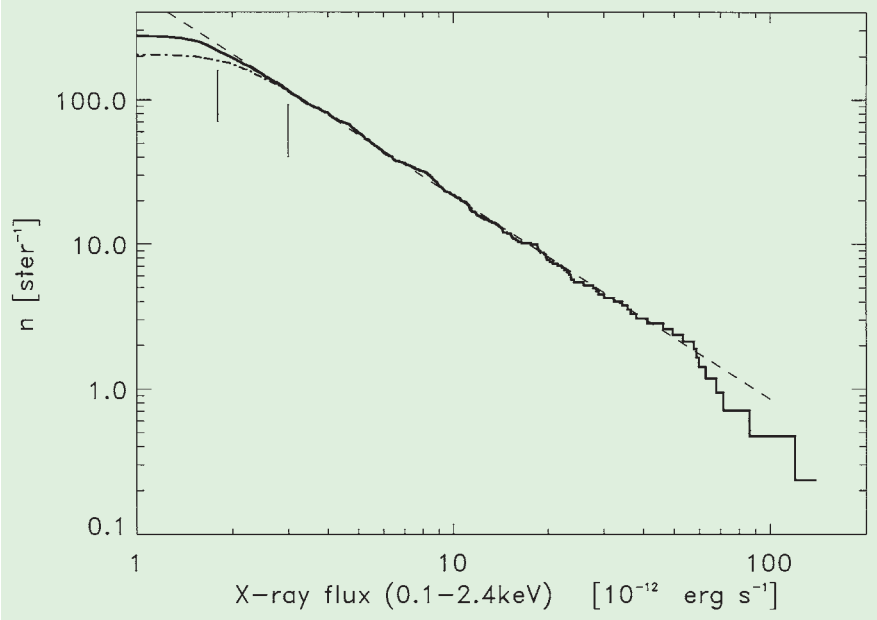

Figure 13: Number count sky density of the REFLEX II survey clusters and cluster candidates as a function of X-ray flux. The solid line gives the total list of clusters and still-to-observe cluster candidates, while the dashed line designates the confirmed clusters with redshifts. The thin line indicates a logarithmic slope of –1.4, the slope approximately expected for a complete sample. The two vertical bars indicate the flux limit of REFLEX and the prospected flux limit of REFLEX II, 1.8 · 10^{-12} erg s^{-1} cm^{-2}. Note, that a high completeness is still to be expected for REFLEX II flux limit.

7. Outlook

Having now well tested the reliability of the REFLEX catalogue by a series of investigations and having demonstrated its scientific value, not least by the studies described here, we are preparing the publication of the catalogue of the REFLEX I Survey as conducted within the frame of the ESO key programme "A Redshift Survey of Southern ROSAT Clusters of Galaxies" prospectively for January 2002. This survey is restricted to a flux limit well above the depth of the ROSAT All-Sky Survey which guarantees that clusters are still well characterised as X-ray sources. We have explored the value of a further extension of the REFLEX Survey and found that it is still possible to essentially preserve most of the sample quality while extending the flux limit from presently $3 \cdot 10^{-12}$ erg s^{-1} cm^{-2} to a value of $\sim 1.8 \cdot 10^{-12}$ erg s^{-1} cm^{-2}. This increases the sample from currently 452 to about 900 clusters providing a significantly higher precision for the measurement of large-scale structure and cosmological parameters. We have already embarked on this extension with the REFLEX II programme and so far conducted three further observing runs at the ESO 3.6-m telescope. A number count diagram of the clusters and cluster candidates is shown in Figure 13. It illustrates how little is left to complete the survey with a high degree of completeness. With about three further campaigns we can finish this extension project.

We could continue describing further important REFLEX-based studies. In particular the extended sample, taken together with NORAS, which will provide a denser sampling of the cluster distribution in space will allow us not only to improve the statistical measures of large-scale structure but also to look, for example for alignment effects, supercluster structure, and to attempt a three-dimensional reconstruction of the dark matter distribution. In addition the cluster catalogue will serve as a shopping list for many future studies of cluster physics.

References

Abell, G.O., 1958, *ApJS*, **3**, 211.

Abell, G.O., Corwin, H.G. & Olowin, R.P., 1989, *ApJS*, **70**, 1.

Andreani, P., Böhringer, H., Dall'Oglio, G., Martinis, L., Shaver, P., Lemke, R., Nyman, L.-A, Booth, R., Pizzo, L., Whyborn, N., Tanaka, Y., Liang, H., 1999, *ApJ*, **513**, 23.

Barone, L.T., Molinari, E., Böhringer, H., Chincarini, G., Collins, C.A., Guzzo, L., Lynam, P.D., Neumann, D.M., Reiprich, T.H., Schindler, S., Schuecker, P., 2000, in *Constructing the Universe with Clusters of Galaxies,* IAP 2000 meeting, Paris, France, July 2000, Florence Durret & Daniel Gerbal Eds., available on CD-Rom and at http://www.iap.fr/Conferences/Colloque/coll2000/contributions.

Bertin, e. & Arnouts, S., 1996, *A&A Suppl.*, **117**, 393.

Böhringer, H., Guzzo, L., Collins, C.A., et al., 1998, *The Messenger*, **94**, 21.

Böhringer, H., Voges, W., Huchra, J.P., Giacconi, R., Rosati, P., McLean, B., Mader, J., Schuecker, P., Simic, D., Komossa, S., Reiprich, T.H., Retzlaff, J., & Trumper, J., 2000, *ApJS*, **129**, 435.

Böhringer, H., Schuecker, P., Guzzo, L., et al., 2001, *A&A*, **369**, 826–850.

Böhringer, H., Collins, C.A., Guzzo, L.,Schuecker, P., Voges, W., Neumann, D.M., Schindler, S., DeGrandi, S., Chincarini, G., Cruddace, R.G., Edge, A.C., Shaver, P., 2002, *ApJ*, **566**, 1.

Collins, C.A., Guzzo, L., Böhringer, H., Schuecker, P., Chincarini, G., Cruddace, R., De Grandi, S., Neumann, D., Schindler, S., & Voges, W., 2000, *MNRAS*, **319**, 939.

Guzzo, L., Böhringer, H., Schuecker, P., et al. 1999, *The Messenger*, **95**, 27.

Lauer, T.R. & Postman, M., 1994, *ApJ*, **425**, 418.

Lynam, P.D., Collins, C.A., James, P.A., Böhringer, H., Neumann, D.M., 2002, *MNRAS*, to be submitted.

Reiprich, T.H. & Böhringer, H., 2002, *ApJ*, in press.

Schuecker, P., Böhringer, H., Guzzo, L., Collins, C.A., Neumann, D.M., Schindler, S., Voges, W., Chincarini, G., Cruddace, R.G., De Grandi, S., Edge, A.C., Muller, V., Reiprich, T.H., Retzlaff, J., & Shaver, P., 2001a, *A&A*, **368**, 86.

Schuecker, P., Böhringer, H., Reiprich, T.H., Feretti, L., 2001b, *A&A*, in press.

Tucker, W. H., Tananbaum, H., Remillard, R. A., 1995, *ApJ*, **444**, 532.

Tucker, W., Blanco, P., Rappoport, S., David, L., Fabricant, D., Falco, E. E., Forman, W., Dressler, A., Ramella, M., 1998, *ApJ*, **496**, 5.

Catching the Sounds of Stars

ASTEROSEISMOLOGY, THE RIGHT TOOL TO UNDERSTAND STELLAR INTERIORS

F. BOUCHY, F. CARRIER

Contact e-mail: francois.bouchy@obs.unige.ch
Observatoire de Genève, Switzerland

1. Why Measure Stellar Acoustic Oscillations?

The physics of stellar interiors is poorly known. There are serious uncertainties about the modelling of the inner structure and about the stellar evolution. The main problem is the lack of observational constraints. We have usually only two observables: the effective temperature and the luminosity. In some cases, the detailed analysis of the spectrum allows us to determine surface abundances and to estimate surface gravity. However, all these observables trace only the physical conditions prevailing in a thin layer of the stellar internal structure, the photosphere. Masses and radius are known for a limited number of double systems. As a consequence, the stellar internal structure and the evolution theory is not well tested.

Geologists learn about the inner structure of our planet by monitoring how seismic waves generated by earthquakes propagate through the Earth. In a way, they show us the method needed to study the inside of a star. By chance almost every star undergoes perturbations that generate seismic waves (see Fig. 1). The principle is to detect and measure seismic oscillation modes of a star in order to understand its inner structure.

2. Acoustic Spectrum of Solar-like Stars

The discovery of the propagating sound waves in the Sun by Leighton et al. (1962) and their interpretation by Ulrich (1970) has opened a new area in stellar physics. Since the Sun is a sphere of hot gas, its interior transmits acoustic waves very well. Convection near the stellar surface produces vigorous turbulent flows that generate a broad spectrum of random acoustical waves. The process of destructive and constructive interferences transforms this random convective noise into a very rich acoustic spectrum in the subaudible domain with periods of few minutes (see Fig. 2). The resulting oscillations are pressure waves, also called p-modes. Each acoustic eigenmode is trapped in a spherical-shell cavity between the stellar surface and a specific inner layer. Frequencies and amplitudes of these oscillation modes depend on the physical conditions prevailing in the layers crossed by the waves and provide a powerful seismological tool. Helioseismology led to major revisions in the "standard model" of the Sun and provided for instance measures of the sun's inner rotation, the size of the convective zone and the structure of the external layers.

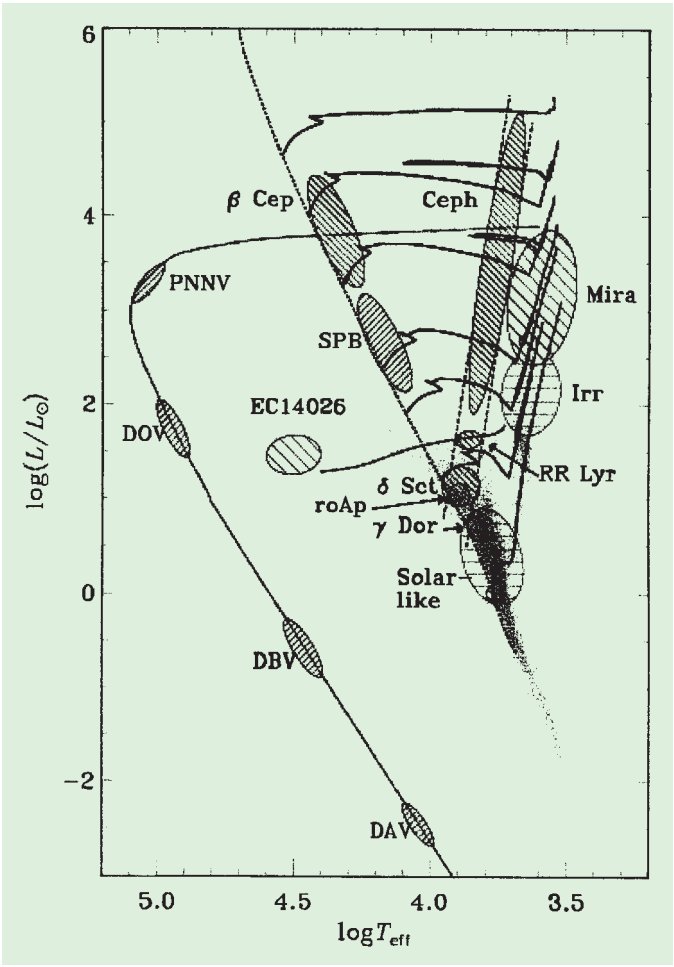

Figure 1: Schematic location of classes of pulsating stars in the HR diagram. Solar-like stars correspond to stars with intermediate masses near the main sequence. This class undergoes nonradial oscillations generated by the stochastic excitation of their outer convective zone.

Each oscillation mode can be characterised by the two quantum numbers *n* and *l* which are respectively the radial order (see footnote number 1) and the angular degree (see footnote number 2) of modes. In stars where the disk is not resolved, it is only possible to measure the lowest-degree modes ($l \leq 3$). Fortunately, these modes are especially interesting because they penetrate more deeply into the stellar interior and probe the physical conditions near the stellar core. The p-mode oscillations produce a characteristic comb-like structure in the power spectrum with mode frequencies $\nu_{n,l}$ well approximated by the asymptotic relation:

$$\nu_{n,l} = \Delta\nu_0(n + l/2 + \epsilon) - l(l+1)\delta\nu_0/6$$

The parameters $\Delta\nu_0$, ε and $\delta\nu_0$ are related to the stellar structure. The large separation $\Delta\nu_0$ reflects the average stellar density while ε is related to the physical conditions at the boundaries of the acoustic cavity and therefore it is sensitive to physical conditions in the surface layers. The small separation $\delta\nu_0$ depends on the mean molecular weight down to the central regions of the star and it is thus an indicator of the stellar age. A considerable advantage of the asteroseismology comes from the fact that the measurement of the frequencies $\nu_{n,l}$ and their amplitudes A_{osc} allows to constrain directly the internal structure of models independently of any intermediate steps like radiation transfer in the atmosphere or photometric calibrations.

The oscillation characteristics of solar-like stars are expected in first approximation to scale from solar values (Kjeldsen & Bedding 1995) as a func-

[1]Number of nodes in the radial direction.
[2]Number of nodes around a circumference.

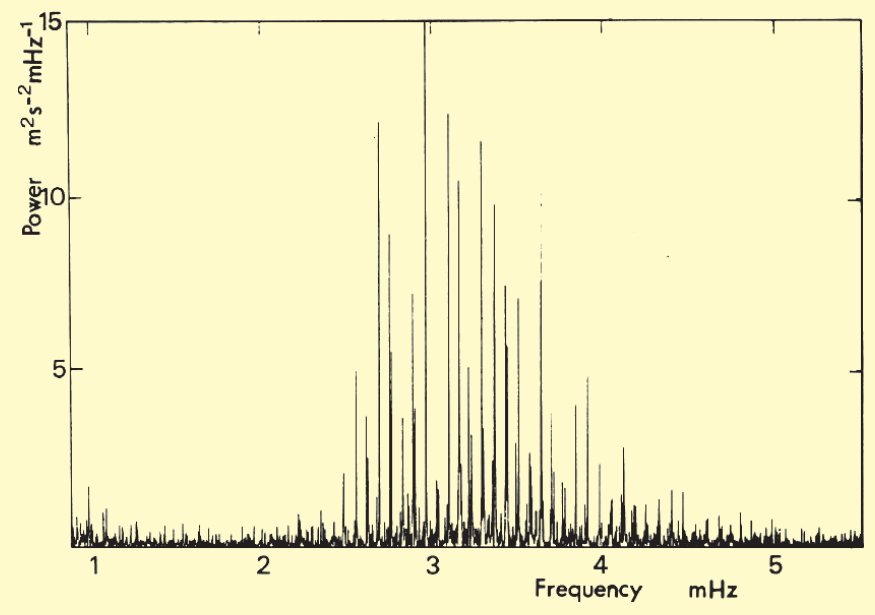

Figure 2: Acoustic spectrum of the full solar disk (Grec et al. 1983) showing the presence of several tens of eigen frequencies with periods in the range 3 to 8 minutes. The individual Doppler amplitudes of these acoustic modes are lower than 25 cm s^{-1}.

tion of the stellar luminosity (or radius), mass and temperature according to:

$$A_{osc} = \frac{L/L_\odot}{M/M_\odot} 23.4\ cm\ s^{-1},$$

$$\nu_{max} = \frac{M/M_\odot}{(R/R_\odot)^2 \sqrt{Teff/5777K}} 3.05\ mHz,$$

$$\Delta\nu_0 = \frac{(M/M_\odot)^{1/2}}{(R/R_\odot)^{3/2}} 134.9\ \mu Hz.$$

Solar-like oscillation modes generate periodic motions of the stellar surface (see Fig. 3) with periods in the range 3–30 mn but with extremely small amplitudes. Essentially two methods exist to detect such a motion: photometry and Doppler spectroscopy. In photometry, the amplitudes of the oscillation of solar-like stars are in the range 2–20 ppm (see footnote number 3) while they are in the range 10–100 cm s^{-1} in radial velocity measurements. Photometric measurements made from ground are strongly limited by scintillation noise. To reach the needed accuracy it actually requires measurements made from space. The accuracy of Doppler spectroscopy has recently been improved, mostly driven by intensive search for extra-solar planet programmes. Actually they have reached the accuracy needed to detect p-mode oscillations from the ground on bright solar-like stars.

[3]Part per million or 10^{-6} L where L is the stellar luminosity.

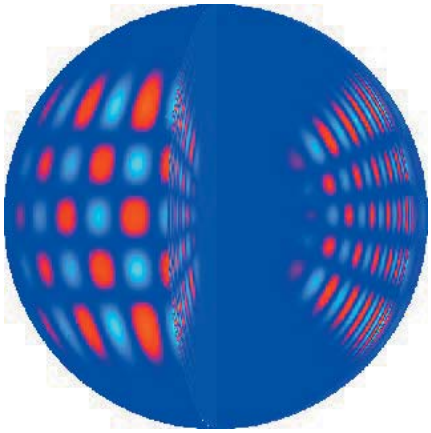

Figure 3: Representation of resonating acoustic waves in the interior of a solar-like star. Red and blue colours show the displacement of elements in opposite directions.

3. Listen to Solar-like Stars by Precise Doppler Measurements

The detection of acoustic oscillations of stars needs long and intensive sequences of high-precision radial velocity measurements. In order to reach a precision of few m s^{-1} one needs first high flux and enough spectral information to compute the radial velocity without being limited by photon noise. Second, a stable wavelength reference is necessary to measure and to correct systematic errors of the spectrograph. The photon noise limit depends on the wavelength spectral range and on the spectral resolution of the spectrograph. It depends as well on the spectral type and the rotational broadening *v* sin *i* (see footnote number 4) of the star. A detailed analysis of the fundamental photon noise limit on radial velocity measurements can be found in Bouchy et al. (2001). For illustration, Figure 4 shows the expected radial velocity errors with the high-resolution echelle spectrograph CORALIE (Queloz et al. 2001) for a 100 s exposure time on a 5th-magnitude star versus effective temperature and rotational broadening.

Essentially two different methods can be used to gather precise Doppler measurements (see Fig. 5). Both mon-

[4]Equatorial stellar velocity projected on the line of sight causing Doppler broadening of the stellar lines.

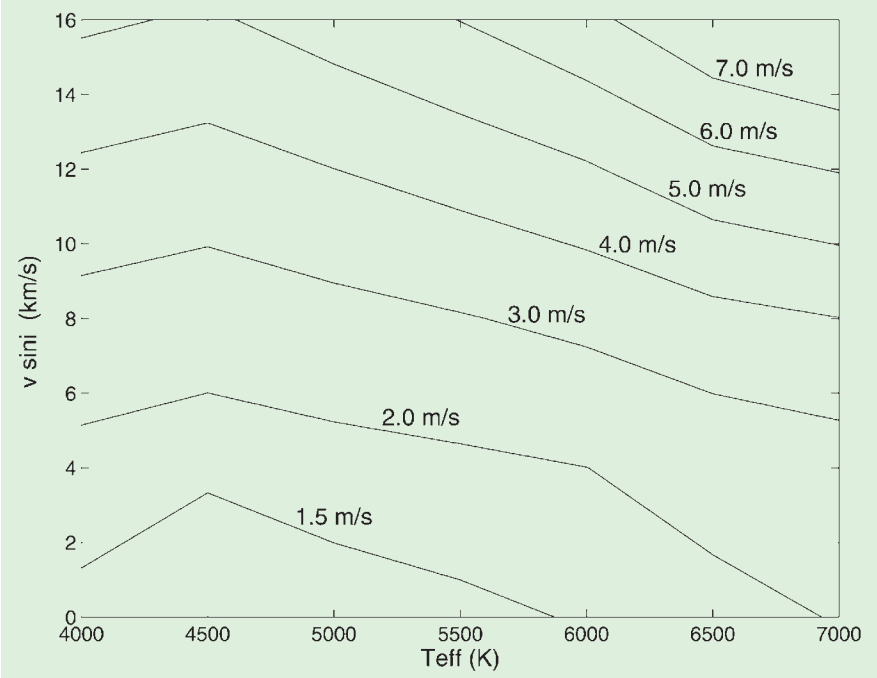

Figure 4: Radial velocity uncertainty predictions for the spectrograph CORALIE for a flux given by t_{exp} (s) = 2.512^{mv}. This spectrograph, installed on the Euler 1.2-m telescope, covers a spectral range of 3000 Å with a resolution of 50,000 and a total efficiency peak of 1.5%.

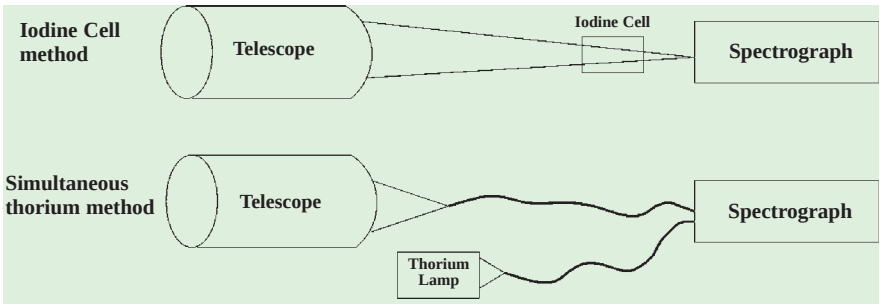

Figure 5: The different methods of radial velocity measurements.

itor instrumental changes by comparison with a set of stable reference lines. One method, called the Iodine cell method, inserts in the input stellar beam an iodine cell to impress stable absorption lines on the incoming starlight. Another method, called the simultaneous thorium method, uses an optical fibre for the star light, in conjunction with a second fibre carrying light from a thorium lamp. A variant consists in replacing the thorium lamp by a fixed Fabry-Perot interferometer illuminated by a white lamp. Both methods have recently shown precision of only few m s^{-1}. However, although very reliable, the iodine cell approach increases the photon noise errors by limiting the spectral range to about 1000 Å and reducing the total efficiency by a factor of ~ 2. Hence, for a given photon noise limit, this technique requires telescopes at least 2 times larger than for an instrument using the simultaneous thorium method.

Figure 6: α Cen A is the brightest star of the picture. One can see the Southern Cross on the left.

Even if the precision of individual measurements of the radial velocity is greater than 1 m s^{-1}, periodic Doppler variations as small as 10 cm s^{-1} can be detected if a large amount of measurements is made. The relation between mean noise level in the power spectrum σ_{PS} and the dispersion of the time series Doppler measurements σ_{obs} is given by:

$$\sigma_{PS} = \frac{4\,\sigma_{obs}^2}{N},$$

where *N* is the number of measurements. If the noise is Gaussian then the mean noise level in the amplitude spectrum σ_{amp} *is* given by:

$$\sigma_{amp} = \sqrt{\frac{\pi\,\sigma_{PS}}{4}}.$$

For example, 400 measurements with 2 m s^{-1} precision allow us to reach a noise level in the amplitude spectrum of 18 cm s^{-1}.

The difficulty is not only to reach a high signal-to-noise level but to have a sufficiently long duration of observation to resolve and to characterise the eigen frequencies with sufficient accuracy. For example, in the Sun, the small separation $\delta\nu_0$ is equal to about 9 μHz. The solar oscillation modes are broadened by their limited lifetime (few days) and have a typical mean width of about 2 μHz. For these reasons, one needs frequency resolution at least equal to 2 μHz to characterise the acoustic modes with accuracy. This implies a duration of observation at least equal to 6 nights.

With single-site observations, the identification of oscillation modes can be complicated by the observation window limited by the diurnal cycle. Each mode in the power spectrum presents the day aliasings at 11.57 μHz. In order to improve the spectral window and reduce these aliases, it is useful to realise multi-longitude observations as they already exist for helioseismology (IRIS, BiSON, GONG, see Pallé 1997).

4. Recent Progress in Solar-like Seismology

Many attempts to detect signature of p-mode oscillations on solar-like stars have been made since the 1980's. Until 1999, they reached only upper limits or the detections were not very reliable.

The first good evidence of excess power due to mode oscillations was obtained by Martic et al. (1999) on the F5 subgiant Procyon. Bedding et al. (2001) obtained a quite similar excess power on the G2 subgiant β Hyi, an evolved solar-mass star that corresponds to the future evolution of the Sun. These two results have been confirmed independently by our group based on observations made with the CORALIE spectrograph (Carrier et al. 2001a, 2001b).

A primary and challenging target for the search for p-mode oscillations was the nearby solar twin Rigil Centaurus (α Cen A). In May 2001, we made for the first time on this star an unambiguous detection of solar-like acoustic modes (Bouchy & Carrier 2001; Carrier et al. 2001c). The observations and analysis are presented in the next section.

The main parameters of these three stars, Procyon, β Hyi and α Cen *A,* and the characteristic of their observed seismic signal are reported in Table 1 and are compared with the Sun.

The seismic parameters of these three stars are in agreement with the expected values scaled from the Sun. So far the low signal to noise obtained and the day aliasings coming from the single-site window function have not allowed to identify modes on Procyon and β Hyi. On α Cen A, the high signal to noise obtained and the fact that modes are more separated in frequency and less sensible to the day aliasings, allow to identify them.

Table 1: Main parameters of the solar-like stars where seismological signal was obtained.

	Sun	α CMi HR2943	β Hyi HR98	α Cen A HR5459
Spectral type	G2V	F5IV-V	G2IV	G2V
mv	–27	0.34	2.80	0.0
T_{eff} (K)	5777	6530	5800	5780
L/L_θ	1	7.1	3.5	1.5
M/M_θ	1	1.5	1.1	1.12
A_{osc} (cm s^{-1})	23.4	50	50	31
ν_{max} (mHz)	3.05	1	1.1	2.3
$\Delta\nu_0$ (μHz)	134.9	55	58	105.5
$\delta\nu_0$ (μHz)	9	–	–	6.6

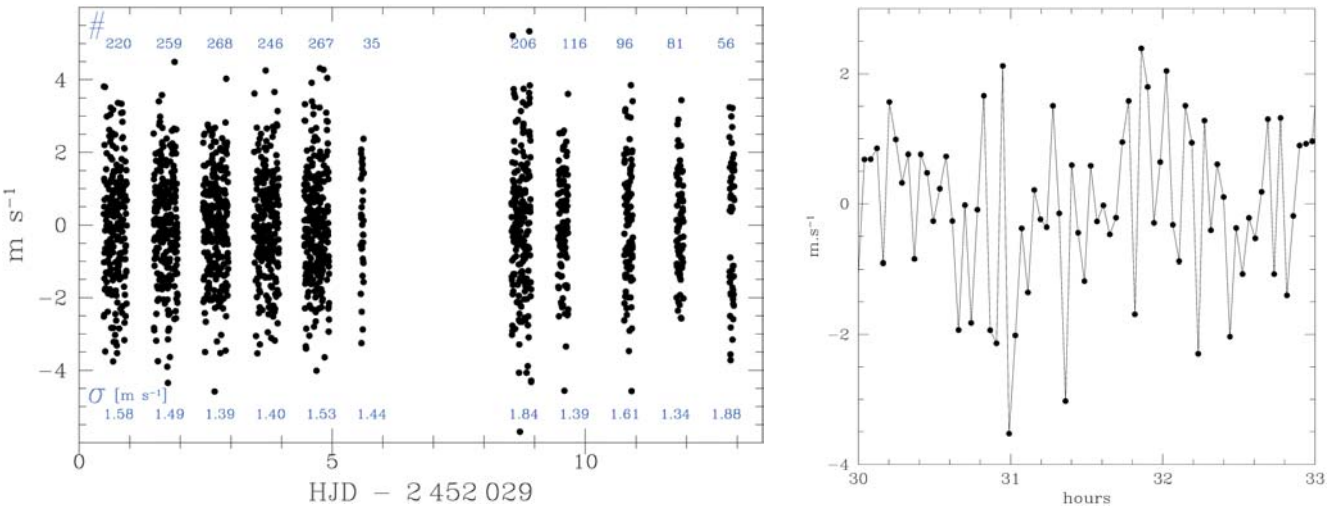

Figure 7: Left: Radial velocity measurements of the star α Cen A. A 3-order polynomial fit subtraction was applied on each night. The number of Doppler measurements and their dispersion are indicated for each night. Right: Portion of 3 hours of the radial velocity measurements obtained during the third night. On this part the dispersion reaches 1.25 m s⁻¹.

5. Acoustic Waves in Solar-twin α Cen A

5.1 Observations

The star α Cen A (see Fig. 6) was observed with the CORALIE fibre-fed echelle spectrograph (Queloz et al. 2000) mounted on the 1.2-m Swiss telescope at the ESO La Silla Observatory. CORALIE is the southern hemisphere twin of the ELODIE spectrograph (Baranne et al. 1996), both of them well known for their discoveries of extra-solar planets. The wavelength domain ranges from 3875 to 6820 Å recorded on 68 orders. Using a 2k by 2k CCD with 15-μm pixels, CORALIE reaches a spectral resolution of 50,000 with 3-pixel sampling. The total efficiency including atmosphere, telescope, spectrograph and detector reaches about 1.5% at 5500 Å in the best seeing case. During stellar exposures, the spectrum of a thorium lamp carried by a second fibre is simultaneously recorded in order to monitor the spectrograph instability and thus to obtain high-precision velocity measurements.

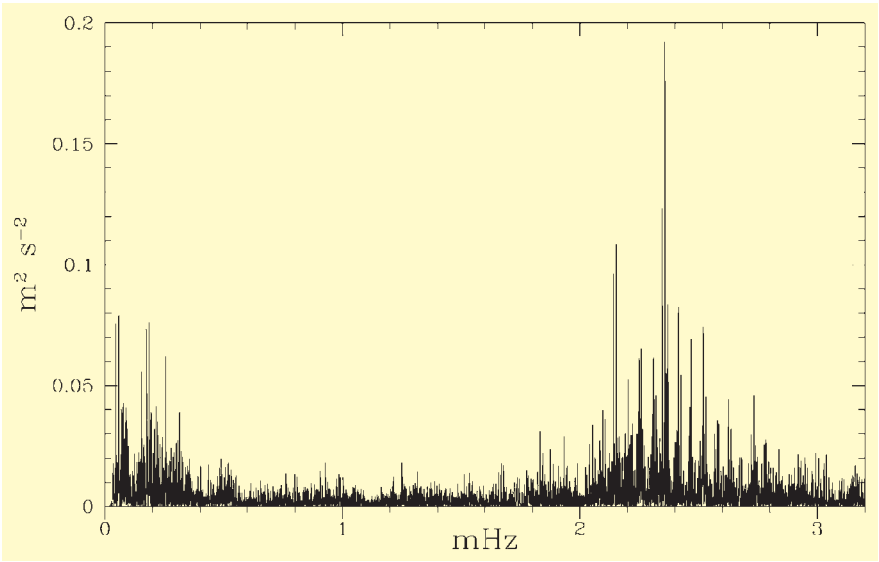

Figure 8: Power spectrum of 13 nights of radial velocity measurements of the star α Cen A. The series of peaks between 1.8 and 2.9 mHz is the unambiguous signature of solar-like oscillations.

α Cen A was observed over 13 nights in May 2001. Exposure time was 40 s, with a dead time of 110 s between exposure. In total, 1850 spectra were collected with typical signal-to-noise ratio

Table 2: Mode frequencies (in μHz). The frequency resolution of the time series is 0.9 μHz. The last row shows the average large spacing $\Delta\nu_{n,l} = \nu_{n,l} - \nu_{n-1,l}$ computed for l = 0, 1 and 2.

	l = 0	l = 1	l = 2
n = 15			1833.0
n = 16	1841.2	1887.2	1935.0
n = 17		1991.9	2041.5
n = 18		2095.6	2145.9
n = 19	2152.8	2202.8	2251.3
n = 20	2258.3	2308.9	2358.3
n = 21	2364.2	2414.2	2464.1
n = 22	2470.0	2519.3	2568.5
n = 23	2573.2	2625.5	2672.2
n = 24	2679.7	2733.0	2782.9
n = 25		2837.4	
$\Delta\nu_0$	105.4 ± 0.5	105.6 ± 0.4	105.5 ± 0.8

Table 3: Upper panel: Observational constraints adopted for the calibration of models. Lower Panel: Global characteristics derived from the calibrated models.

Models	A_{BV}, A_{ov} & A_{CM}	A_{GD}
$M/M_\odot$	1.16 ± 0.031	1.1015 ± 0.008
T_{eff} [K]	5790 ± 30	5770 ± 50
log *g*	4.32 ± 0.05	4.28 ± 0.02
$[\frac{Fe}{H}]_i$	0.20 ± 0.02	0.22 ± 0.02
$L/L_\odot$	1.534 ± 0.103	1.572 ± 0.135

Models	A_{BV}	A_{ov}	A_{CM}	A_{GD}
t [*Myr*]	2710	3530	4086	5640
Y_i	0.284	0.279	0.271	0.300
$(\frac{Z}{X})_i$	0.0443	0.0450	0.0450	0.0480
α	1.53	1.64	0.96	1.86

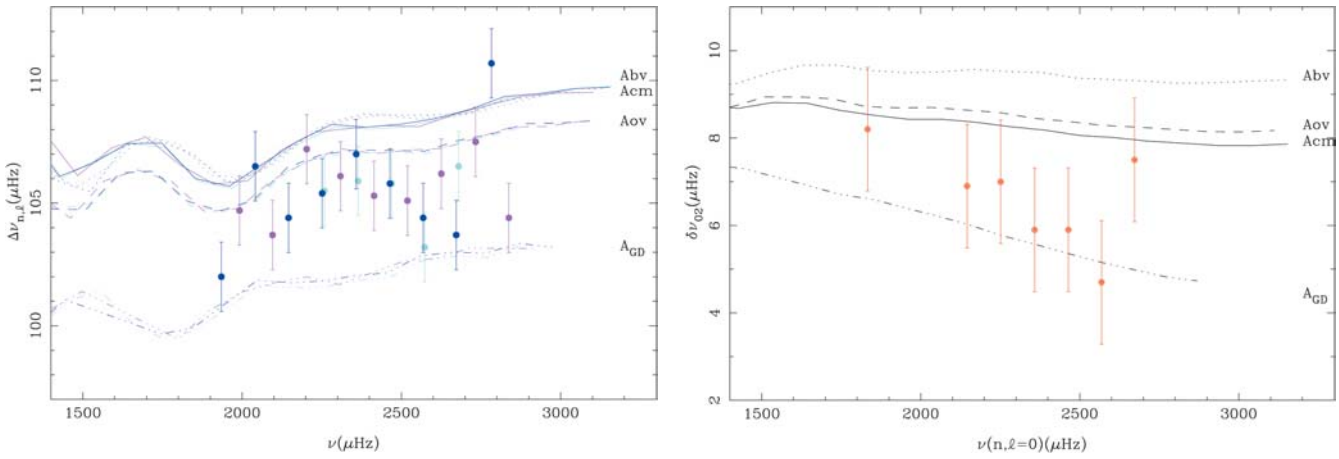

Figure 9: Left: Variations of the large spacing between modes of consecutive radial order $\Delta\nu_{n,l} = n_{n,l} - \nu_{n-1,l}$ for p-modes of degree l = 0 (light blue line), l = 1 (purple line) and l = 2 (dark blue line) versus frequency. Right: Variations of the small frequency spacing $\delta\nu_{02} = \nu_{n,0} - \nu_{n-1,2}$ versus frequency.

in the range 300–420 at 550 nm. The data reduction, based on the optimum-weight procedure, is described in Bouchy et al. (2001). The resulting velocities are presented in Figure 7. The dispersion of these measurements reaches 1.53 m s^{-1}. The photon noise uncertainties coming from the stellar spectrum and from the simultaneous thorium spectrum used in the instrumental tracking are typically the same and equal to 0.50 m s^{-1}. The quadratic sum of these two photon noise contributions is 0.70 m s^{-1}.

5.2 Acoustic spectrum analysis

The power spectrum shown in Figure 8 exhibits a series of peaks between 1.8 and 2.9 mHz modulated by a broad envelope. This is the typical signature of solar-like oscillations and can be compared with the acoustic spectrum of the Sun in Figure 2.

Toward the lowest frequencies (ν < 0.6 mHz), the power rises and scales inversely with frequency squared as expected for instrumental instabilities. The mean white noise level σ_{PS}, computed in the range 0.6–1.5 mHz reaches 2.39 × 10^{-3} m^2 s^{-2}, namely 4.3 cm s^{-1} in amplitude. This noise level corresponds to a velocity accuracy of 1.05 m s^{-1} which is to be compared with the estimated photon noise uncertainty of about 0.70 m s^{-1}. The average amplitude of the highest modes is estimated in the range 29–33 cm s^{-1}.

The strongest identified modes are listed in Table 2. The values of *n* and *l* are deduced from the asymptotic relation with parameter ε estimated to 1.41.

The average large and small spacing are deduced from this table:

$$< \Delta\nu_0 > = < \nu_{n,l} - \nu_{n-1,l} > = 105.5 \pm 0.3\ \mu Hz,$$

$$< \delta\nu_0 > = < \nu_{n,0} - \nu_{n-1,2} > = 6.6 \pm 0.4\ \mu Hz.$$

The modes corresponding to *l* = 3 are expected to be separated by about 11 μHz to the modes *l* = 1. This expected separation is near the day aliasing at 11.57 μHz and explains why they cannot be identified.

5.3 Astrophysical interpretation

The variation with the frequency of the large and small spacings obtained from our observations are compared in Figure 9 with the values deduced from three models developed by Morel et al. (2000) (A_{BV}, A_{ov} and A_{CM}) and one model developed by Guenther & Demarque (2000) (A_{GD}) The observational constraints for the model calibrations and the properties of the calibrated models are given in Table 3. The two sets of models differ essentially by the estimated mass and the age of the star.

For α Cen A, our observations clearly suggest a model with properties intermediate between the two sets of models, i.e. a mass near 1.13 $M_\odot$. The age of αCen A seems to be close to 5 Gyr. New models of α Cen A are presently developped by the OCA team (Provost, Berthomieu, Morel and Thevenin) with different properties in order to better interpret the observed oscillations.

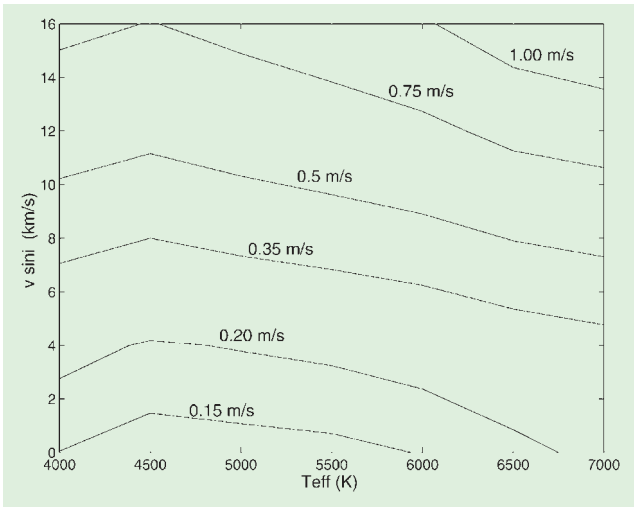

Figure 10: Radial velocity uncertainty predictions for the spectrograph HARPS for a flux given by t_{exp} (s) = 2.512^{mv}. This spectrograph, installed at the ESO 3.6-m telescope, covers a spectral range of 3000 Å with a resolution of 90,000 and a total efficiency peak of 4.5%.

6. Future Prospects with ESO Instruments

This result on a Cen A demonstrates the power of the simultaneous thorium radial velocity method and shows that Doppler asteroseismology can be further developed from the ground. With the CORALIE spectrograph installed on a small 1.2-m telescope, we are limited to observe targets brighter than 3rd or 4th magnitude. But ESO has developed and develops spectrographs fully adapted for Doppler asteroseismology.

The FEROS spectrograph based on the 1.52-m telescope at La Silla observatory has recently shown its capability to obtain high-precision radial velocity measurements (Setiawan et al. 2000) with the simultaneous thorium method. Considering its very high efficiency, the estimated gain is 2 magnitude compared to CORALIE.

The state of the art will be the future spectrograph HARPS (High Accuracy Radial velocity Planetary Searcher) which will be installed on the 3.6-m ESO telescope at La Silla observatory (Queloz et al. 2001). This instrument is optimised and dedicated to high-precision radial velocity measurements and it is designed to reach 1 m s^{-1} precision. A detailed photon noise study for HARPS can be found in Bouchy et al. (2001). The expected radial velocity errors due to the photon noise for a 100 s exposure time on a 5th-magnitude star

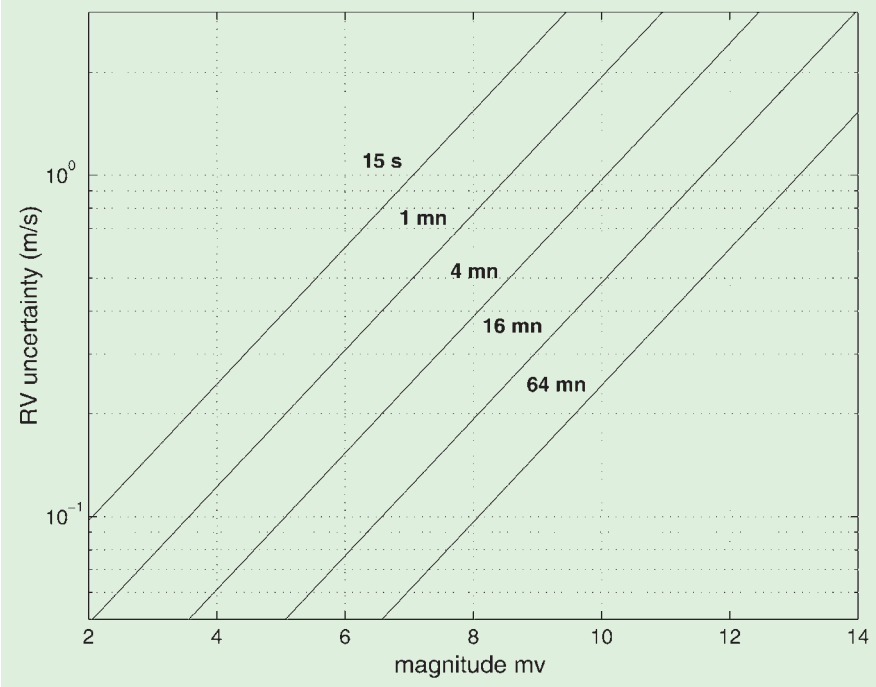

Figure 11: Radial velocity uncertainty predictions for HARPS versus magnitude for a star spectrum with T_{eff} = 4500 K and v sin i = 0 km s^{-1}.

is presented in Figure 10 versus effective temperature and rotational broadening. Figure 11 shows the photon noise uncertainty versus stellar magnitude for the best stellar case (T_{eff} = 4500 K, *v* sin *i* = 0 km s^{-1}) for various exposure times. This quantity is less than 1 m s^{-1} for exposure time of 1 mn on stars with magnitude lower than 8. Typically, a gain of 5 magnitudes is expected compared to CORALIE.

UVES (Ultraviolet and Visual Echelle Spectrograph) is a cross-dispersed echelle spectrograph located at the second Unit Telescope of the 8.2-m ESO VLT. FLAMES (Fibre Large Array Multi Element Spectrograph) is a VLT large-field fibre facility that consists of several components, including a fibre link to the UVES spectrograph. The light is collected at the Nasmyth focus through 8 fibres in a usable field of up to 25 arcmin in diameter. Considering that one fibre is used for the simultaneous Thorium spectrum, 7 objects can be simultaneously measured with UVES. The photon-noise study for HARPS has been extrapolated to UVES and shows a gain between 1 and 2 magnitudes.

All these prospects show that Doppler ground-based asteroseismology will undergo intensive developments these next years and will be able to enlarge our understanding on stellar physics.

Acknowledgements

We would like to thank M. Mayor who encourages our programme and gives us time allocation at the Euler Swiss telescope. D. Queloz and all people associated with the CORALIE and HARPS projects are acknowledged for their help and for ongoing discussions and helpful comments.

References

Baranne, A., Queloz, D., Mayor, M., et al., 1996, *A&ASS*, **119**, 373.

Bouchy, F., & Carrier, F., 2001, *A&A*, **374**, L5.

Bouchy, F., Pepe, F., Queloz, D., 2001, *A&A*, **374**, 733.

Bedding, T.R., Butler, R.P., Kjeldsen, H., et al., 2001, *ApJ*, **549**, L105.

Carrier, F., Bouchy, F., Kienzle, F., & Blecha, A., 2001a, IAU 185, ASP Conf. Ser., in press.

Carrier, F., Bouchy, F., Kieuzle, F., et al., 2001b, *A&A*, **378**, 142.

Carrier, F., Bouchy, F., Provost, J., et al., 2001c, IAU 185, ASP Conf. Ser., in press.

Grec, G., Fossat, E., Pomerantz, M.A., 1983, *Solar Physics*, **82**, 55.

Guenther, D.B., & Demarque, P., 2000, *ApJ*, **531**, 503.

Kjeldsen, H., & Bedding, T., 1995, *A&A*, **293**, 87.

Leighton, R.B., Noyes, R.W., & Simon, G.W., 1962, *ApJ*, **135**, 474.

Martic, M., Schmitt, J., Lebrun, J.-C., et al., 1999, *A&A*, **351**, 993.

Morel, P., Provost, J., Lebreton, Y., et al., 2000, *A&A*, **363**, 675.

Pallé, P., 1997, Proc. IAU Symp. 181, Provost & Schmider (eds), 15.

Queloz, D., Mayor, M., Weber, L., et al., 2000, *A&A*, **354**, 99.

Queloz, D., Mayor, M., et al., 2001, *The Messenger*, **105**, 1.

Setiawan, J., Pasquini, L., da Silva, L., et al., 2000, *The Messenger*, **102**, 13.

Ulrich, R.K., 1970, *ApJ*, **162**, 993.

Discovery of Lead Stars with the ESO 3.6-m Telescope and CES

S. VAN ECK (Institut d'Astronomie et d'Astrophysique, Université Libre de Bruxelles), svaneck@astro.ulb.ac.be

S. GORIELY and A. JORISSEN (Institut d'Astronomie, Bruxelles), and B. PLEZ (GRAAL, Montpellier)

1. The Synthesis of Elements Heavier than Iron in Stars

In a seminal paper, Burbidge et al. (1957) lay the foundations of our understanding of the origin of the elements heavier than iron: these elements cannot be formed by the mainstream nucleosynthesis processes feeding the stellar energy. They require instead that pre-existing seed nuclei, like the abundant iron-group elements, form heavier and heavier nuclei by successive captures of neutrons. In this neutron-capture chain, unstable nuclei are formed. Depending on the respective time scales for β-decay and neutron-capture (respectively τ_β and τ_n), the neutron-capture process will either be dubbed slow (s-process: $\tau_\beta < \tau_n$) or rapid (r-process: $\tau_\beta > \tau_n$). The r-process occurs during the supernova event, and is able to produce heavy elements up to the actinides (Th, U). These actinides are injected into the interstellar medium by the supernova remnant, and are subsequently incorporated into the next

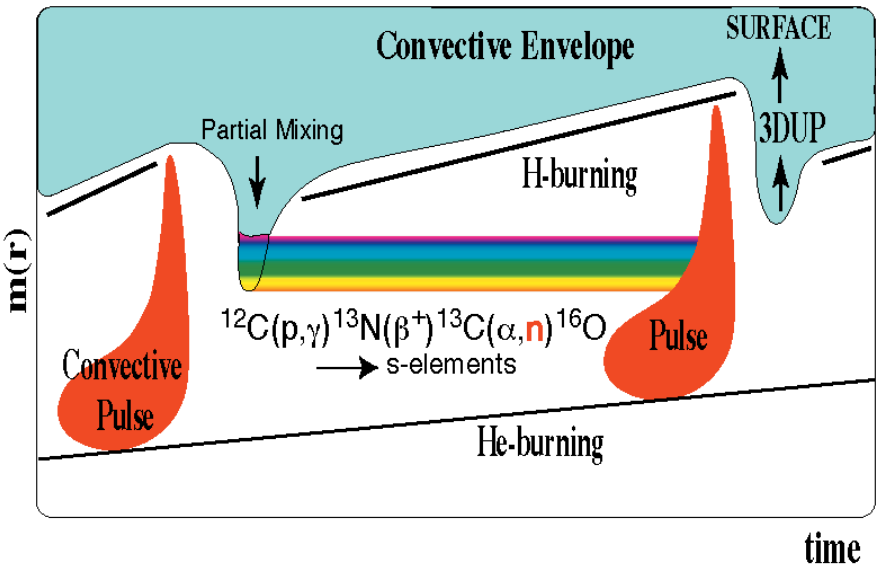

Figure 1: Temporal evolution of the structure of the intershell region of an AGB star, sketching the partial proton mixing in the He intershell zone, and the subsequent s-process nucleosynthesis occurring in the region depicted with rainbow colours.

generation of stars, at the surface of which they may be observed. A success in that story has recently been achieved by a member of this team (BP) who reported the detection of Uranium in the atmosphere of a very metal-poor star using UVES (Cayrel et al. 2001).

The s-process operates in stars either during core He-burning in massive stars (Prantzos et al. 1987) or during the asymptotic giant branch (AGB) phase in the evolution of low- and intermediate-mass stars (e.g., Gallino et al. 1998). At that phase, stars develop a complex structure, consisting of a degenerate core, H- and He-burning layers, and a deep convective envelope (Fig. 1). The double-shell structure is thermally unstable, with a thermal runaway ('thermal pulse') occurring recurrently in the He-burning layer. The energy liberated by this thermal pulse disturbs the envelope, which then relaxes through a temporary deepening of its lower boundary. The convective envelope then penetrates the intershell region where He-burning operated in a convective pocket associated with the thermal pulse (Fig. 1). With this mixing process, called the 'third dredge-up' (3DUP), elements produced in the intershell zone are brought into the convective envelope, and hence become visible at the stellar surface. Carbon stars are formed in this way during the AGB.

Neutrons may possibly be produced in this context through the reaction chain $^{12}C(p,\gamma)^{13}N(\beta)^{13}C(\alpha,n)^{16}O$ if protons from the hydrogen shell can be partially mixed downward into the intershell zone enriched in ^{12}C from the former thermal pulse.

Recent studies (Herwig et al. 1997, Langer et al. 1999) have suggested that the transport processes accompanying the 3DUP could induce the required partial mixing of protons (PMP).

Although this scenario is nowadays the most widely accepted one, its main ingredient (the partial mixing of protons in the deep carbon-rich layers) cannot yet be derived from first physical principles due to the difficulties inherent to the description of convection, diffusion or rotational transport in 1-D models.

It is therefore of prime importance to devise predictions that may test this proton mixing scenario against abundance observations. Although the presence of the unstable element Tc (whose isotope ^{99}Tc is produced by the s-process and has a half life of only 2.1×10^5 y) at the surface of S stars (e.g., Van Eck & Jorissen 1999) clearly indicates that the s-process takes place in these AGB stars, it does not provide strong constraints on its detailed operation. A more stringent prediction, expressed by Goriely & Mowlavi (2000ab), is that low-metallicity AGB stars should exhibit large overabundances of Pb-Bi as compared to lighter s-elements. This is because at low metallicities the pre-existing seed nuclei are comparatively less abundant, so that the available neutrons are then numerous enough to convert all the seed nuclei into Pb and Bi. Within the PMP scenario, the prediction that [Pb/s] should be large (where $[A/X] \equiv \log(N_A/N_X) - \log(N_A/N_X)_\odot$, and s stands for any element produced by the s-process) is found to be quite robust with respect to the model parameters (like the abundance profile of the protons in the partially mixed layers, or the extent of the partial mixing zone) and uncertainties (e.g., reaction rates). All s-process enriched AGB stars with metallicities $[Fe/H] \leq -1.3$ are thus predicted to be 'Pb stars' (Goriely & Mowlavi 2000a), independently of their mass or metallicity (provided the partial mixing of protons takes place). 'Pb stars' are characterised not only by large [Pb/Fe] and [s/Fe] abundance ratios, but also by large [Pb/s] abundance ratios. In particular, [Pb/hs] (where hs denotes the so-called heavy s-process elements such as Ba, La or Ce) ratios as large as 1.5 are predicted by Goriely & Mowlavi (2000a) in AGB stars with $[Fe/H] \leq -1.3$.

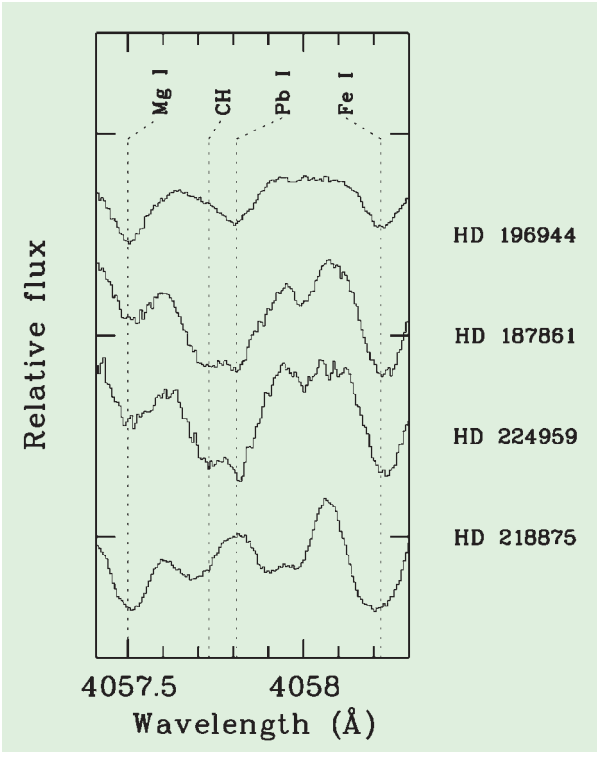

Figure 2: The CES spectra were obtained with the medium-resolution image slicer and the thinned, back-side illuminated CCD#61 (EEV, 2K × 4K pixels) yielding a resolution of 135,000; exposure times lie in the range 1 h 30 to 2 h 30. Note how strong the Pb I λ405.781 nm line is in the three CH stars. It is absent in the comparison R star HD 218875 (lower spectrum).

2. Observations: A Success Story

With this prediction about the existence of Pb stars in hand (first presented at the 1999 Liège Astrophysical Colloquium: Goriely & Mowlavi 2000b), we rushed to introduce an ESO observing

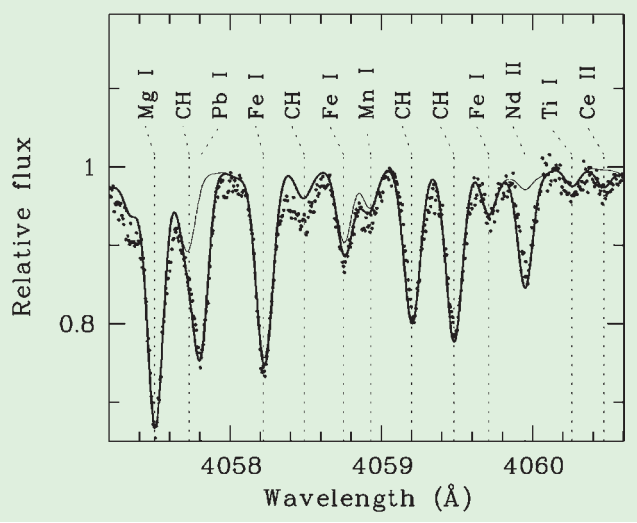

Figure 3: Comparison between the observed spectrum of HD 196944 with synthetic spectra corresponding to [s/Fe] = 0 (thin solid line; in this case the Pb line is not visible) and with the best matching [s/Fe] abundance set as given by Van Eck et al. (2001; thick solid line).

proposal. Luck was then with us twice: first when time was allocated at once to our project by the OPC, and second when the finishing Chilean winter offered us two good nights in September 2000. The Very Long Camera of the CES fed by the 3.6-m telescope provides the ideal instrumental set-up for testing our prediction. Although the recently refurbished CES/VLC (Kürster 1998ab) offers a resolution as high as R = 235,000, we chose R = 135,000 as a compromise between resolution and sensitivity. This set-up already allows us to separate the Pb I λ405.781 nm line from a CH line lying less than 0.1 Å bluewards.

As genuine low-metallicity AGB stars are rare in the solar neighbourhood, the target list comprised CH stars instead, a class of low-metallicity binary stars whose atmosphere bears the evidence for pollution by s-process-rich matter, probably coming from their companion formerly on the AGB (now a dim white dwarf; McClure & Woodsworth 1990).

At the telescope, it was immediately obvious that all the CH stars targeted by the programme had a very strong Pb I line. Figure 2 compares the CES/VLC spectra of CH stars with that of a warm carbon comparison star of spectral type R which does not appear to be enriched in lead.

The abundances were derived from spectral synthesis in the 404.5–407.1 nm spectral window using POSMARCS model atmospheres (Plez et al. 1992) matching their CNO abundances and metallicity. Solar oscillator strengths were derived from a synthesis of the solar spectrum, except for the 405.781 nm Pb I line, for which the laboratory value log gf = –0.22 has been adopted (Biémont et al., 2000). Although efforts were made to improve upon existing CN and CH line lists, the larger errors affecting the abundances in the two carbon-rich stars (HD 187861 and HD 224959, see Figure 4 and Van Eck et al. 2001) are mainly due to remaining inaccuracies in the CN line list.

3. Comparison with Predicted Abundances

Figure 4 presents the abundance pattern derived as described in Van Eck et al. (2001) for our three CH stars which have metallicities in the range –2.45 ≤ [Fe/H] ≤ –1.65, and compared to the predictions for the operation of the PMP in AGB stars of the same metallicities (see Goriely & Mowlavi 2000a for details about the models). Despite the fact that few elements have useful lines in the narrow (26 Å) spectral window offered by the CES/VLC around the Pb I line, the available data are in very good agreement with the PMP predictions.

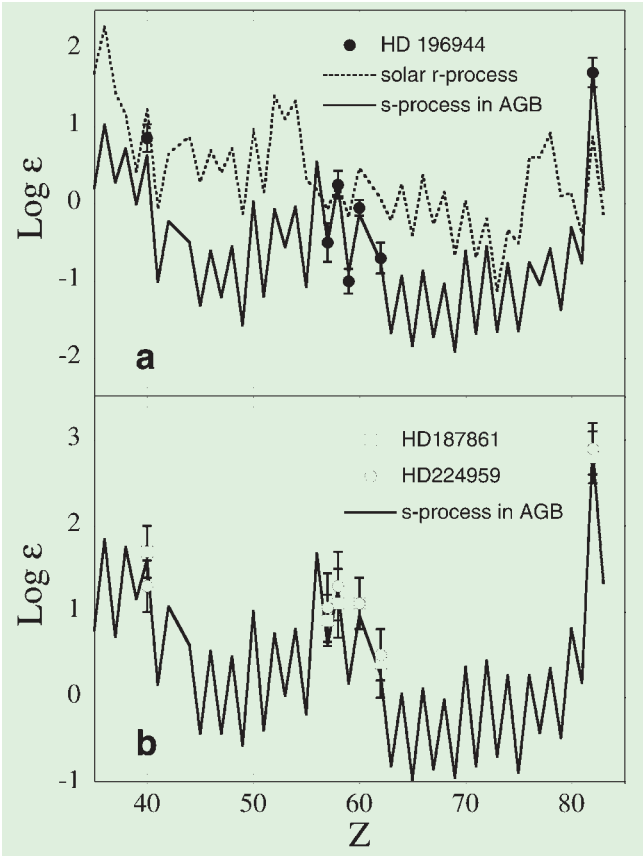

Figure 4: Comparison of the observed abundances with PMP abundance predictions. The model abundances are obtained as described in Goriely & Mowlavi (2000a) for stars of the same metallicities as the programme stars. The abundances are given in the scale log(ε_H) = 12. The upper panel (a) displays as well the solar system r-abundance distribution normalised to Ce. This comparison clearly shows that the large [Pb/hs] ~ 1.2 abundance ratio cannot be understood in terms of an r-process enrichment.

Although this good agreement strongly supports the PMP mechanism for the operation of the s-process in AGB stars, alarm signals came in at about the same time from the observations by Aoki et al. (2001) of [Pb/hs] ratios not larger than 0.4 (despite large Pb overabundances of the order of [Pb/Fe] = 2.3 to 2.6) in the slightly more metal-deficient carbon stars LP 625-44 and LP 706-7 ([Fe/H] about –2.7). Since these [Pb/hs] ratios are incompatible with the seemingly robust predictions from the PMP mechanism, they raise the questions whether the s-process operates in totally different ways in AGB stars with metallicities above and below [Fe/H] of about –2.5, as suggested by Fujimoto et al. (2000).

4. Future Prospects

The faintness of many other good candidate lead stars strongly limited the target list for the 3.6-m telescope and CES. UVES offers better prospects both on the ground of limiting magnitude and of spectral coverage. Its good UV sensitivity opens the way to the study of other Pb I lines lying in the UV, as well as of many other heavy elements.

The different abundance patterns observed among very low-metallicity, s-process-rich stars will undoubtedly stimulate the nucleosynthesis modelling of AGB stars of low (or even zero) metallicity, as initiated by Fujimoto et al. (2000) and followed by many other works since then (e.g., Goriely & Siess, 2001).

Finally, our data will help to fix the Pb yields from low-mass stars at low metallicities, that may then be used in models of the chemical evolution of the Galaxy (e.g., Travaglio et al. 1999). This would make the splitting between the s- and r-contribution to the solar Pb possible.

Acknowledgement

It is a pleasure to thank Dr. M. Kürster and the whole 3.6-m team for their operational support.

References

Aoki, W., Ryan, S.G., Norris, J.E., et al., 2001, *ApJ*, in press (astro-ph/0107040).

Biémont, E., Garnir, H. P., Palmeri, P., Li, Z. S. & Svanberg, S., 2000, *Mon. Not. R. Astron. Soc*. **312**, 116–122.

Burbidge, E.M., Burbidge, G.R., Fowler, W.A., Hoyle, F., 1957, *Rev. Mod. Phys.* **29**, 547.

Cayrel, R., Hill, V., Beers, T. C., et al., 2001, *Nature* **409**, 691.

Fujimoto, M.Y., Ikeda, Y., Iben, I.Jr. 2000, *ApJ* **529**, L25.

Gallino, R., Arlandini, C., Busso, M., et al., 1998, *ApJ* **497**, 388.

Goriely, S., Mowlavi, N., 2000a, *A&A* **362**, 599.

Goriely, S., Mowlavi, N., 2000b, in "The Galactic Halo: From Globular Clusters to Field Stars", A. Noels P. Magain, D. Caro, E. Jehin, G. Parmentier, A. Thoul (eds.), Proc. of the 35th Liège Intern. Astrophys. Coll. (Université de Liège, Belgium), 25.

Goriely, S., Siess, L., 2001, *A&A* **378,** L25.

Herwig, F., Blöcker, T., Schönberner, D., El Eid, M., 1997, *A&A* **324**, L81.

Kürster, M., 1998a, *The Messenger* **92**, 18.

Kürster, M., 1998b, *The Messenger* **94**, 12.

Langer, N., Heger, A., Wellstein, S., Herwig, F., 1999, *A&A* **346**, L37.

McClure, R.D., Woodsworth, A.W., 1990, *ApJ* **352**, 709.

Plez, B., Brett, J.M., Nordlund, A., 1992, *A&A* **256**, 551

Prantzos, N., Arnould, M., Arcoragi, J.-P., 1987, *ApJ* **315**, 209.

Travaglio, C., Galli, D., Gallino, R., et al., 1999, *ApJ* **521**, 691.

Van Eck, S., Jorissen, A., 1999, *A&A* **345**, 127.

Van Eck, S., Goriely, S., Jorissen, A., Plez, B., 2001, *Nature* **412**, 793.

SIMBA Explores the Southern Sky

L.-Å. NYMAN and M. LERNER, SEST and Onsala Space Observatory
M. NIELBOCK, M. ANCIAUX and K. BROOKS, ESO
R. CHINI, M. ALBRECHT and R. LEMKE, Astronomical Institute of Ruhr University of Bochum
E. KREYSA and R. ZYLKA, Max Planck Institute for Radio Astronomy
L.E.B. JOHANSSON, Onsala Space Observatory
L. BRONFMAN, Department of Astronomy, University of Chile
S. KONTINEN, Observatory, University of Helsinki
H. LINZ and B. STECKLUM, Thüringer Landessternwarte Tautenburg

SIMBA

SIMBA (the SEST Imaging Bolometer Array) was installed on the SEST in June this year through a collaboration between the University of Bochum, the Max-Planck-Institute for Radio Astronomy, the Swedish National Facility for Radio Astronomy and ESO. It is a 37-channel bolometer array operating at a wavelength of 1.2 mm.

Images produced by SIMBA are taken with the telescope in a fast scanning mode with speeds up to 160″/s without using a nutating subreflector. The beam size of SEST is 24″ at 1.2 mm and the pixel size in the SIMBA maps presented here is set to 8″. A map with a size of 15′ by 6′ with a rms noise of 40–50 mJy is obtained in only 12 minutes. More technical information about SIMBA is given on the SEST home page, and preliminary results were presented in ESO Press Release 20/01.

The strength of SIMBA is certainly the efficient coverage of large areas in a short time. It has therefore been used to map and survey regions of star formation in our own Galaxy as well as in nearby galaxies where cold dust and ionised regions emit strongly at 1.2 mm wavelength. SIMBA has also been used to study planetary nebulae, quasars, and maps of the deep fields in the Southern sky (the Hubble deep field South, the Chandra deep field, and the Phoenix deep field) have been obtained.

The SIMBA images presented in this article are preliminary in the sense that they were reduced with the on-line data reduction system. The data reduction software MOPSI – which so far has only been used for data obtained with a chopping secondary – is presently being adapted to the fast scanning mode and it is expected that all existing maps will improve in terms of intensity calibration and noise performance. Consequently, parts of extended, faint emission might have escaped detection so far but should appear more frequently after the upgrade.

The Orion region

Figure 1 displays the SIMBA map of the entire integral shaped Orion A molecular cloud complex at a wavelength of 1.2 mm. It has been created from 13 single maps during a total integration time of about 3.5 hours. The 1-sigma residual noise is about 40 mJy/beam.

The Orion A complex is usually divided into three regions, known as OMC-1, OMC-2 and OMC-3 (right panel), and the Orion Nebula (M 42) which belongs to the most luminous HII regions known. M42 is located in front of OMC-1 at a distance of 470 pc. This region also encompasses the brightest millimetre peaks of the SIMBA map, coincident with the Becklin-Neugebauer (BN) object adjacent to the Kleinmann-Low (KL) Nebula. The BN object is thought to be a young massive star of about 25 L_0 with a considerable mass loss.

Both M 42 and OMC-1 are regions of current massive star formation. OMC-1 itself is heated by stars from the nearby OB cluster within the Orion Nebula, including the Orion Trapezium. Its UV radiation is also responsible for photodissociation regions (PDR) on the surface of OMC-1 and southern parts of OMC-2.

OMC-2 and OMC-3 also show star-formation activity which is obvious from the numerous dense cores located within the filament. Some of them coincide with VLA radio sources, which is usually a sign of free-free emission from bow shocks of protostellar molecular outflows. In contrast to OMC-1, however, preferably low-mass stars are created there. Both OMC-2 and OMC-3 possess comparable amounts of gas and dust, although OMC-3 seems to be less evolved than OMC-2. Six of ten compact millimetre sources in OMC-3 have been identified as Class 0 protostars, while all sources in OMC-2 are at least of Class I. Furthermore, temperatures are lower and outflows are less

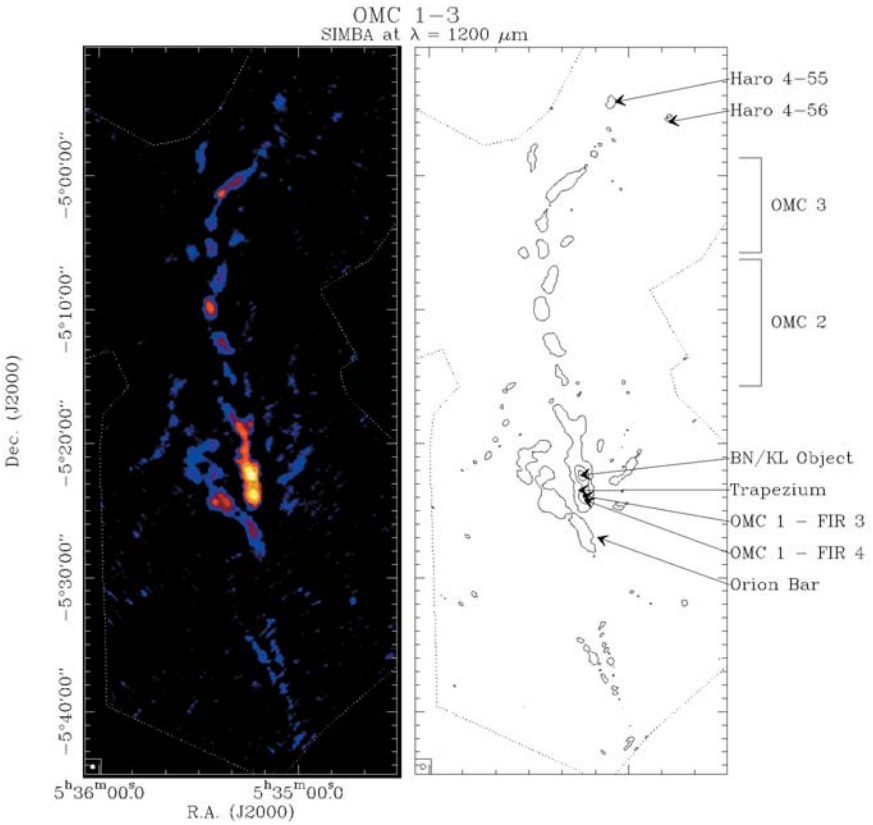

Figure 1: The Orion A molecular cloud complex. The left image shows the 1.2 mm SIMBA map. Some sources and regions of special interest are shown in the contour plot to the right. The circle in the lower or upper left corner seen in all figures except Fig. 4 depicts the SEST beamsize at 1.2 mm (24″ FWHM).

energetic in OMC-3 than in OMC-2. This suggests an evolutionary trend in the star formation history in Orion. Actually, it can be traced back to the Orion belt with a group of 6 to 12 Myr old stars. From there it advanced to the region of Orion's sword, where stars of 3 to 6 Myr age lie in front of the Orion nebula, where the next chapter of star formation took place. The evolution headed farther away from us to OMC-1, before turning back to the north and finally reaching the currently youngest region, OMC-3.

η Carinae and the Keyhole Nebula

The Keyhole Nebula is part of the Carina Nebula, an HII region/molecular cloud complex at a distance of 2.2 kpc. Herschel (1847) was the first to note the interesting optical features of the Keyhole Nebula which include bright arcs and filaments interwoven with dark patches, the most prominent of which is in the shape of a keyhole (see Malin 1993). The region is associated with Trumpler 16, an open cluster that contains numerous massive stars, including three O3-type stars as well as one of the most massive stars known – η Car. Such a high concentration of massive stars has created an extremely harsh environment within the Keyhole Nebula. There are bright ionisation fronts with complex kinematics and all that remains of the GMC in this region are externally heated molecular globules.

Figure 2 shows a SIMBA map of η Car and the surrounding regions. In addition to emission from η Car, there is a striking linear ridge of emission that extends more than 1 arcmin in length with a gap near the centre. Surrounding this ridge are a number of smaller emission clumps, one of which is located in the north and is in the shape of an arc that curves towards η Car. The emission detected by SIMBA closely follows the distribution of the 4.8-GHz continuum emission, which arises from thermal emission from ionised gas associated with one of the peaks in the Carina HII region (Car II). The main emission components are thought to be ionisation fronts possibly originating from η Car. It is not clear what is responsible for their striking shapes.

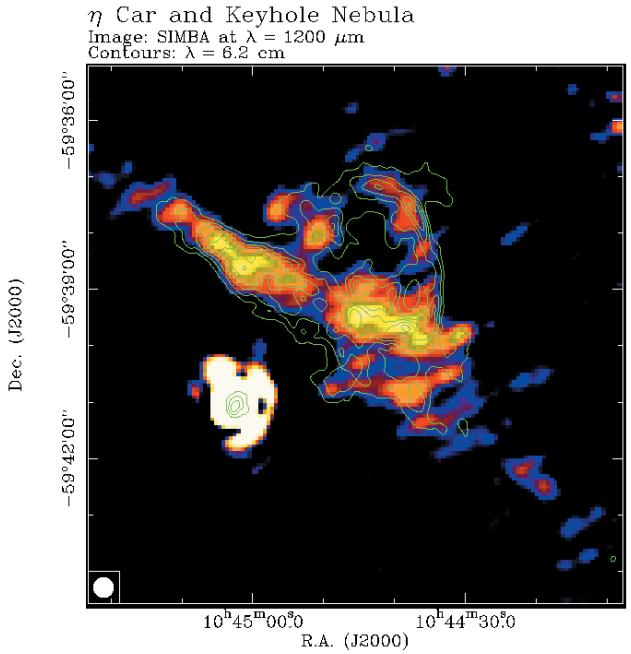

Figure 2: η Carinae and the Keyhole Nebula. η Carina is the bright region to the left in the map. The contours overlayed on the SIMBA map show the free-free emission from ionised gas at 4.8 GHz taken from a map obtained with the Australia Telescope Compact Array.

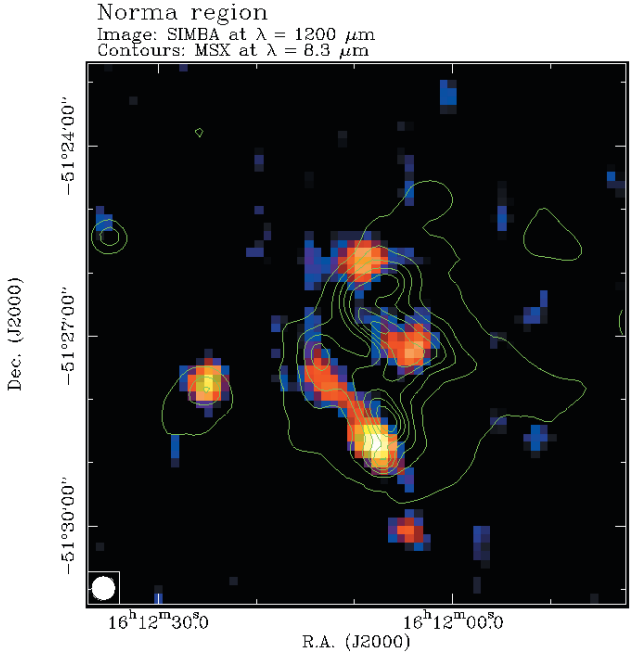

Figure 3: 1.2 mm emission from a dense core in the Norma spiral arm tangent point. The contours outline the 8.3 micron emission obtained with the MSX satellite.

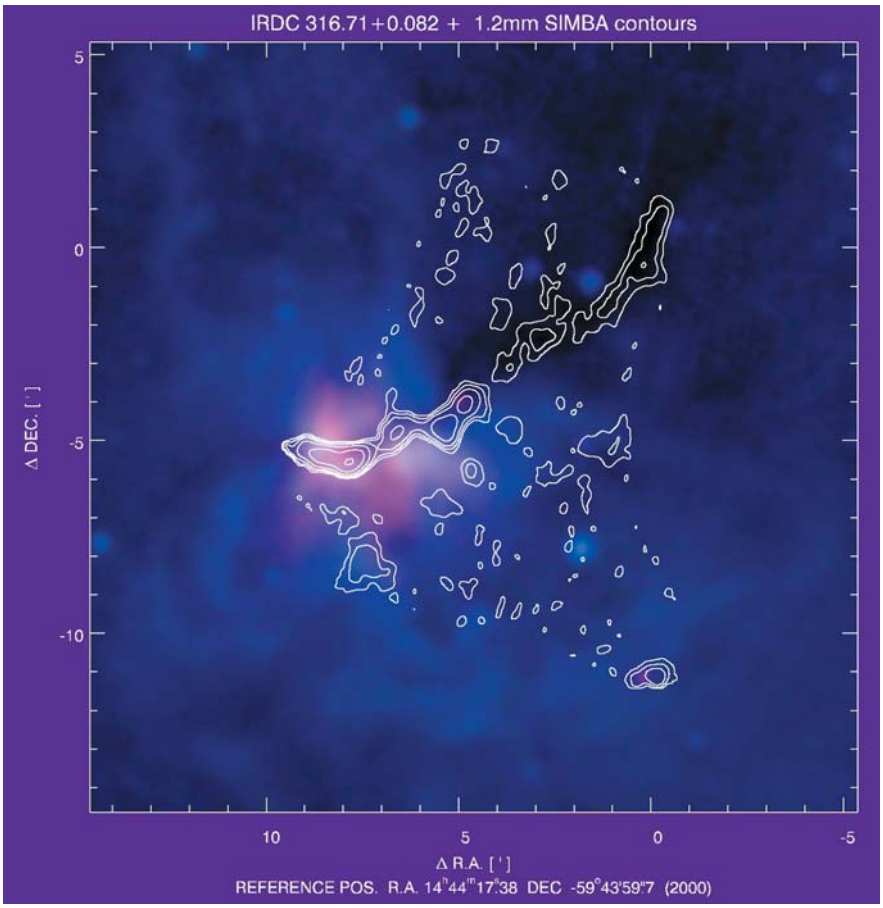

Figure 4: 1.2 mm emission from an infrared dark cloud. Contours from the SIMBA map are overlayed on a true colour MSX image.

Massive Star Formation in the Norma Spiral Arm

The Norma Spiral Arm contains the most massive molecular clouds as well as the most luminous regions of massive star formation in the Galactic disk. Eight embedded regions of OB star formation (identified in a survey of IRAS point sources with FIR colours of UC H II regions), situated in the spiral arm's tangent at $l \sim 330$ deg and at a distance of 7 kpc from the sun, have been previously mapped in CS(2-1) with the SEST. Figure 3 shows the SIMBA map of one of these dense cores; the most extended one (20 pc × 20 pc) observed so far in CS emission. As traced by SIMBA, it apparently contains UC HII regions, and more interestingly several massive stars in earlier stages of evolution. These data are consistent with a scenario of massive star formation occurring by fragmentation and condensation of the gas within the dense cores of giant molecular clouds.

Infrared Dark Clouds

The presence of a large number of so-called InfraRed Dark Clouds (IRDCs) was revealed by a mid-infrared survey of the Galactic plane conducted with the SPIRIT III instrument on board of the Midcourse Space Experiment (MSX). These clouds have MIR extinction values in excess of 2 magnitudes at 8 micron and are thought to contain cold ($T < 20$ K) and dense ($n(H_2) > 10^5$ cm^{-3}) material. Until now only a few IRDCs are examined in more detail. Several southern IRDCs were mapped with SIMBA to trace possible mm dust emission arising from the cold dust within the clouds. Figure 4 displays an interesting example of a non-spherical IRDC in the farther vicinity of a site of massive star formation. The contours are overlaid on a true colour MSX image which shows the 8, 13, and 21 micron emission coded blue, green, and red. The blue background results from the higher sensitivity and the ubiquitous PAH emission features covered by this band. This can be compared to the case of the Orion Trapezium region where the silhouette proplyds are seen against the optical emission. The superimposed SIMBA 1.2 mm contours in the right upper part match nicely the dark extincted region in the MSX image. A more extended lane of emission reaches down to the bright MIR region where several Galactic radio sources as well as OH, H_2O and methanol masers are located. Star formation probably started at the eastern end and spread along the filament. In fact, a very red source (which is not included even in the MSX catalogue) almost coincides with the 1.2 mm peak at the offset position (5′, –4′). It might be the youngest (massive) protostar seen so far.

The R CrA Star Forming Region

The Coronae Australis dark cloud complex is a nearby (130 pc) region of low-mass star formation. The cloud can be divided roughly into two parts; the north-western dense gas region, known as the R CrA core, and the south-eastern tail consisting of a quiescent dense core. The cloud complex is located 17 to 22 degrees below the galactic plane in a region which appears to be free of foreground or background dust and molecular gas.

A number of variable stars and embedded IR objects are associated with the R CrA Cloud. The brightest star, TY CrA (a Herbig Be star), has almost reached the main sequence. Others, like S CrA, T CrA, VV CrA and R CrA are still above the zero age main sequence. Some of the infrared objects have optical counterparts while some deeply embedded objects can only be detected in infrared. With SIMBA, it is possible to detect dust emission from small clumps giving rise to a single star or a stellar system and identify larger-scale dust structures.

The SIMBA data (shown in Fig. 5), taken together with the $C^{18}O$ and $C^{17}O$ column densities, can be used to estimate the degree of CO depletion onto dust grains. This is important because the freezing out of gaseous species onto grain surfaces strongly affects the physical and chemical properties of molecular clouds. This includes the deuterium fractionation and the degree of ionisation, one of the fundamental parameters regulating the rate of star formation, through the ion-neutral drift or ambipolar diffusion process. With SIMBA maps combined with spectral line observations, it is possible to correlate the dust emission characteristics with the degree of depletion and the chemical composition of dense clumps. This might reveal the importance of chemistry and depletion vs. desorption for the dynamical evolution of the cloud.

A region of 40′ times 20′ was observed with the SIMBA. The mapped area consists of 40 fast maps, varying from 400″ × 900″ to 792″ × 1400″ in size. The faint sources at the south-eastern quiescent core were resolved with 20 fast maps, which equals roughly 10 hours of observations. The other 20 scans were used to map the central and northwestern region of the cloud.

The Dark Globule B68

Stars form within dark clouds. While the study of protostars has been quite

successful during recent years, little is known about the initial conditions of star formation, i.e. the internal structure of the parental clouds. This is mainly due to the unknown amount of molecular hydrogen, which cannot be observed directly at the low temperatures of the clouds. The traditional way out of this dilemma was so far either to use tracer molecules such as CO and correlate their emission with the molecular hydrogen column density or to measure the optically thin emission of dust and derive the gas mass by adopting a gas-to-dust ratio. Both methods are based on a couple of assumptions on unknown conversion factors, which makes the determination of the amount of molecular hydrogen rather uncertain.

Recently, a new method to determine the line-of-sight distribution of dust in dark clouds has been applied successfully to some starless clouds like e.g. B 68 (Alves et al. 2001). The extinction could be directly measured from various IR colours towards background stars, yielding detailed maps of the dust column density. The penetrated optical depths (to a visual extinction of about 40 magnitudes) and the achieved spatial resolution (about 10) were an order of magnitude higher than previously possible from optical star count techniques.

Using these IR techniques in parallel to mm imaging seems to be an ideal tool to calibrate the mass absorption coefficient at 1.2 mm by comparing the IR-derived optical extinction with the mm-derived (optically thin) emission. Once this calibration has been established for a number of starless dust clouds, the total amount of dust can be determined for every dark cloud, independent of its optical depth and far beyond the capabilities of current IR techniques which are limited by the number of background stars detectable at high extinctions.

The application of this method is then wide spread. In particular, it allows to measure the total mass and the density structure of a cloud, the latter one on various scales from the global radial density profile until small-scale clumping. In addition, it is possible to study the initial conditions of star formation in a regime of optical depths where the current promising IR techniques cannot penetrate any longer the dust along the line of sight. Figure 6 shows a first example where we have mapped B 68 with SIMBA; the image consists of 130 coverages. From a preliminary analysis of the data and in comparison with the extinction map by Alves et al. (2001), we find that SIMBA traces the 1.2 mm emission until an equivalent optical extinction of 10 magnitudes; lower extinction values might be accessible soon when the reduction software has been optimised.

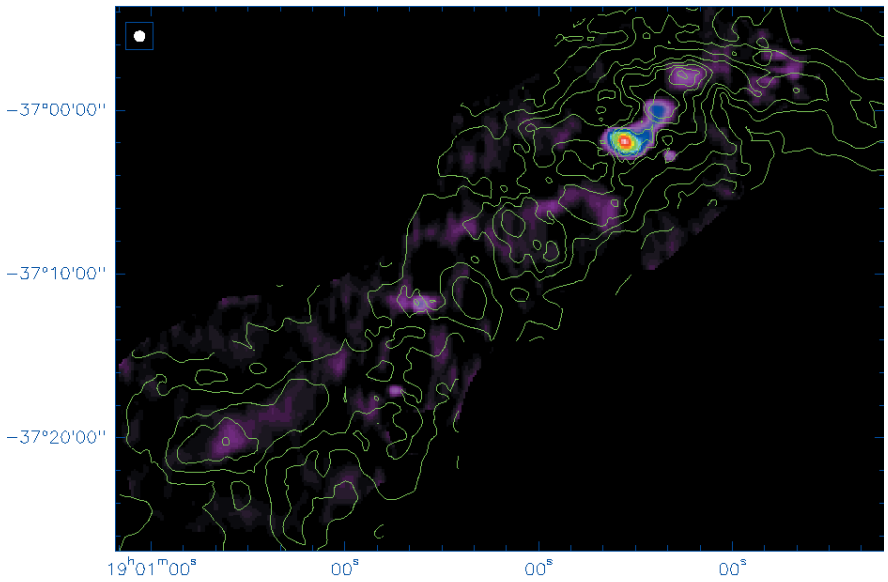

Figure 5: A SIMBA map of the low-mass star forming region R CrA. The contours show the integrated $C^{18}O$(1-0) emission from a map obtained by Harju et al. (1993) taken with the SEST. The lowest levels in the SIMBA map are set to reveal possible faint, extended structures.

30 Dor and N159 in the Large Magellanic Cloud

In Figures 7 and 8 SIMBA maps are presented of the 30 Doradus nebula (centred on the young cluster R 136) and an area including the HII region N 159 as well as prominent CO complexes. The distributions of the 1.2 mm flux are compared with those at 8.3 micron (from the MSX satellite) and the ^{12}CO(1-0) emission (obtained at SEST), respectively. Both regions show an excellent agreement between the 1.2 mm and 8.3 micron maps with respect to peak locations and extents, while the CO distribution, although closely associated with the 1.2 mm flux in general, deviates significantly in some cases. Most notable is the lack of 1.2 mm emission from the CO cloud south of N 159. CO excitation analysis indicates that this cloud is cold with kinetic temperatures probably less than 15 K. It is

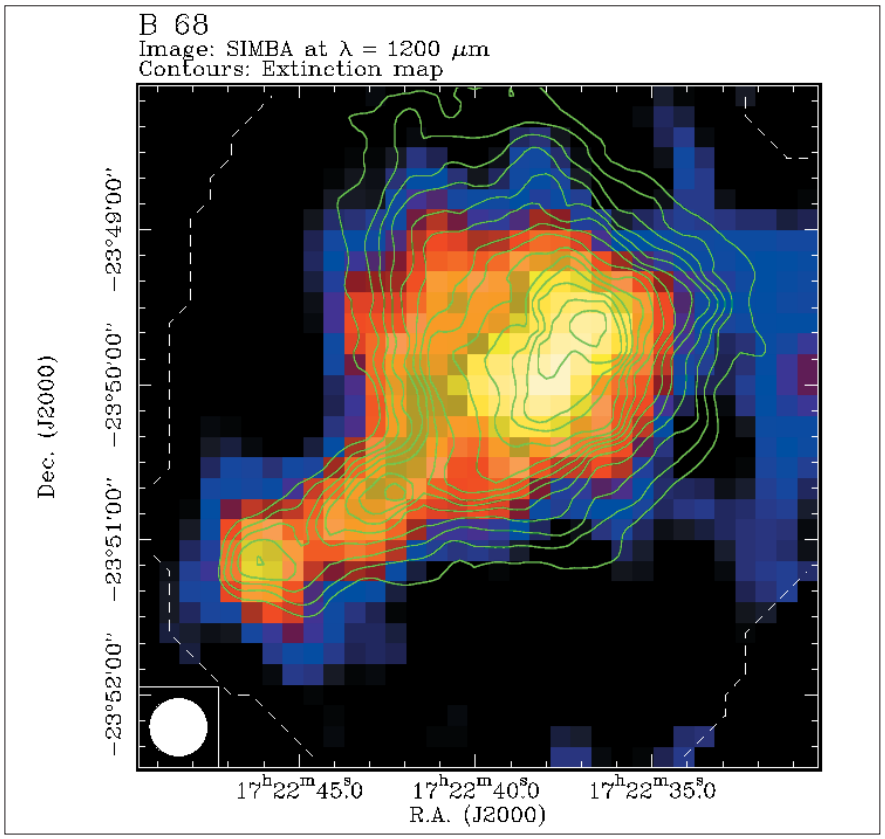

Figure 6: 1.2 mm emission from the dark globule B68. The contours are taken from the extinction map obtained by Alves et al. (2001).

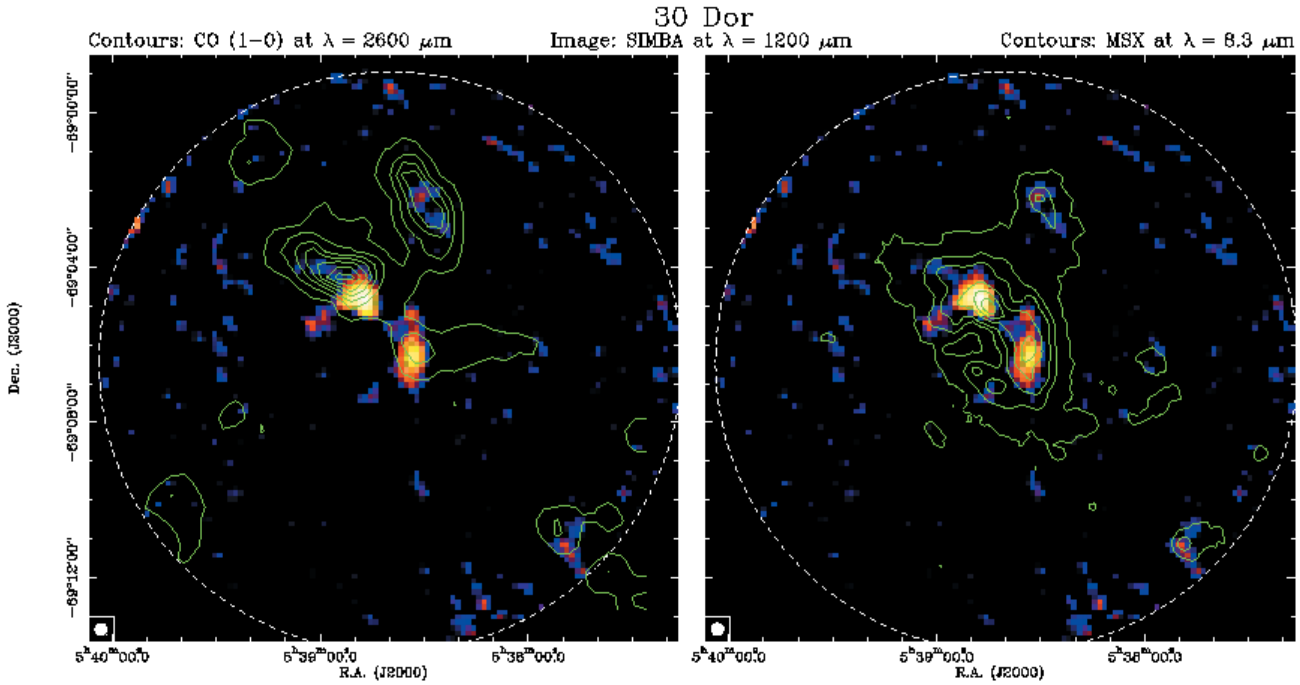

Figure 7: SIMBA 1.2 mm images of the 30 Dor region in the LMC. The contours show the integrated CO(1-0) emission (left panel), and the 8.3 micron contours from the MSX satellite image (right panel). The circle in the lower left corner depicts the SEST beamsize at 1.2 mm (24″ FWHM).

not associated with the formation of massive stars, in contrast to most of the CO complexes visible in these maps. The strongest 1.2 mm peak is associated with a region where the warmest CO cloud in the sample studied is located; according to the CO excitation analysis the kinetic temperature of this cloud is in the range 40–80 K.

Acknowledgements

We thank Joao Alves for permission to use the extinction map of B 68. We acknowledge the help of Katrin Kaempgen and Vera Hoffmeister for reducing the B 68 data. This article made use of data products from the Midcourse Space Experiment. Processing of the data was funded by the Ballistic Missile Defense Organization with additional support from NASA Office of Space Science. This article has also made use of the NASA/IPAC Infrared Science Archive, which is operated by the Jet Propulsion Laboratory, California Institute of Technology, under contract with the National Aeronautics and Space Administration.

References

Alves J., Lada C., Lada E., 2001, *The Messenger* No. 103.

Harju et al., 1993, *A&A* **278**, 569.

Herschel J.F.W., 1847, Results of Astronomical Observations at the Cape of Good Hope, London, p. 153.

Malin D., 1993, A View of the Universe. Cambridge University Press, pages 104, 155.

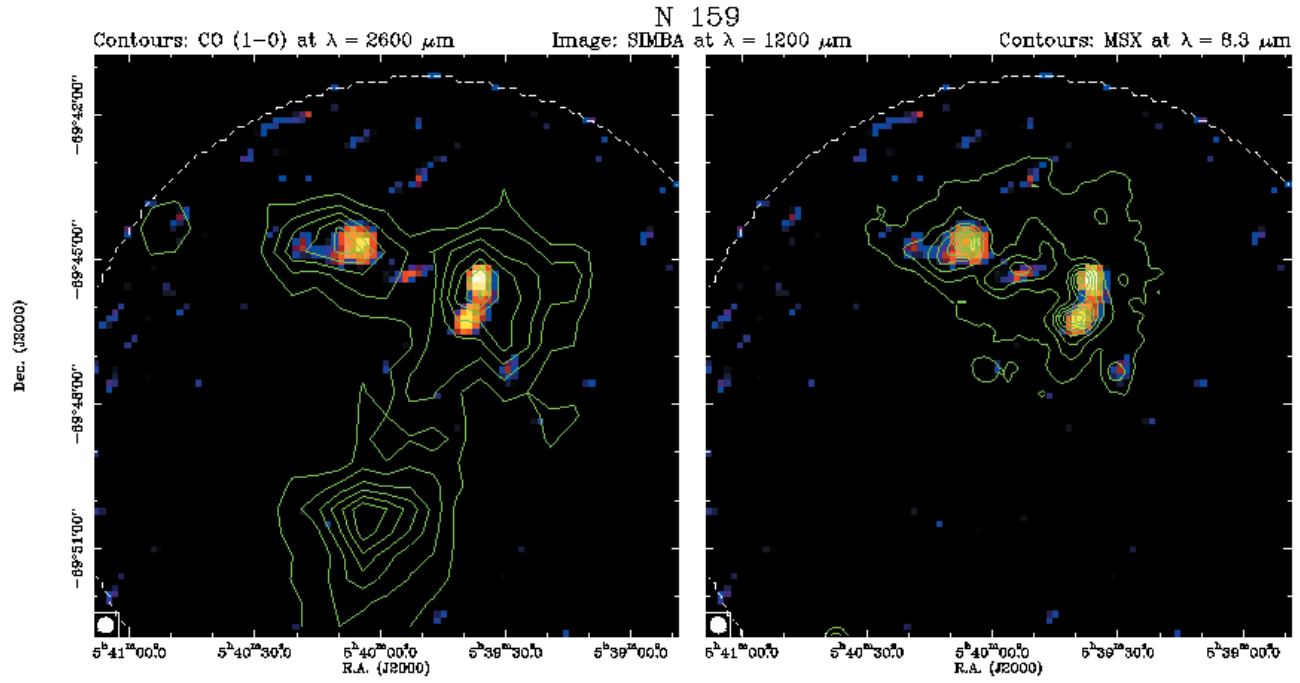

Figure 8: SIMBA 1.2 mm images of the N159 region in the LMC. The contours show the integrated CO(1-0) emission (left panel), and the 8.3 micron contours from the MSX satellite image (right panel).

News from Santiago

With the ever-growing number of astronomers in Chile, the ESO Topical Meetings in Santiago provide an important forum for the community to meet, exchange ideas and discuss recent research.

The series started with three successive meetings in October/November 1999 ("The Distant Universe", "Physics of Galaxies", "From Stars to Planets"), then continued in December 2000 with a Topical Meeting oriented towards telescopes/instruments ("New Facilities for Astronomy in Chile").

In 2001, we have complemented the series with two Topical Meetings recently held at ESO/Santiago. Below are short summaries of these lively and fruitful scientific meetings. Names in parentheses are speakers at the Workshops. Acronyms are written out at the end. D. Alloin

ESO Topical Meeting: "Astrophysical Niches for High Resolution Spectroscopy"

ESO/Santiago, 2001 October 2–3
S. Ellison

This Topical Meeting was held in Vitacura on October 2–3. The technique of high-resolution spectroscopy is exploited in many areas of astronomy, as was reflected by the breadth of scientific talks given over the two days and the attendance of astronomers and students from universities in Santiago and Concepción as well as several visitors from Europe and other Latin American countries.

One of the most exciting and widely publicised uses of high-resolution spectrographs in recent years has focussed on their exquisite radial velocity accuracy necessary for detecting extra-solar planets.

D. Queloz presented a progress report of the on-going planet search project with CORALIE and reviewed some of the important conclusions to come out of this programme. The distribution of planet masses, which exhibits a sharp increase down to around 1 Jupiter mass before dropping sharply due to incompleteness, highlighted the motivation for future instrumentation such as HARPS, which will provide the next important step in radial velocities by routinely providing 1 m/s accuracy (F. Pepe).

Another exciting prospect is using the transit method to detect extra-solar planets. G. Mallen-Ornelas presented some recent radial velocity follow-up measurements from UVES of the first extra-solar planet candidates to be detected via the transit method, an important discovery and a complement to radial velocity techniques.

Stellar spectroscopy naturally had a significant presence at the Topical Meeting, addressing many wide-ranging issues. Important new results have surfaced in the field of metal-poor stars, as reviewed by E. Jehin. Although many puzzles still remain (e.g. the oxygen abundance in very metal-poor stars and the issue of deep mixing), new avenues are continually opening, such as the possibility of using radioactive isotopes for age-dating. Chemical profiling was a recurrent theme of this meeting and talks by D. Minniti, J. Arenas and D. Geisler highlighted this technique in three very different populations: the Galactic bulge, the metal-poor halo and Sculptor dwarf spheroidal.

High resolution is essential for the detailed analysis of stellar magnetic fields due to the small scale of line splitting, as discussed by G. Mathys and S. Bagnulo.

High-resolution spectroscopy has also had an important impact on cosmological fields. B. Leibundgut reviewed an ESO large programme aiming at characterising the elusive SNIa progenitor population, whose nature remains unknown despite its key role as a standard candle.

The study of high-redshift quasars proves to be interesting not only for investigation of the AGN and its environment (P. Hall), but also as a tool for probing intervening matter such as the intergalactic medium and distant galaxies (S. Lopez and S. Ellison). Quasar absorption lines remain one of the best diagnostics of the high-redshift Universe, allowing us to determine detailed chemical profiles, probe primordial abundances and even measure the temperature of the CMB.

European and Chilean astronomers now have an exciting suite of spectroscopic capability available to them. In addition to the most recent addition of UVES to the ESO arsenal, the science presented at this meeting utilised a host of instrumentation including FEROS (the most over-subscribed of all ESO instruments), CORALIE and the VLC (on the 3.6-m). Instruments such as EMMI, which are not dedicated high-resolution facilities also offer an important contribution, as demonstrated in talks on cataclysmic variables (E. Mason and R. Mennickent).

Of course, high-resolution spectroscopy is not confined to the Optical and several speakers discussed results in the IR and sub-mm regime to probe the environments of AGN (E. Galliano) and to investigate the properties of star-forming regions (P. Cox).

With new instruments on the horizon, such as HARPS, FLAMES and CRIRES, the capabilities and possibilities for the future are very exciting and research in this domain will certainly continue to blossom.

ESO Topical Meeting: "Brown Dwarfs and Planets"

ESO/Santiago, 2001 October 16
M. Sterzik

On October 16, the second in the series of the 2001 Topical Meetings at ESO/Vitacura was about "Brown Dwarfs and Planets". More than 30 participants, the majority being researchers and students based in Chile, discussed the current status and future prospects in this rapidly growing field, a field that was actually pioneered with the discovery of the first free-floating brown dwarf, Kelu-1, in 1997 by the Chilean astronomer M.T. Ruiz. The topic was introduced by a review on the theories of star and planet formation, in the perspective of planet searches (G. Wuechterl).

Then, coming to the question of discoveries, the whole variety of observational methods employed in brown dwarf and planet search programmes was discussed.

Precise radial velocity Doppler measurements are currently the most successful method in discovering planetary mass companions (e.g. with the spectrographs CES, UVES, CORALIE and in the future HARPS) as was discussed by M. Kuerster.

But also direct imaging methods are now promising, ranging from Deep NIR

imaging with ISAAC in star-forming regions down to sensitivities of planetary masses for free-floating objects (F. Comerón), as well as photometric transit and microlensing searches which are currently pursued or planned (D. Minitti).

Searches for faint companions, mostly done with adaptive optics in the NIR, also reach sensitivities below the hydrogen burning limit (S. Hubrig). However, the brown dwarf companion frequency inferred from such observations appears to be low, and the so-called "brown dwarf desert", already well-known from radial velocity surveys, likely extends over a broader distance range (M. Sterzik). The promises of adaptive optics for planetary science studies in general was also highlighted at the meeting (F. Marchis).

Among other predicted observable signatures of planets are e.g. their interaction with circumstellar disks. This will be visible with future high-sensitivity, high-resolution IR imaging techniques (O. Schuetz). Atmospheric signatures, especially OH features, can eventually be identified with the next-generation high-resolution VLT/MIR spectrograph CRIRES (U. Kaeufl).

In the near future, a very powerful way to identify new brown dwarf and planetary mass companions will involve the VLT interferometer, measuring both astrometric variations in close binary systems, and also direct imaging by nulling techniques (M. Schoeller, M. Wittkowski).

In conclusion, we should expect in the coming years very exciting discoveries in this area of research, thanks to performing and inventive new instruments. The quest for extra-solar planets has just started to bring us beautiful results. There is no doubt that this success will continue and unveil at some point the awaited Earth-like planets.

HARPS: High-Accuracy Radial-velocity Planetary Search
FEROS: Fiber-fed Extended Range Optical Spectrograph
FLAMES: VLT Fibre Large Array Multi Element Spectrograph
UVES: VLT UV-Visual Echelle Spectrograph
ISAAC: VLT Infrared Spectrometer And Array Camera
CRIRES: VLT Cryogenic high-resolution InfraRed Echelle Spectrograph
VLC: Very Long Camera (used together with the CES, Coudé Echelle Spectrometer)

The ESO Users Committee

L. WISOTZKI, Chairperson of the UC

Founded as an advisory body to the Director General, the Users Committee mainly works at the interface between 'common users' and ESO representatives. This article describes the role of the UC, highlights some of its recent activities, and outlines some areas where the communication between ESO and its users can be improved.

ESO's status as an international organisation requires that its member states are appropriately represented in the shaping of decisions and policies. As part of this principle, several panels were created where delegates from the ESO member countries participate to define various aspects of ESO policies. Among these, the Observing Programmes Committee (OPC) with its biannual verdicts on the submitted proposals is probably most prominently present in the daily life of many astronomers. Other important institutions are the Scientific Technical Committee (STC), the Finance Committee, and ultimately the ESO Council. Wait – there's something else: the **Users Committee (UC).** Maybe less central in high ESO politics, it nevertheless fulfils an important function: representation of the 'common user' towards ESO, and support of the communication between ESO and its users. This article is meant to give a little background information on tasks and challenges of the UC and its members.

Suppose you have been granted observing time and enjoyed the trip to Chile (or alternatively, enjoyed preparing your Observing Blocks at home). If the weather is good, you'll get a lot of data and can start doing science. Usually, that's all there is to be said, most users are quite satisfied with the way their needs are taken care of, with the support on the mountains, and with the quality of their data. But nothing is perfect, and ESO is no exception to this rule – instruments might not work properly, there might be conflicts with staff members, or certain things might just run somewhat below optimum. Now what are you – as an ESO user – supposed to do if you run into troubles that cannot be solved on the spot? For such cases, a number of options exist:

• Don't do anything at all. Or, to make it worse, tell your colleagues at the next conference that ESO is a lost case. This method has the virtue of being at least partly self-fulfilling, in that you certainly don't accomplish a lot.

• Complain to your ESO friend, ideally to the person highest up within the ESO hierarchy you can get hold of. Works sometimes, but this route is clearly not always open.

• Fill in a detailed comment in your end-of-mission questionnaire. Actually, that's what these forms are for, and ESO *does* react on them. Unfortunately, not too many people make use of this option, see below.

• Talk to the User Support Group. It is their task (among others) to take com-

Contact your representative in the Users Committee

Belgium:	Hans van Winckel, Katholieke Universiteit Leuven	hans@ster.kuleuven.ac.be
Chile:	Mónica Rubio, Universidad de Chile	mrubio@das.uchile.cl
Denmark:	Jens Viggo Clausen, Niels-Bohr Institute	jvc@astro.ku.dk
France:	Marguerite Pierre, CE Saclay	mpierre@cea.fr
Germany:	Lutz Wisotzki, Universität Potsdam	lutz@astro.physik.uni-potsdam.de
Italy:	Paolo Molaro, Osservatorio Astronomico di Trieste	molaro@oat.ts.astro.it
Netherlands:	Paul van der Werf, Sterrewacht Leiden	pvdwerf@strw.LeidenUniv.nl
Portugal:	João Lin Yun, Observatório Astronómico de Lisboa	yun@oal.ul.pt
Sweden:	Göran Östlin, Stockholm Observatory	ostlin@astro.su.se
Switzerland:	Werner Schmutz, PMOD / WRC,	schmutz@astro.phys.ethz.ch
United Kingdom:	Malcolm Bremer, University of Bristol (Observer)	m.bremer@bristol.ac.uk

This list is updated every year. Check at http://www.eso.org/gen-fac/commit/uc/

plaints serious and to communicate them to the appropriate places.

• Inform your national representative in the Users Committee and ask her or him to discuss the case with ESO officials, especially if you feel you need support with your problem.

Tasks of the UC

Officially, the ESO Users Committee 'advises the ESO Director General on matters concerning the use of ESO telescopes, instruments, computers, etc.' Its members are appointed by the Director General as representatives of the user community, one from each ESO member country plus Chile, with a (not immediately renewable) tenure of four years. The current composition of the UC is listed in Table 1. In its annual spring meetings, the UC works down a densely packed agenda: Presenting problem reports collected from the user community over the year; discussing specific aspects of performance and user friendliness of ESO facilities; receiving briefings from ESO to communicate things back to the users; recommending improvements; and last not least, helping to collect user expertise as input for the shaping of future policies. Let me expand and comment on these tasks in more detail.

Problem reporting

Dealing with problem reports is the most traditional function of the UC, perhaps the one with which most users associate the UC. There are two types of issues between ESO and its users:

• Individual problems, typically related to some not-quite-average request, or to a mistake that has been made by either side. Most of these cases (at least, of those that I heard of) have in fact been sorted out and solved directly between the user and ESO.

• General problems, most commonly originating in some sort of incompatibility between user requests (concerning scheduling, operation, documentation, etc.), and ESO's ability to implement such requests.

Although the UC is usually not needed for addressing this first kind of problems, several similar, seemingly isolated cases make a general one. General problems may sometimes be hard to solve, but in order to tackle them, it is important to recognise them as general problems. This is where the UC and its national representatives come in: as an instance to bundle problem reports and requests, giving them additional weight by demonstrating that the community as a whole is affected.

For this reason, the UC members greatly appreciate if users could keep them informed about any kind of problems between them and ESO, *even if these problems have already been sorted out.* Just send a brief summary of the case to your national representative, or forward e-mails exchanged on that topic. (Since mid-2000, problems mentioned in the end-of-mission questionnaires will be reviewed by the UC anyway).

Monitoring performance

A substantial fraction of each UC meeting is dedicated to a certain 'special topic', which usually means that one specific aspect of using ESO facilities comes under close scrutiny. This year, we chose the topic 'service observing and user support', received briefings from ESO representatives and discussed about aspects that in our experience were unclear or not well treated. While the UC meeting is a very good forum to present our questions, criticism, and suggestions to ESO officials, it is slightly less obvious how the results of that meeting should be communicated back to the users. In case of the above-mentioned special topic of 2001, the UC thought it was so important that the responsible people at ESO were asked to publicise the subject, with special emphasis on describing the service mode scheduling process. This has already generated a response: Please take a look at Dave Silva's helpful and detailed article on service observing which appeared in the September 2001 issue of *The Messenger*.

User polls

One important activity of the UC in 1998/1999 was to conduct a survey ("La Silla 2000+") within the ESO community, by means of an electronic questionnaire, giving the community a platform to express their ideas for the future of the La Silla observatory. The results of this survey have greatly helped shape the recommendations of a corresponding ESO working group . These recommendations are public and can be found at ESO's web site under `http://www.eso.org/gen-fac/commit/ls2000pl1.html`.
It should be noted that nearly all of the top priority recommendations as well as a number of second-priority items have already been implemented or brought on their way.

The wide acceptance of the survey, as quantified by the high return rate (256 filled questionnaires), demonstrates that the users take an active interest in these policy issues. This case also further illustrates the role of the UC: it is not a 'policy-making' panel – these are the tasks of the STC and ultimately of Council –, but the UC takes responsibility that also the community of 'normal users' receives attention.

Recommendations

As an advisory body, the UC cannot make 'decisions' that are binding to ESO. However, each year the UC issues recommendations and action items in order to improve the use of ESO facilities and/or the communication between ESO and the users (mostly as a consequence of a significant number of corresponding complaints from the community). ESO is expected to at least react on these items, either by following the recommendations, or else by stating very clearly *why* a certain issue cannot be resolved as desired. Note that since the 2000 meeting, UC recommendations and action items are accessible via the web under `http://www.eso.org/gen-fac/commit/`, as part of the minutes of the UC meetings.

To our great satisfaction, in many cases ESO has been able to follow the UC recommendations, demonstrating that user opinion is of substantial value. Sometimes it takes a bit to convince the people in charge, in which case action items may reappear in subsequent years. One illuminating example: For a long time, users had been annoyed that observing proposals rejected by the OPC did not get feedback comments by default, despite the generally acknowledged usefulness of such comments and despite the fact that most other time allocation committees provide them. The UC repeatedly criticised this attitude and asked to alter it, until ESO announced last year to change its policy and return comments. After a bit over one year of experience, it is probably fair to say that the new OPC procedure has been very well received by the community.

Another case, slightly more subtle but important in 'daily life', are the headers of FITS files distributed by ESO: these contain non-standard 'hierarchy keywords' which are not understood by (sometimes even screwing up) non-ESO data-processing packages – a continued source of embarrassment for quite a few users. Pleading to solve this incompatibility was almost one of the 'running items' at past UC meetings. But not in vain: ESO now provides a small 'Stand-Alone FITS Tool' (saft) which converts the hierarchy keywords into standard FITS keywords. This tool is quite new and we have not yet obtained a lot of feedback as to its usefulness, but the example clearly shows that such things can be changed for the better.

Improving Feedback

With all these proceedings going on within the UC and during the annual UC meetings, it is clearly an important task to make the results public and available to the community. In the past, this task

has been handled by the representatives independently, each for his/her national users community. This was not ideal: Apart from the fact that some will do this more thoroughly than others, it always means that much of the work (compiling information, writing reports, etc.) is done redundantly. It would be much better if the same information were available to all users, regardless of nationality or affiliation. Last year we implemented some important changes in this direction:

• The official minutes of the annual UC meetings are public and available over the web, including the approved recommendations and action items. Visit `http://www.eso.org/gen-fac/commit/` to see the available documents.

• For the first time, we have drafted an informal feedback report to the users community as a whole. This report has been publicised by e-mail and is available at the author's homepage under `http://www.astro.physik.uni-potsdam.de/~lutz/eso-uc.html`

An additional valuable source of information would be the presentation material given by ESO staff during the UC meetings. We hope that in the near future this can also routinely be placed in a public web area.

Improving User Input

One of the problems of the UC in the past has been that only a relatively limited group of users reported regularly to their UC representatives; as a result, the problem reports collected by the UC were not really representative. Additional insight is now provided by the end-of-mission reports, but the use of these reports is limited. First, there are still too many 'silent users' who do not even fill in the end-of-mission reports (only roughly 50% do so). Second, among those who do, there are many who just mark everything as 'excellent'. No doubt, this proves that indeed the users are highly satisfied with the way ESO is operated, but does it really mean that everything is perfect? It is great for ESO staff members to hear that they are on the right track, but they also need to know where remaining problems are. In my opinion – especially in the current atmosphere of mutual satisfaction –, users should feel encouraged to come up with constructive criticism.

Furthermore, the end-of-mission questionnaires clearly do not cover the full range of user/ESO interactions. Most significantly, nothing comparable is available to Service Mode observers, and hence not much is known about the general level of satisfaction among those. ESO has stated in the last UC meeting that they are working on implementing a scheme similar to the end-of-mission reports, but so far we are faced with more than two years of Service observing and very little, if any, systematic feedback from the users.

On an even longer time scale, the ultimate figure of merit is the user satisfaction with the scientific data obtained. This is often known only when the data are fully reduced and analysed, i.e. typically at least one year after the observations. Only then is it possible to recognise, e.g., inadequate calibration facilities, or scattered light effects not obvious in the raw data, just to give a few examples. However, learning about end-product data quality in a systematic way is certainly not easy. ESO has started with VLT instrument performance review sessions (organised by the STC), but from the UC point of view it would be desirable to also draw upon the enormous resources of the general users' experience. I suggest that we seriously consider some sort of new user poll with respect to instrument performance and data quality.

We all acknowledge that ESO staff is highly committed to excellent technical and scientific performance, and user-friendliness is one important aspect. It is probably fair to say that ESO is already one of the most user-friendly observatories in the world. In those (presumably rare) cases where things do not appear as you would like them to be, there's only one way to change that: Say something! Being critical means that you care, not that you are obnoxious (it's always a matter of *how* to say things, of course). In this sense, achieving good performance is to some extent also a responsibility of the users; it is the role of the UC to help in this process.

ESO Presentation in Brussels

Following the events in Bern and Porto, ESO continued its series of high-level presentations in the member states on November 20 with a meeting in the Belgian capital. The event in Brussels coincides with the Belgian Presidency of the European Union (and thus of the European Research Council), a fact that was reflected by participants to the meeting, which included members of the Belgian Senate, the Belgian Federal Government Commissioner for Science Policy, Yvan Ylieff, the Secretary General of the Federal Office for Scientific, Technical and Cultural Affairs, Eric Beka, the European Commissioner for Research, Philippe Busquin, and other high officials from the Directorate General for Research of the European Commission. All in all about 100 invited guests representing politics, public administration, the Belgian astronomical research community, industry and media listened to speeches by the ESO Director General, Commissioners Busquin and Ylieff. After the showing of the ESO video 'Astronomy to the Power of Four', Maarten Baes (PhD, University of Ghent) and Jean-Pierre Chisogne, commercial manager of A.M.O.S., Liège, presented impressive examples of Belgian participation in ESO, both in science and technology. The event, which took place at the Planetarium on the Heysel, was organised jointly by the Belgian Federal Office for Scientific, Technical and Cultural Affairs, the Belgian Royal Observatory and ESO.

C. MADSEN, ESO

The ESO Director General in conversation with the European Commissioner for Research, Philippe Busquin, and Prof. Paul Pâquet, Director of the Belgian Royal Observatory, Uccle.

International Max-Planck research School on Astrophysics at the University of Munich IMPRS

PhD programme

For the second time, the International Max-Planck Research School on Astrophysics (IMPRS) is accepting applications for its PhD programme. IMPRS is a joint collaboration between the European Southern Observatory, Max-Planck-Institut für Extraterrestrische Physik (MPE), the Observatory of the Ludwig-Maximilians University of Munich (USM) and the Max-Planck-Institut für Astrophysik (MPA). Also participating as associated partners are the Astro-particle physics groups at the Technical University of Munich (TUM) and the Werner-Heisenberg-Institut for Physics (MPP).

IMPRS is offering a highly competitive PhD programme, including lectures, seminars, and a research project supervised by scientists at one of the participating institutions. Course language is English. Students have access to ground- and space-based observatories and instrumentation operated by the participating institutes as well as supercomputers for advanced numerical simulations and theoretical studies. Successful completion of the 3-year programme by meeting LMU requirements leads to a doctoral ("PhD") degree in natural sciences (rerum naturalium) awarded by the Ludwig-Maximilians University of Munich.

Applications for the programme are open to students from all countries world-wide fulfilling the LMU admission requirements. More details on the IMPRS programme and admission requirements can be found at the website http://www.imprs-astro.mpg.de/ . For more information on research and science activities at ESO, please consult http://www.eso.org/projects/ and http://www.eso.org/science/ .

The closing date for applications for the programme starting in September 2002 is January 15, 2002.

Please apply by using the IMPRS application form available on-line (http://www.imprs-astro.mpg.de/admission.html).

Book Review: Reflecting Telescope Optics II, by Ray Wilson

Springer-Verlag, Corrected Second Printing, 2001, ISBN 3-540-60356-5, 554 pages, 240 illustrations, PRICE DM 159,90

Volume I appeared in 1996 and was reprinted with significant corrections in 2000. It deals with the historical development of the reflecting telescope with essentially "classical" technology from its invention up to about 1980 and gives the complete optical design and related theory of virtually all known telescope forms. An interesting addition in the reprint is the recently researched identity of Cassegrain in the Portrait Gallery of App. B.

Volume II appeared in 1999 and deals with all aspects of the technological "revolution" from about 1970–1980 onwards, which allowed the breakthrough of the absolute barriers to further progress both in size and optical quality imposed by the limitations of classical technology. A corrected reprint appeared in mid-2001.

The frontispiece added in the reprint shows one of the 8-metre ESO VLT telescopes, the first 8-metre-class telescope using modern active technology for *monolithic* mirrors; while the unchanged cover shows the two 10-metre Keck telescopes using modern active technology for *segmented* mirrors. These two technologies, in combination, seem set to dominate coming developments of super-large telescopes. Volume II deals with all practical aspects of the production and operation of such telescopes designed for use in the visual and infrared wavebands. All techniques required to build them, in particular for large telescopes, are described in considerable detail.

Chapter 1 gives a description of what is often the most demanding task in such projects, the manufacture of the surfaces of the mirrors. Many of the techniques have not changed considerably over the last years, but are nowadays much more effective owing to the use of computers. New methods like stress and ion beam polishing can be used for special applications or fine tuning, respectively.

The success of the figuring depends critically on the procedures used for the test of the optical surfaces. Computer techniques have completely revolutionised the precision, speed and convenience of test procedures. The method has to be adapted to the type of mirror. Interferometric methods are discussed in detail, also the null systems required to generate aspheric surfaces. Special attention is given to the complex test procedures for convex mirrors. Chapter 2 deals with the test and alignment of the telescope in function. After an introduction to the optical theory of misaligned two-mirror telescopes, an alignment procedure for such telescopes is described in detail. Methods for measuring the quality of telescope optics range from simple methods like the evaluation of defocused images to computer-based procedures such as Shack-Hartmann and curvature sensing.

The central Chapter 3 discusses modern telescope developments which are, in one way or the other, all aimed at overcoming the classical scaling laws for the total mass and related flexure of telescopes as functions of the diameter of the mirror. The four possibilities treated are the use of (usually hexagonal) segments, the coupling of separate telescopes, the light-weighting of the mirrors, or the use of actively controlled thin meniscus mirrors. Whereas most mirrors of large telescopes are made of low-

expansion glass ceramics, there are other possible blank materials such as, for example, metal or silicon carbide. All materials have advantages and face specific problems. A problem closely related to the type of the blank is its support.

The summary of the support theories includes basic laws of elasticity theory, the early theory of Couder and modern theories, in particular of G. Schwesinger, to whom the book is also dedicated. Both the axial and the lateral support of meniscus mirrors are treated. It is nowadays accepted that mirrors with diameters larger than approximately three metres have to be actively controlled. Since the author was the inventor of this method as applied to *monoliths* and used for the first time in the ESO NTT 3.5-m telescope, the history and basic principles are comprehensively presented.

Of equal importance is the control of the local environment, that is the avoidance of temperature inhomogeneities introduced by the telescope itself. Particularly significant is the attempt to keep the temperature of the primary mirror in equilibrium with the temperature of the ambient air. The local environment can, for example, be passively influenced by the dome design and also actively by cooling the air in the dome or certain components such as the primary mirror. Chapter 4 treats the question of how the optical quality can be assessed in one or a few figures of merit and how the specification for the overall quality can be broken down into specifications for the subsystems. The method using the so-called Central Intensity Ratio, a kind of Strehl Ratio for telescopes working in the atmosphere, was extensively applied during the manufacture of the ESO VLT.

Chapter 5 includes a summary of the fast growing area of adaptive optics, the purpose of which is to correct the aberrations introduced by the atmosphere and reach the diffraction limit of the telescope. After a comprehensive introduction to the theory of atmospheric optics based on the work of Tatarski, Fried and Roddier, the design and performance of the first adaptive optics systems are discussed.

Chapters 6 and 7 deal with topics which usually receive much less attention, namely the reflecting coatings of the mirrors, the design of the adapters, and the reduction of straylight through the use of baffles. Even the best coatings reflect at most 90% of the light over a reasonable range of wavelength, and the reflectivity degrades considerably if the mirrors are not regularly cleaned. Modern approaches as described in Chapter 6 are required to improve the situation. In modern telescopes, the adapters and rotators, which are often integrated into one unit, have to fulfil many tasks including guiding and wavefront sensing.

Finally, the short Chapter 8 stresses the importance of regular and systematic maintenance to preserve or even improve the quality reached after the commissioning of the telescope.

The book contains many more aspects and details than could be mentioned in this review. In fact, to the reviewer's knowledge it is the only monograph currently available which treats the whole range of modern optical technology of reflecting telescopes in a comprehensive way, whereby, as mentioned in the preface, interferometry between telescopes as well as solar and X-ray telescopes have been deliberately excluded as subjects which are too extensive or too specialised. (In contrast, a number of other modern treatments of the theory of Volume I exist, notably Schroeder's "Astronomical Optics"). It should be stressed that most of Volume II does not require a deep knowledge of the optical theory presented in Volume I. It should therefore also be of use to readers who are working in specialised areas or who simply want to get an overview of modern telescope technology. Special topics can easily be found with the help of the extensive name and subject indices, and thanks to the long list of references, the book is an entry point for more detailed studies.

Furthermore, amateur telescopes are getting bigger and better and are more and more computer controlled. Since many of the techniques and conclusions in this book can also be applied to these telescopes, the book should also be of interest for more ambitious amateur astronomers.

With the extensive name and subject index this volume should also be useful as a reference book.

L. NOETHE

PERSONNEL MOVEMENTS

International Staff

(1 October 2001 – 31 December 2001)

ARRIVALS

EUROPE

CIONI, Maria Rosa (I), Fellow
CORBETT, Ian F. (GB), Head of Administration
CRETTON, Nicolas (CH), Fellow
DADDI, Emanuele (I), Fellow
ETTORI, Stefano (I), Fellow
GONTÉ, Frédéric (F), Optical Engineer
KUNTSCHNER, Harald (D), Fellow
RICCIARDI, Francesco (I), Software Engineer
ROSSI, Silvio (I), Electronics Engineer/Senior Technician
SOMMER, Heiko (D), Software Designer/Developer
TACCONI-GARMAN, Lowell (USA), User Support Astronomer

CHILE

HEINZ, Volker (D), Mechanical Engineer
LO CURTO, Gaspare (I), Operations Staff Astronomer
MARCHESI, Massimiliano (I), Mechanical Engineer
RASSIA, Effrosyni (GR), Student

DEPARTURES

EUROPE

ANDERSEN, Torben (DK), ALMA Antenna Team Manager
BOGUN, Stefan (D), Astronomical Data Reduction Specialist
KÖNIG, Norbert (D) on 30.09.01, Head of Administration
LEDOUX, Cédric (F), Fellow
MOUTOU, Claire (F), Fellow
RAHMER, Gustavo (RCH), CCD System Engineer
SOLLERMAN, Jesper (S), Fellow
ZINS, Gérard (F), Software Engineer

CHILE

GRAY, Peter (AUS), Head of Engineering Department PAO
LEISY, Pierre (F), Operations Staff Astronomer
ROUCHER, Jacques (F), Electronics Technician

Local Staff

(1 September – 30 November 2001)

DEPARTURES

GARAGORRI ALA A PEDRO, Assistente Administrativo
NUÑEZ CRUZ, HERNAN, on 31.8.01, Telescope Instruments Operator
OSORIO BR LE MARIA ISABEL, Technical Secretary
RIJO ARANCIBIA ARIELA, Electronics Technician, Paranal
SANCHEZ VARAS FELIPE, Telescope Instruments Operator, La Silla

LES HOUCHES

centre de physique

EUROWINTER SCHOOL

Observing with the Very Large Telescope Interferometer

3-8 FEBRUARY 2002

The European Southern Observatory (ESO) in collaboration with European institutes will start operating the Very Large Telescope Interferometer (VLTI) in 2003. Two scientific instruments, AMBER in the near-infrared and MIDI in the thermal infrared, will be offered to the European community.

The expected performances of the VLTI and its instruments will be unique in terms of flux sensitivity and angular resolution, because of the large collecting area of the 8-m and 1.8-m telescopes and multiple baselines up to 200 meters. However the scientific outcome will be at the same level as the VLTI performance only if astronomers get prepared to interferometric observations. With this objective in mind, we organize a winter school to train European astronomers to the optimal use of the VLTI and to the preparation of the first observations.

The objective of the school is focused on practical exercizes. The curriculum of the school consists in general lectures for 30% of the time, practical training for 50% of it and informal seminars for the remaining time. The school is opened to a maximum of 50 participants from any country and any nationality.

The financial support from the European Union together with other sponsors will allow us to cover the most of the costs of the school (housing and travel) for all European participants. This financial aspect should prevent any student or scientist from not taking part to this school.

ORGANIZING COMMITTEES

SCHOOL CHAIRS

F. Malbet (LAOG, Grenoble)
<Fabien.Malbet@obs.ujf-grenoble.fr>,
G. Perrin (Observatoire de Paris, Meudon)
<Guy.Perrin@obspm.fr>

SCIENTIFIC ORGANIZING COMMITTEE

A. Boden *(JPL/Caltech)*, M. Fridlund *(ESA)*, A. Glindemann *(ESO)*, C. Haniff *(MRAO, Cambridge)*, C. Leinert *(MPIA, Heidelberg)*, R. Le Poole *(NEVEC, Leiden)*, D. Mourard *(Observatoire de Nice)*, F. Paresce *(ESO)*, R. Petrov *(Université de Nice)*, J. Surdej *(Université de Liège)*, D. Queloz *(Observatoire de Genève)*, G. Weigelt *(MPIfR, Bonn)*

LOCAL ORGANIZING COMMITTEE

G. Duvert, A. Chelli, X. Delfosse, D. Mouillet, K. Perraut, E. Le Coarer, S. Ortuno, F. Bouillet, G. Buisson

CENTRE DE PHYSIQUE DES HOUCHES

M. Ducloy, R. Romestain, B. Rousset, I. Lelièvre

LOCATION

Les Houches is a resort village in the Chamonix Valley of the french Alps. Established in 1951, the School is located in a group of mountain chalets surrounded by meadows and woods at 1150 m elevation. It is ideally located for mountaineering, skiing or touring as well as for intellectual pursuits.

INFORMATION AND APPLICATION

http://www-laog.obs.ujf-grenoble.fr/~jmmc/obsvlti

With the support of

EUROPEAN HIGH LEVEL SCIENTIFIC CONFERENCE, Supported by EC contract n° HCF-2001-00120

**The Centre de Physique in Les Houches is affiliated to Université Joseph Fourier and l'Institut National Polytechnique in Grenoble.
It is subsidized by the MENRT, CNRS and Commissariat à l'Energie Atomique. CENTRE DE PHYSIQUE DES HOUCHES - Côte des Chavants - F-74310 Les Houches
Tel. (33) 4 50 54 40 69 - (33) 1 49 40 39 00 - Fax (33) 4 50 55 53 25**

The ESO MESSENGER is published four times a year: normally in March, June, September and December. ESO also publishes Conference Proceedings, Preprints, Technical Notes and other material connected to its activities. Press Releases inform the media about particular events. For further information, contact the ESO Education and Public Relations Department at the following address:

EUROPEAN
SOUTHERN OBSERVATORY
Karl-Schwarzschild-Str. 2
D-85748 Garching bei München
Germany
Tel. (089) 320 06-0
Telefax (089) 3202362
ips@eso.org (internet)
URL: http://www.eso.org
http://www.eso.org/gen-fac/pubs/messenger/

The ESO Messenger:
Editor: Marie-Hélène Demoulin
Technical editor: Kurt Kjär

Printed by
J. Gotteswinter GmbH
Buch- und Offsetdruck
Joseph-Dollinger-Bogen 22
D-80807 München
Germany

ISSN 0722-6691

List of Scientific Preprints

October–December 2001

1444. H. Boehnhardt et al.: Visible and Near-IR Observations of Transneptunian Objects. Results from ESO and Calar Alto Telescopes. *A&A*.
1445. A.C. Delsanti et al.: BVRI Photometry of 27 Kuiper Belt Objects with ESO/Very Large Telescope. *A&A*.
1446. S. Arnouts et al.: Measuring the Redshift Evolution of Clustering: the Hubble Deep Field South. *M.N.R.A.S.*
1447. G. Carraro and F. Patat: Star clusters in the Carina complex: *UBVRI* photometry of NGC 3114, Collinder 228 and vdB-Hagen 99. *A&A*.
1448. D.H. Jones, P. L. Shopbell and J. Bland-Hawthorn: Detection and Measurement from Narrowband Tunable Filter Scans. *M.N.R.A.S.*
1449. E.V. Held et al.: RR Lyrae Variables in the Dwarf Spheroidal Galaxy Leo I. *ApJ*.
1450. J. Gorosabel et al.: Strategies for prompt searches for GRB afterglows: the discovery of the GRB 001011 optical/near-infrared counterpart using colour-colour selection. *A&A*.
1451. A. Kaufer, R.K. Prinja and O. Stahl: Evidence for a connection between photospheric and wind structure in HD 6470. *A&A*.
1452. M.A. Prieto et al.: On the relation between the coronal line emission and the IR / X-ray emission in Seyfert galaxies. *M.N.R.A.S.*
1453. M. Fernández and F. Comerón: Intense accretion and mass loss of a very low mass young stellar object. *A&A*.

Contents

TELESCOPES AND INSTRUMENTATION

REPORTS FROM OBSERVERS

OTHER ASTRONOMICAL NEWS

ANNOUNCEMENTS